

EUROPEAN ORGANISATION FOR NUCLEAR RESEARCH (CERN)



Submitted to: JHEP



CERN-EP-2018-083
31st July 2018

Search for dark matter in events with a hadronically decaying vector boson and missing transverse momentum in pp collisions at $\sqrt{s} = 13$ TeV with the ATLAS detector

The ATLAS Collaboration

A search for dark matter (DM) particles produced in association with a hadronically decaying vector boson is performed using pp collision data at a centre-of-mass energy of $\sqrt{s} = 13$ TeV corresponding to an integrated luminosity of 36.1 fb^{-1} , recorded by the ATLAS detector at the Large Hadron Collider. This analysis improves on previous searches for processes with hadronic decays of W and Z bosons in association with large missing transverse momentum (mono- W/Z searches) due to the larger dataset and further optimization of the event selection and signal region definitions. In addition to the mono- W/Z search, the as yet unexplored hypothesis of a new vector boson Z' produced in association with dark matter is considered (mono- Z' search). No significant excess over the Standard Model prediction is observed. The results of the mono- W/Z search are interpreted in terms of limits on invisible Higgs boson decays into dark matter particles, constraints on the parameter space of the simplified vector-mediator model and generic upper limits on the visible cross sections for $W/Z+\text{DM}$ production. The results of the mono- Z' search are shown in the framework of several simplified-model scenarios involving DM production in association with the Z' boson.

1 Introduction

Numerous cosmological observations indicate that a large part of the mass of the universe is composed of dark matter (DM), yet its exact, possibly particle, nature and its connection to the Standard Model (SM) of particle physics remain unknown. Discovery of DM particles and understanding their interactions with SM particles is one of the greatest quests in particle physics and cosmology today. Several different experimental approaches are being exploited. Indirect detection experiments search for signs of DM annihilation or decays in outer space, while direct detection experiments are sensitive to low-energy recoils of nuclei induced by interactions with DM particles from the galactic halo. The interpretation of these searches is subject to astrophysical uncertainties in DM abundance and composition. Searches at particle colliders, for which these uncertainties are irrelevant, are complementary if DM candidates can be produced in particle collisions. Weakly interacting massive particles (WIMPs), one of the leading DM candidates, could be produced in proton–proton (pp) collisions at the Large Hadron Collider (LHC) and detected by measuring the momentum imbalance associated with the recoiling SM particles.

A typical DM signature which can be detected by the LHC experiments is a large overall missing transverse momentum E_T^{miss} from a pair of DM particles which are recoiling against one or more SM particles. Several searches for such signatures performed with LHC pp collision data at centre-of-mass energies of 7, 8 and 13 TeV observed no deviations from SM predictions and set limits on various DM particle models. Measurements include those probing DM production in association with a hadronically decaying W or Z boson [1–4] and dedicated searches for the so-called invisible decays of the Higgs boson into a pair of DM particles, targeting Higgs boson production in association with a hadronically decaying vector boson [5–7]. In the SM, the invisible Higgs boson decays occur through the $H \rightarrow ZZ^* \rightarrow vvvv$ process with a branching ratio $\mathcal{B}_{H \rightarrow \text{inv.}}^{\text{SM}}$ of 1.06×10^{-3} for a Higgs boson mass $m_H = 125$ GeV [8]. Some extensions of the SM allow invisible decays of the Higgs boson into DM or neutral long-lived massive particles [9–13] with a significantly larger branching ratio $\mathcal{B}_{H \rightarrow \text{inv.}}$. In this case H is required to have properties similar to those of a SM Higgs boson and is assumed to be the Higgs boson with mass of 125 GeV that was discovered at the LHC. At present, the most stringent upper limit on $\mathcal{B}_{H \rightarrow \text{inv.}}$ is about 23% at 95% confidence level (CL) for $m_H = 125$ GeV, obtained from a combination of direct searches and indirect constraints from Higgs boson coupling measurements [5, 14].

In this paper, a search for DM particles produced in association with a hadronically decaying W or Z boson (mono- W/Z search) is performed for specific DM models, including DM production via invisible Higgs boson decays. The analysis uses LHC pp collision data at a centre-of-mass energy of 13 TeV collected by the ATLAS experiment in 2015 and 2016, corresponding to a total integrated luminosity of 36.1 fb^{-1} . The results are also expressed in terms of upper limits on visible cross sections, allowing the reinterpretation of the search results in alternative models. In addition to the mono- W/Z search, the as yet unexplored hypothesis of DM production in association with a potentially new vector boson Z' [15] is studied using the same collision data (mono- Z' search). Compared to the analysis presented in Ref. [1], the results are obtained from a larger data sample, and event selection and definition of the signal regions are further optimized, including new signal regions based on the tagging of jets from heavy-flavour hadrons and on jet topologies. Event topologies with two well separated jets from the vector boson decay are studied (referred to as the *resolved topology*), as well as topologies with one large-radius jet from a highly boosted vector boson (referred to as the *merged topology*).

The paper is organized as follows. A brief introduction to the ATLAS detector is given in Section 2. The signal models are introduced in Section 3, while the samples of simulated signal and background processes are described in Section 4. The algorithms for the reconstruction and identification of final-state

particles are summarized in Section 5. Section 6 describes the criteria for the selection of candidate signal events. The background contributions are estimated with the help of dedicated control regions in data, as described in Section 7. The experimental and theoretical systematic uncertainties (Section 8) are taken into account in the statistical interpretation of data, with the results presented in Section 9. Concluding remarks are given in Section 10.

2 ATLAS detector

The ATLAS detector [16] is a general-purpose detector with forward-backward symmetric cylindrical geometry.¹ It consists of an inner tracking detector (ID), electromagnetic (EM) and hadronic calorimeters and a muon spectrometer (MS) surrounding the interaction point. A new innermost silicon pixel layer [17, 18] was added to the ID before the start of data-taking in 2015. The inner tracking system, providing precision tracking in the pseudorapidity range $|\eta| < 2.5$, is immersed in a 2 T axial magnetic field, while toroidal magnets in the MS provide a field integral ranging from 2 Tm to 6 Tm across most of the MS. The electromagnetic calorimeter is a lead/liquid-argon (LAr) sampling calorimeter with an accordion geometry covering the pseudorapidity range $|\eta| < 3.2$. The hadronic calorimetry is provided by a steel/scintillator-tile calorimeter in the range $|\eta| < 1.7$ and two copper/LAr calorimeters spanning $1.5 < |\eta| < 3.2$. The calorimeter coverage is extended to $|\eta| < 4.9$ by copper/LAr and tungsten/LAr forward calorimeters providing both electromagnetic and hadronic energy measurements. The data are collected with a two-level trigger system [19]. The first-level trigger selects events based on custom-made hardware and uses information from muon detectors and calorimeters with coarse granularity. The second-level trigger is based on software algorithms similar to those applied in the offline event reconstruction and uses the full detector granularity.

3 Signal models

Two signal models are used to describe DM production in the mono-W/Z final state. The first is a *simplified vector-mediator model*, illustrated by the Feynman diagram in Figure 1(a), in which a pair of Dirac DM particles is produced via an s -channel exchange of a vector mediator (Z') [20, 21]. There are four free parameters in this model: the DM and the mediator masses (m_χ and $m_{Z'}$, respectively), and the mediator couplings to the SM and DM particles (g_{SM} and g_{DM} , respectively). The minimal total mediator decay width is assumed, allowing only vector mediator decays into DM or quarks. Its value is determined by the choice of the coupling values g_{SM} and g_{DM} [21] and it is much smaller than the mediator mass. The second is a model with *invisible Higgs boson decays* in which a Higgs boson H produced in SM Higgs boson production processes decays into a pair of DM particles which escape detection. The production process with a final state closest to the mono-W/Z signature is associated production with a hadronically decaying W or Z boson (VH production, see Figure 1(b)). The WH and ZH signals are predominantly produced via quark–antiquark annihilation ($q\bar{q} \rightarrow VH$), with an additional ZH contribution from gluon–gluon fusion ($gg \rightarrow ZH$). The production of a Higgs boson via gluon–gluon fusion (ggH) or vector

¹ The ATLAS experiment uses a right-handed coordinate system with its origin at the nominal interaction point (IP) in the centre of the detector and the z -axis along the beam pipe. The x -axis points from the IP to the centre of the LHC ring, and the y -axis points upward. Cylindrical coordinates (r, ϕ) are used in the transverse plane, ϕ being the azimuthal angle around the z -axis. The pseudorapidity is defined in terms of the polar angle θ as $\eta = -\ln \tan(\theta/2)$. Transverse momentum is computed from the three-momentum, \mathbf{p} , as $p_T = |\mathbf{p}| \sin \theta$.

boson fusion (VBF) followed by the Higgs boson decay into DM particles can also lead to events with large E_T^{miss} and two or more jets. Especially the ggH signal has a contribution comparable to or even stronger than the VH process, since its cross section is about 20 times larger and the jets originating from initial state radiation are more central than in the VBF process. The free parameter of this model is the branching ratio $\mathcal{B}_{H \rightarrow \text{inv.}}$. The cross sections for the different Higgs boson production modes are taken to be given by the SM predictions.

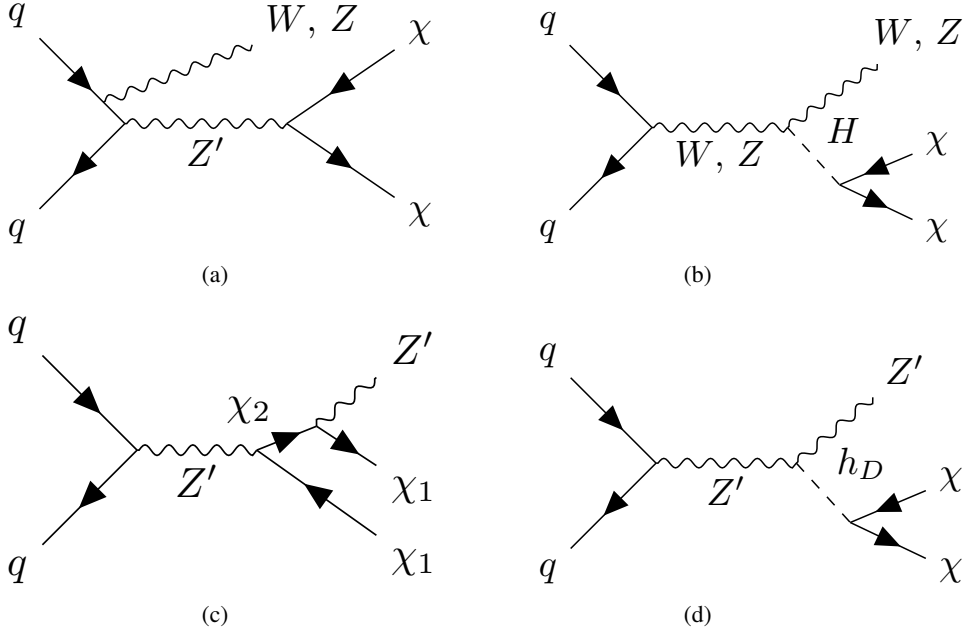


Figure 1: Examples of dark matter particle (χ) pair-production (a) in association with a W or Z boson in a simplified model with a vector mediator Z' between the dark sector and the SM [20]; (b) via decay of the Higgs boson H produced in association with the vector boson [9–13]; (c) in association with a final-state Z' boson via an additional heavy dark-sector fermion (χ_2) [15] or (d) via a dark-sector Higgs boson (h_D) [15].

Two signal models describe DM production in the mono- Z' final state [15]. Both models contain a Z' boson in the final state; the Z' boson is allowed to decay only hadronically. The $Z' \rightarrow t\bar{t}$ decay channel, kinematically allowed for very heavy Z' resonances, is expected to contribute only negligibly to the selected signal events and therefore the branching ratio $\mathcal{B}_{Z' \rightarrow t\bar{t}}$ is set to zero. In the first model, the so-called *dark-fermion model*, the intermediate Z' boson couples to a heavier dark-sector fermion χ_2 as well as the lighter DM candidate fermion χ_1 , see Figure 1(c). The mass m_{χ_2} of the heavy fermion χ_2 is a free parameter of the model, in addition to the DM candidate mass m_{χ_1} , the mediator mass $m_{Z'}$, and the Z' couplings to $\chi_1\chi_2$ (g_{DM}) and to all SM particles (g_{SM}). The total Z' and χ_2 decay widths are determined by the choice of the mass and coupling parameter values, assuming that the only allowed decay modes are $\chi_2 \rightarrow Z'\chi_1$, $Z' \rightarrow q\bar{q}$ and $Z' \rightarrow \chi_2\chi_1$. Under these assumptions the decay widths are small compared to the experimental dijet and large-radius-jet mass resolutions. In the second, so-called *dark-Higgs model*, a dark-sector Higgs boson h_D which decays to a $\chi\chi$ pair is radiated from the Z' boson as illustrated in Figure 1(d). The masses m_{h_D} , m_χ , $m_{Z'}$ and the constants g_{SM} and g_{DM} are free parameters of the model. The latter is defined as the coupling of the dark Higgs boson h_D to the vector boson Z' . Similar to the dark-fermion model, the total decay widths of the Z' and h_D bosons are determined by the values of the mass and coupling parameters, assuming that the Z' boson can only decay into quarks or radiate an h_D

boson. The dark Higgs boson is assumed to decay only into $\chi\chi$ or $Z'Z^{(*)}$. The latter decay mode is suppressed for $m_{h_D} < 2m_{Z'}$, which is the case for the parameter space considered in this paper.

4 Simulated signal and background samples

All signal and background processes from hard-scatter pp collisions were modelled by simulating the detector response to particles produced with Monte Carlo (MC) event generators. The interaction of generated particles with the detector material was modelled with the GEANT4 [22, 23] package and the same particle reconstruction algorithms were employed in simulation as in the data. Additional pp interactions in the same and nearby bunch crossings (pile-up) were taken into account in simulation. The pile-up events were generated using PYTHIA 8.186 [24] with the A2 set of tuned parameters [25] and the MSTW2008LO set of parton distribution functions (PDF) [26]. The simulation samples were weighted to reproduce the observed distribution of the mean number of interactions per bunch crossing in the data.

The mono- W/Z signal processes within the simplified Z' vector-mediator model, as well as all mono- Z' signal processes, were modelled at leading-order (LO) accuracy with the MadGraph5_aMC@NLO v2.2.2 generator [27] interfaced to the PYTHIA 8.186 and PYTHIA 8.210 parton shower models, respectively. The A14 set of tuned parameters [28] was used together with the NNPDF23lo PDF set [29] for these signal samples. The mono- W/Z signal samples within the simplified vector-mediator model were generated in a grid of mediator and DM particle masses, with coupling values set to $g_{SM} = 0.25$ and $g_{DM} = 1$ following the ‘V1’ scenario from Ref. [30]. The mediator mass $m_{Z'}$ and the DM particle mass m_χ range from 10 GeV to 10 TeV and from 1 GeV to 1 TeV respectively. Two samples with $m_\chi = 1$ GeV were used to evaluate the impact of theory uncertainties on the signal, one with a mediator mass of 300 GeV and the other with a mediator mass of 600 GeV. The mono- Z' samples were simulated for mediator masses between 50 GeV and 500 GeV, with the g_{DM} coupling value set to $g_{DM} = 1$. Following the current experimental constraints from dijet resonance searches [31–34], in particular those for the mediator mass range below about 500 GeV studied in this analysis, the g_{SM} coupling value was set to 0.1. For this choice of the couplings, the width of the Z' boson is negligible compared to the experimental resolution, allowing limits to be set on the coupling product $g_{SM} \cdot g_{DM}$. For each choice of $m_{Z'}$, two signal samples were simulated in both mono- Z' models, each with a different choice of masses m_{χ_2} or m_{h_D} of intermediate dark-sector particles as summarized in Table 1. Out of the two samples for a given $m_{Z'}$ value, the one with a lower (higher) mass of the intermediate dark-sector particle is referred to as the ‘light dark sector’ (‘heavy dark sector’) scenario. The mass m_χ in the dark-Higgs model was set to 5 GeV, since it can be assumed that the kinematic properties are determined by the masses $m_{Z'}$ and m_{h_D} unless the mass m_χ is too large.

Processes in the mono- W/Z final state involving invisible Higgs boson decays originate from the VH , ggH and VBF SM Higgs boson production mechanisms and were all generated with the PowHEG-Box v2 [35–37] generator interfaced to PYTHIA 8.212 for the parton shower, hadronization and the underlying event modelling. The detailed description of all generated production processes together with the corresponding cross-section calculations can be found in Refs. [38, 39]. The Higgs boson mass in these samples was set to $m_H = 125$ GeV and the Higgs boson was decayed through the $H \rightarrow ZZ^* \rightarrow vvvv$ process to emulate the decay of the Higgs boson into invisible particles with a branching ratio of $\mathcal{B}_{H \rightarrow \text{inv.}} = 100\%$.

The major sources of background are the production of top-quark pairs ($t\bar{t}$) and the production of W and Z bosons in association with jets ($V+\text{jets}$, where $V \equiv W$ or Z). The event rates and the shape of the final discriminant observables for these processes are constrained with data from dedicated control regions

Table 1: Particle mass settings in the simulated mono- Z' samples for a given mediator mass $m_{Z'}$.

Scenario	Dark-fermion model	Dark-Higgs model
	$m_{\chi_1} = 5 \text{ GeV}$	$m_\chi = 5 \text{ GeV}$
Light dark sector	$m_{\chi_2} = m_{\chi_1} + m_{Z'} + 25 \text{ GeV}$	$m_{h_D} = \begin{cases} m_{Z'} & , m_{Z'} < 125 \text{ GeV} \\ 125 \text{ GeV} & , m_{Z'} > 125 \text{ GeV} \end{cases}$
	$m_{\chi_1} = m_{Z'}/2$	$m_\chi = 5 \text{ GeV}$
Heavy dark sector	$m_{\chi_2} = 2m_{Z'}$	$m_{h_D} = \begin{cases} 125 \text{ GeV} & , m_{Z'} < 125 \text{ GeV} \\ m_{Z'} & , m_{Z'} > 125 \text{ GeV} \end{cases}$

(see Section 7). Other small background contributions include diboson (WW , WZ and ZZ) and single top-quark production. Their contribution is estimated from simulation.

Events containing leptonically decaying W or Z bosons with associated jets were simulated using the SHERPA 2.2.1 generator [40], with matrix elements calculated for up to two partons at next-to-leading order (NLO) and four partons at LO using COMIX [41] and OPENLOOPS [42] and merged with the SHERPA parton shower [43] using the ME+PS@NLO prescription [44]. The NNPDF3.0 next-to-next-to-leading order (NNLO) PDF set [29] was used in conjunction with dedicated parton shower tuning developed by the SHERPA authors. The inclusive cross section was calculated up to NNLO in QCD [45].

For the generation of $t\bar{t}$ events, PowHeg-Box v2 was used with the CT10 PDF set [46] in the NLO matrix element calculations. Electroweak t -channel, s -channel and Wt -channel single-top-quark events were generated with PowHeg-Box v1. This event generator uses the four-flavour scheme for the NLO matrix element calculations together with the fixed four-flavour PDF set CT10f4 [46]. For all top-quark processes, top-quark spin correlations are preserved (for t -channel top-quark production, top quarks were decayed using MADSPIN [47]). The parton shower, hadronization, and the underlying event were simulated using PYTHIA 6.428 [48] with the CTEQ6L1 PDF set [49] and the corresponding Perugia 2012 set of tuned parameters [50]. The top-quark mass was set to 172.5 GeV. The EvtGen 1.2.0 program [51] was used for the properties of b - and c -hadron decays. The inclusive $t\bar{t}$ cross section was calculated up to NNLO with soft gluon resummation at next-to-next-to-leading-logarithm (NNLL) accuracy [52]. Single top-quark production cross sections were calculated at NLO accuracy [53–56].

Diboson events with one of the bosons decaying hadronically and the other leptonically were generated with the SHERPA 2.1.1 event generator. Matrix elements were calculated for up to one (ZZ) or zero (WW , WZ) additional partons at NLO and up to three additional partons at LO using COMIX and OPENLOOPS, and merged with the SHERPA parton shower according to the ME+PS@NLO prescription. The CT10 PDF set was used in conjunction with dedicated parton shower tuning developed by the SHERPA authors. The event generator cross sections at NLO were used in this case. In addition, the Sherpa diboson sample cross section is scaled to account for the cross section change when switching to the G_μ scheme for the electroweak parameters, resulting in an effective value of $\alpha \approx 1/132$.

5 Object reconstruction and identification

The selection of mono- W/Z and mono- Z' candidate signal events and events in dedicated one-muon and two-lepton (electron or muon) control regions relies on the reconstruction and identification of jets, electrons and muons, as well as on the reconstruction of the missing transverse momentum. These are described in the following.

Three types of jets are employed in the search. They are reconstructed from noise-suppressed topological calorimeter energy clusters [57] (“*small- R* ” and “*large- R* ” jets) or inner detector tracks (“*track*” jets) using the anti- k_t jet clustering algorithm [58, 59] with different values of the radius parameter R .

Small- R jets (j) with radius parameter $R = 0.4$ are used to identify vector bosons with a relatively low boost. Central jets (forward jets) within $|\eta| < 2.5$ ($2.5 \leq |\eta| < 4.5$) are required to satisfy $p_T > 20$ GeV ($p_T > 30$ GeV). The small- R jets satisfying $p_T < 60$ GeV and $|\eta| < 2.4$ are required to be associated with the primary vertex using the jet-vertex-tagger discriminant [60] in order to reject jets originating from pile-up vertices. The vertex with the highest $\sum p_T^2$ of reconstructed tracks is selected as the primary vertex. Jet energy scale and resolution, as well as the corresponding systematic uncertainties, are determined with simulation and data at $\sqrt{s} = 13$ TeV [61, 62]. Jets within $|\eta| < 2.5$ containing b -hadrons are identified using the MV2c10 b -tagging algorithm [63–65] at an operating point with a 70% b -tagging efficiency measured in simulated $t\bar{t}$ events.

Large- R jets (J) [66, 67] are reconstructed with a radius parameter of $R = 1.0$ to allow the detection of merged particle jets from a boosted vector boson decay. The trimming algorithm [68] is applied to remove the energy deposits from pile-up, the underlying event and soft radiation, by reclustering the large- R jet constituents into sub-jets with radius parameter $R = 0.2$. The sub-jets with transverse momenta below 5% of the original jet transverse momentum are removed from the large- R jet. The jet mass is calculated as the resolution-weighted mean of the mass measured using only calorimeter information and the track-assisted mass measurement [69]. Large- R jets are required to satisfy $p_T > 200$ GeV and $|\eta| < 2.0$. In the mono- W/Z search, these jets are tagged as originating from a hadronic W - or Z -boson decay using p_T -dependent requirements on the jet mass and substructure variable $D_2^{(\beta=1)}$ [70, 71]. The latter is used to select jets with two distinct concentrations of energy within the large- R jet [72, 73]. The jet mass and $D_2^{(\beta=1)}$ selection criteria are adjusted as a function of jet p_T to select W or Z bosons with a constant efficiency of 50% measured in simulated events. In the mono- Z' search, large- R jets are tagged as originating from the hadronic decay of a Z' boson using a jet-mass requirement and requiring $D_2^{(\beta=1)} < 1.2$, chosen to optimize the search sensitivity. The momenta of both the large- R and small- R jets are corrected for energy losses in passive material and for the non-compensating response of the calorimeter. Small- R jets are also corrected for the average additional energy due to pile-up interactions.

Track jets with radius parameter $R = 0.2$ [74] are used to identify large- R jets containing b -hadrons [75]. Inner detector tracks originating from the primary vertex, selected by impact parameter requirements, are used in the track jet reconstruction. Track jets are required to satisfy $p_T > 10$ GeV and $|\eta| < 2.5$, and are matched to the large- R jets via ghost-association [76]. As for the small- R jets, the track jets containing b -hadrons are identified using the MV2c10 algorithm at a working point with 70% efficiency.

Simulated jets are labelled according to the flavour of the hadrons with $p_T > 5$ GeV which are found within a cone of size $\Delta R \equiv \sqrt{(\Delta\phi)^2 + (\Delta\eta)^2} = 0.3$ around the jet axis. If a b -hadron is found, the jet is labelled as a b -jet. If no b -hadron, but a c -hadron is found, the jet is labelled as a c -jet. Otherwise the jet is labelled as a light jet (l) originating from u -, d -, or s -quarks or gluons. Simulated $V+jets$ events are categorized

according to this particle-level labelling into three separate categories: $V +$ heavy flavour ($V+HF$) events, $V + cl$ events and $V +$ light flavour ($V+LF$) events. The first category consists of $V + bb$, $V + bc$, $V + cc$ and $V + bl$ components, while the last one is given by the $V + ll$ component alone. In the very rare case that after the final selection only one jet is present in addition to the V boson, the missing jet is labelled as a light jet.

Electron candidates are reconstructed from energy clusters in the electromagnetic calorimeter that are associated to an inner detector track. The electron candidates are identified using a likelihood-based procedure [77, 78] in combination with additional track hit requirements. All electrons, including those employed for the electron veto in the signal and in the one-muon and two-muon control regions, must satisfy the ‘loose’ likelihood criteria. An additional, more stringent criterion is applied in the two-electron control region, requiring that at least one of the electrons passes the ‘medium’ likelihood criteria. Each electron is required to have $p_T > 7$ GeV, and $|\eta| < 2.47$, with their energy calibrated as described in Ref. [79, 80]. To suppress the jets misidentified as electrons, electron isolation is required, defined as an upper limit on the scalar sum of the p_T^i of the tracks i (excluding the track associated to the electron candidate) within a cone of size $\Delta R = 0.2$ around the electron, $(\sum p_T^i)^{\Delta R=0.2}$, relative to electron p_T . The p_T - and η -dependent limits corresponding to an isolation efficiency of 99% are applied. In addition, to suppress electrons not originating from the primary vertex, requirements are set on the longitudinal impact parameter, $|z_0 \sin \theta| < 0.5$ mm, and the transverse impact parameter significance, $|d_0|/\sigma(d_0) < 5$.

Muon candidates are primarily reconstructed from a combined fit to inner detector hits and muon spectrometer segments [81]. In the central detector region ($|\eta| < 0.1$) lacking muon spectrometer coverage, muons are also identified by matching a reconstructed inner detector track to calorimeter energy deposits consistent with a minimum ionizing particle. Two identification working points with different purity are used. All muons, including those employed for the muon veto in the signal and in the two-electron control regions, must satisfy the ‘loose’ criteria. In addition, the muon in the one-muon control region and at least one of the two muons in the two-muon control region must pass the ‘medium’ selection criteria. Each muon is required to have $p_T > 7$ GeV and $|\eta| < 2.7$ and satisfy the impact parameter criteria $|z_0 \sin \theta| < 0.5$ mm and $|d_0|/\sigma(d_0) < 3$. All muons are required to be isolated by requiring an upper threshold on the scalar sum $(\sum p_T^i)^{\Delta R=0.3}$ relative to the muon p_T that corresponds to a 99% isolation efficiency, similarly to the electrons. In the one-muon control region, tighter isolation criteria with $(\sum p_T^i)^{\Delta R=0.3}/p_T < 0.06$ are applied. In both cases, the muon p_T is subtracted from the scalar sum.

The vector missing transverse momentum E_T^{miss} is calculated as the negative vector sum of the transverse momenta of calibrated small- R jets and leptons, together with the tracks which are associated to the primary interaction vertex but not associated to any of these physics objects [82]. A closely related quantity, $E_T^{\text{miss(no lepton)}}$, is calculated in the same way but excluding the reconstructed muons or electrons. The missing transverse momentum is given by the magnitude of these vectors, $E_T^{\text{miss}} = |E_T^{\text{miss}}|$ and $E_T^{\text{miss(no lepton)}} = |E_T^{\text{miss(no lepton)}}|$. In addition, the track-based missing transverse momentum vector, $\mathbf{p}_T^{\text{miss}}$, and similarly $\mathbf{p}_T^{\text{miss(no lepton)}}$, is calculated as the negative vector sum of the transverse momenta of tracks with $p_T > 0.5$ GeV and $|\eta| < 2.5$ originating from the primary vertex.

6 Event selection and categorization

Events studied in this analysis are accepted by a combination of E_T^{miss} triggers with thresholds between 70 GeV and 110 GeV, depending on the data-taking periods. The trigger efficiency is measured in data

using events with large E_T^{miss} accepted by muon triggers. The triggers are found to be fully efficient for $E_T^{\text{miss}} > 200$ GeV and the inefficiency at lower E_T^{miss} values and the corresponding uncertainty are taken into account. At least one collision vertex with at least two associated tracks is required in each event, and for the signal region selection a veto is imposed on all events with loose electrons or muons in the final state. Depending on the Lorentz boost of the vector boson, two distinct event topologies are considered: a *merged topology* where the decay products of the vector boson are reconstructed as a single large- R jet, and a *resolved topology* where they are reconstructed as individual small- R jets. Each event is first passed through the merged-topology selection and, if it fails, it is passed through the resolved-topology selection. Thus, there is no overlap of events between the two final-state topologies. For the mono- Z' search, the categorization into merged and resolved event topologies is only performed for the mediator mass hypothesis of $m_{Z'}$ below 100 GeV. For heavier mediator masses, the angular separation of jets from the Z' boson decay is expected to be larger than the size of a large- R jet. Thus, only the resolved-topology selection criteria are applied in this case.

The mono- W/Z and mono- Z' event selection criteria applied for each of the two topologies are summarized in Table 2. The criteria have been optimized to obtain the maximum expected signal significance. In the merged (resolved) event topology, at least one large- R jet (at least two small- R jets) and E_T^{miss} values above 250 GeV (above 150 GeV) are required in the final state. In order to suppress the $t\bar{t}$ and $V+\text{jets}$ background with heavy-flavour jets, all events with merged topology containing b -tagged track jets not associated to the large- R jet via ghost-association are rejected. In the resolved topology, all events with more than two b -tagged small- R jets are rejected. The highest- p_T large- R jet in an event is considered as the candidate for a hadronically decaying vector boson in the merged topology. Similarly, in the resolved topology the two highest- p_T (leading) b -tagged small- R jets are selected as the candidate for a hadronically decaying W or Z boson and, if there are fewer than two b -jets in the final state, the highest- p_T remaining jets are used to form the hadronic W or Z boson decay candidate. Additional criteria are applied in both merged and resolved topologies to suppress the contribution from multijet events. Since the vector bosons in signal events are recoiling against the dark matter particles, a threshold is applied on the azimuthal separation between the E_T^{miss} vector and the highest- p_T large- R jet (system of the two highest- p_T jets) in the merged (resolved) topology, $\Delta\phi(E_T^{\text{miss}}, J \text{ or } jj) > 120^\circ$. Also, the angles between E_T^{miss} and each of the up to three highest- p_T small- R jets should be sufficiently large, $\min[\Delta\phi(E_T^{\text{miss}}, j)] > 20^\circ$, in order to suppress events with a significant E_T^{miss} contribution from mismeasured jets. Events with a large E_T^{miss} value originating from calorimeter mismeasurements are additionally suppressed by the requirement of a non-vanishing track-based missing transverse momentum, $p_T^{\text{miss}} > 30$ GeV, and a requirement on the azimuthal separation between the calorimeter-based and track-based missing transverse momenta, $\Delta\phi(E_T^{\text{miss}}, p_T^{\text{miss}}) < 90^\circ$. The p_T^{miss} requirements also reduce non-collision background from beam halo or beam-gas interactions that produce signal in time with the colliding proton bunches. Such events are characterized mainly by energy deposits in the calorimeters in the absence of track activity. In the categories with two b -tagged jets the non-collision background is negligible and the expected discovery significance is higher without the p_T^{miss} requirement, which is not applied. Further criteria are imposed on events with the resolved topology. The leading jet is required to have $p_T^{j_1} > 45$ GeV. To improve the modelling of the trigger efficiency with MC events, the scalar sum of the transverse momenta of all jets is required to be $\sum p_T^{j_i} > 120$ (150) GeV in events with two (at least three) jets.

After these general requirements, the events are classified according to the number of b -tagged jets into events with exactly zero ($0b$), one ($1b$) and two ($2b$) b -tagged jets to improve the signal-to-background ratio and the sensitivity to $Z \rightarrow bb$ decays. Small- R jets (track jets) are used for the b -tagging in the resolved (merged) category. Further selection criteria defining the final signal regions are introduced

separately for the mono- W/Z and mono- Z' searches.

For the mono- W/Z search, the events in the $0b$ and $1b$ categories with merged topology are further classified into high-purity (HP) and low-purity (LP) regions; the former category consists of events satisfying the p_T -dependent requirements on the jet substructure variable $D_2^{(\beta=1)}$, allowing an improved discrimination for jets containing $V \rightarrow q\bar{q}$ decays, while the latter one selects all the remaining signal events. In the signal region with resolved topology, the angular separation ΔR_{jj} between the two leading jets is required to be smaller than 1.4 (1.25) in the $0b$ and $1b$ ($2b$) categories. Finally, a mass window requirement is imposed on the vector boson candidate in each of the eight resulting signal categories. In the $0b$ and $1b$ merged-topology categories, a mass requirement depending on the large- R jet p_T is applied. The large- R jet mass and $D_2^{(\beta=1)}$ requirements have been optimized within a dedicated study of the W/Z tagger performance [66, 67, 83]. In the $2b$ merged-topology category, in which the signal is expected to come predominantly from $Z \rightarrow bb$ decays, a mass window requirement of $75 \text{ GeV} < m_J < 100 \text{ GeV}$ is applied. The large- R jet substructure variable $D_2^{(\beta=1)}$ is not considered in this channel in order to obtain a higher signal efficiency and higher expected discovery significance. In the resolved $0b$ and $1b$ ($2b$) categories, the mass of the dijet system composed of the two leading jets is required to be $65 \text{ GeV} < m_{jj} < 105 \text{ GeV}$ ($65 \text{ GeV} < m_{jj} < 100 \text{ GeV}$). For the mono- Z' search, a similar classification by the b -tagging multiplicity, and by the substructure variable $D_2^{(\beta=1)}$ into high- and low-purity regions in the merged-topology category, is performed, using slightly different requirements on the substructure of the large- R jet. A p_T -independent requirement on the substructure variable $D_2^{(\beta=1)} < 1.2$ is used in signal regions with merged topology, as this is found to provide the maximum expected signal significance. Additional criteria also differ from the criteria applied in the mono- W/Z search. No criteria are applied on the ΔR_{jj} variable in events with the resolved topology, since the high-mass Z' bosons in dark-fermion or dark-Higgs models are less boosted than W or Z bosons in the simplified vector-mediator model, leading to a larger angular separation of jets from the Z' boson decays. The requirements on the mass of the Z' candidate are optimized for each event category as summarized in Table 2.

For both the mono- W/Z and the mono- Z' search, the E_T^{miss} distribution in each event category is used as the final discriminant in the statistical interpretation of the data, since for the models with very large E_T^{miss} values a better sensitivity can be achieved compared to the V -candidate mass discriminant. The E_T^{miss} distributions after the full selection, as well as the m_J and m_{jj} distributions before the mass window requirement, are shown for various signal models in Figures 2 and 3.

Figure 4 shows the product $(\mathcal{A} \times \varepsilon)_{\text{total}}$ of the signal acceptance \mathcal{A} and selection efficiency ε for the simplified vector-mediator model and for the dark-fermion and dark-Higgs mono- Z' signal models after the full event selection. This product is defined as the number of signal events satisfying the full set of selection criteria, divided by the total number of generated signal events. For all signal models, the main efficiency loss is caused by the minimum E_T^{miss} requirement.

In the simplified vector-mediator model, the $(\mathcal{A} \times \varepsilon)_{\text{total}}$, obtained by summing up signal contributions from all event categories, increases from 1% for low to 15% for high mediator mass due to the increase of the missing transverse momentum in the final state.

Similarly, for the mono- Z' signal models, the $(\mathcal{A} \times \varepsilon)_{\text{total}}$ increases with increasing mediator mass from 2% to 15% (from a few % to up to 40%) in scenarios with a light (heavy) dark sector. The $(\mathcal{A} \times \varepsilon)_{\text{total}}$ for invisible Higgs boson decays is 0.5% when summing over all signal regions. About 58% of that signal originates from ggH , 35% from VH and 7% from VBF production processes, with $(\mathcal{A} \times \varepsilon)_{\text{total}}$ values of 0.3%, 5.7% and 0.5%, respectively.

Table 2: Event selection criteria in the mono- W/Z and mono- Z' signal regions with merged and resolved event topologies. The symbols “ j ” and “ J ” denote the reconstructed small- R and large- R jets, respectively. The abbreviations HP and LP denote respectively the high- and low-purity signal regions with merged topology, as defined by the cut on the large- R jet substructure variable $D_2^{(\beta=1)}$.

	Merged topology	Resolved topology
General requirements		
E_T^{miss}	$> 250 \text{ GeV}$	$> 150 \text{ GeV}$
Jets, leptons	$\geq 1J, 0\ell$	$\geq 2j, 0\ell$
b -jets	no b -tagged track jets outside of J	≤ 2 b -tagged small- R jets
Multijet suppression	$\Delta\phi(E_T^{\text{miss}}, J \text{ or } jj) > 120^\circ$ $\min_{i \in \{1,2,3\}} [\Delta\phi(E_T^{\text{miss}}, j_i)] > 20^\circ$ $p_T^{\text{miss}} > 30 \text{ GeV} \text{ or } \geq 2 b\text{-jets}$ $\Delta\phi(E_T^{\text{miss}}, p_T^{\text{miss}}) < 90^\circ$	
Signal properties		$p_T^{j_1} > 45 \text{ GeV}$ $\sum p_T^{j_i} > 120 (150) \text{ GeV} \text{ for } 2 (\geq 3) \text{ jets}$

Mono- W/Z signal regions

	0b HP	0b LP	1b HP	1b LP	2b	0b	1b	2b
ΔR_{jj} $D_2^{(\beta=1)}$ p_T^J -dep.	— pass	— fail	— pass	— fail	— —	< 1.4 —	< 1.4 —	< 1.25 —
Mass requirement [GeV]	m_J W/Z tagger requirement			m_J [75, 100]	m_{jj} [65, 105]			m_{jj} [65, 100]

Mono- Z' signal regions

	0b HP	0b LP	1b HP	1b LP	2b	0b	1b	2b
$D_2^{(\beta=1)} < 1.2$	pass	fail	pass	fail	—	—	—	—
For $m_{Z'} < 100 \text{ GeV}$:						For $m_{Z'} < 200 \text{ GeV}$:		
$[0.85m_{Z'}, m_{Z'} + 10]$						$[0.85m_{Z'}, m_{Z'} + 10]$		
For $m_{Z'} \geq 100 \text{ GeV}$:						For $m_{Z'} \geq 200 \text{ GeV}$:		
no merged-topology selection applied						$[0.85m_{Z'}, m_{Z'} + 20]$		

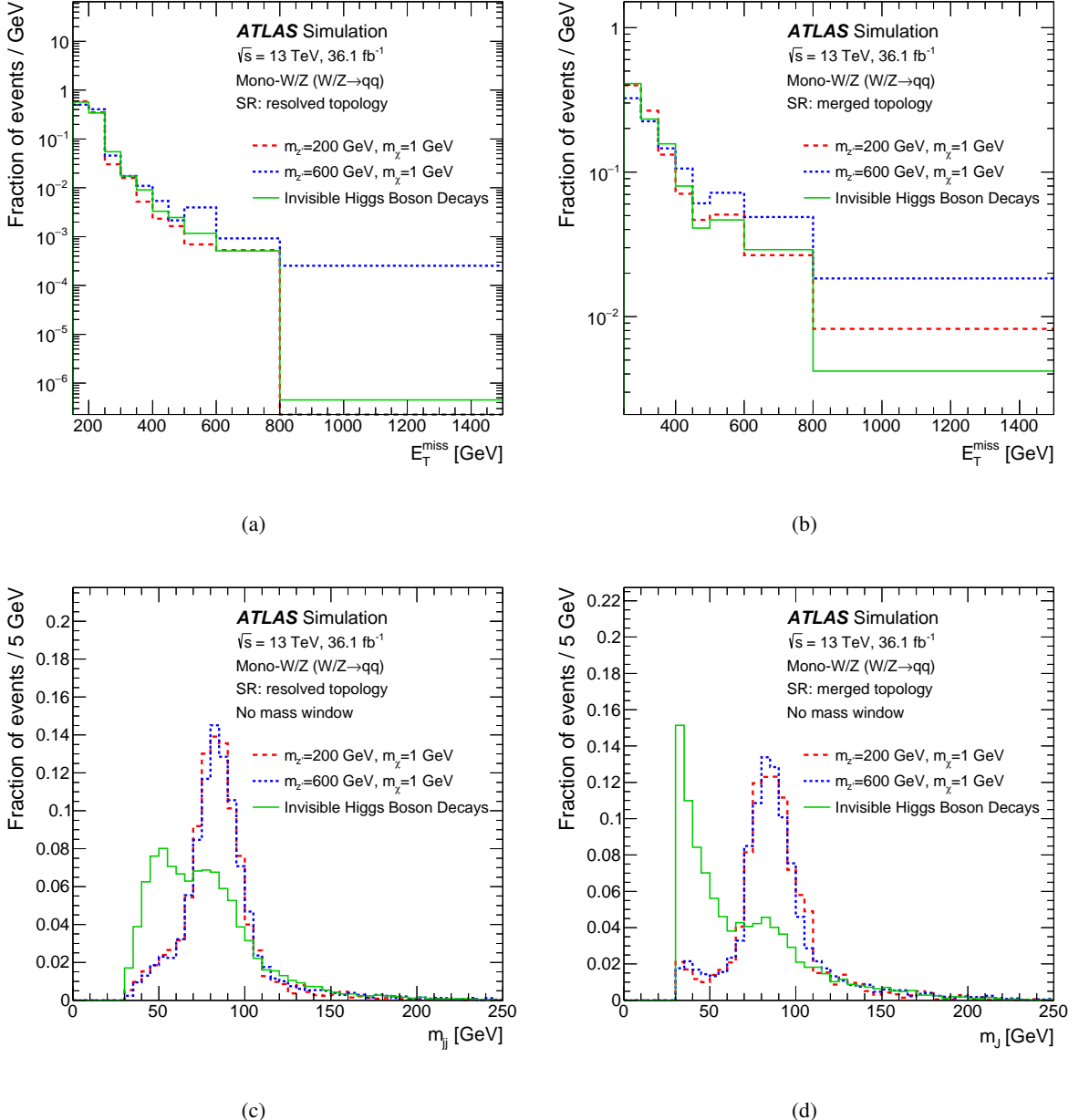


Figure 2: Expected distributions of missing transverse momentum, E_T^{miss} , normalized to unit area, for the simplified vector-mediator model and invisible Higgs boson decays after the full selection in the (a) resolved and (b) merged event topologies, and the expected invariant mass distributions (c) m_{jj} in the resolved and (d) m_J in the merged event topologies, before the mass window requirement. The signal contributions from each resolved (merged) category are summed together. The invisible Higgs boson decays include a large contribution from ggH events, which results in the observed mass distribution.

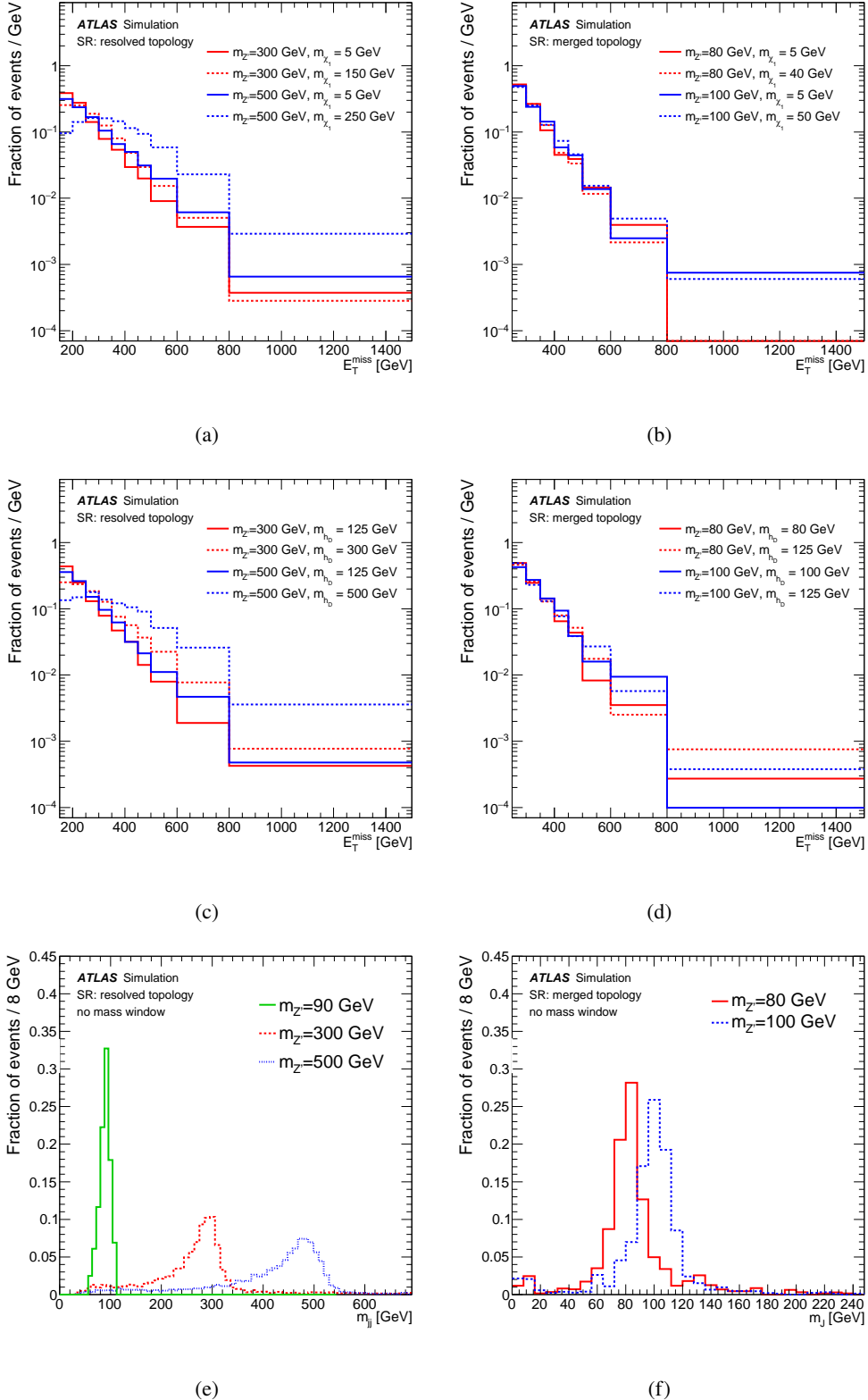


Figure 3: Expected distributions of missing transverse momentum, E_T^{miss} , normalized to unit area, after the full selection for the dark-fermion mono- Z' model in the (a) resolved and (b) merged event topologies, the dark-Higgs mono- Z' model in the (c) resolved and (d) merged event topologies, as well as the expected invariant mass distribution (e) m_{jj} in the resolved and (f) m_j in the merged event topologies for the dark-fermion mono- Z' model in the light dark-sector scenario before the mass window requirement. Similar mass distributions are also observed in the simulation of the other mono- Z' models.

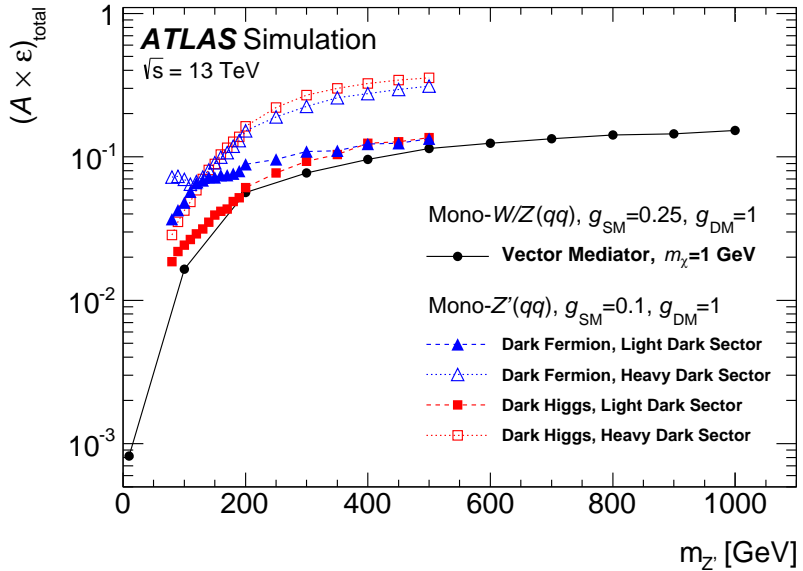


Figure 4: The product of acceptance and efficiency $(\mathcal{A} \times \varepsilon)_{\text{total}}$, defined as the number of signal events satisfying the full set of selection criteria, divided by the total number of generated signal events, for the combined mono- W and mono- Z' signal of the simplified vector-mediator model and for the mono- Z' dark-fermion and dark-Higgs signal models, shown in dependence on the mediator mass $m_{Z'}$. For a given model, the signal contributions from each category are summed together. The lines are drawn to guide the eye.

The number of signal events in a given signal-region category, relative to the total number of signal events selected in all signal categories, depends on the signal model and mediator mass. The largest fraction is expected in the $0b$ category with resolved topology, where it ranges from 40% to 80%. This is followed by the $0b$ -HP and $0b$ -LP merged-topology categories with 10% to 20% of signal events in each of the two. In the mono- Z' signal models, the $1b$ and $2b$ categories with resolved topology contain about 7% to 10% of the total signal contribution. The signal contributions in every other category are below 5%.

7 Background estimation

The dominant background contribution in the signal region originates from $t\bar{t}$ and $V+\text{jets}$ production. In the latter case, the biggest contributions are from decays of Z bosons into neutrinos ($Z \rightarrow \nu\nu$) and $W \rightarrow \tau\nu$, together with $W \rightarrow (e\nu, \mu\nu)$ with non-identified electrons and muons. The normalization of the $t\bar{t}$ and $V+\text{jets}$ background processes and the corresponding shapes of the final E_T^{miss} discriminant are constrained using two dedicated background-enriched data control regions with leptons in the final state. The multijet background contribution is estimated by employing additional multijet-enriched control regions. Events in each control region are selected using criteria similar to, while at the same time disjoint from, those in the signal region. Events are also categorized into merged and resolved topologies, each divided into three categories with different b -tagged jet multiplicities. No requirement is imposed on the large- R jet substructure or ΔR_{jj} and therefore there is no further classification of the merged-topology events into low- and high-purity control regions, as is the case for the signal regions. The remaining small contributions from diboson and single-top-quark production are determined from simulation.

The two control regions with one and two leptons in the final state are defined to constrain the W +jets and Z +jets background respectively, together with the $t\bar{t}$ contribution in the one lepton control region. The latter process is dominant in $2b$ control-region categories. The *one-lepton control region* is defined by requiring no ‘loose’ electrons and exactly one muon with ‘medium’ identification, $p_T > 25$ GeV and satisfying ‘tight’ isolation criteria. Events are collected by E_T^{miss} triggers, as these triggers enhance most efficiently contributions from events with a signal-like topology. The *two-lepton control region* uses events passing a single-lepton trigger. One of the two reconstructed leptons has to be matched to the corresponding trigger lepton. A pair of ‘loose’ muons or electrons with invariant dilepton mass $66 \text{ GeV} < m_{\ell\ell} < 116 \text{ GeV}$ is required in the final state. At least one of the two leptons is required to have $p_T > 25$ GeV and to satisfy the stricter ‘medium’ identification criteria. To emulate the missing transverse momentum from non-reconstructed leptons (neutrinos) in W (Z) boson decays, the $E_T^{\text{miss(no lepton)}}$ and $p_T^{\text{miss(no lepton)}}$ variables are used instead of E_T^{miss} and p_T^{miss} , respectively, for the event selection in the one-lepton and two-lepton control regions. The $E_T^{\text{miss(no lepton)}}$ distribution is employed in the statistical interpretation as the final discriminant in these control regions. The control-region data are also used to confirm the good modelling of other discriminant variables such as the invariant mass of the vector boson candidate and the large- R jet substructure variable $D_2^{(\beta=1)}$ in events with signal-like topology.

The multijet background contribution is estimated separately for each signal region category from a *multipjet control region* selected by inverting the most effective requirement used to discriminate against multijet events in the signal region, i.e. by requiring $\min[\Delta\phi(E_T^{\text{miss}}, j)] \equiv \min[\Delta\phi] < 20^\circ$. The E_T^{miss} distribution observed in this region is used as an expected multijet background shape after a simulation-based subtraction of a small contribution from non-multijet background. To account for the inversion of the $\min[\Delta\phi]$ requirement, the distribution is scaled by the corresponding normalization scale factor. This normalization scale factor is determined in an equivalent control region, but with both the $\min[\Delta\phi]$ and $\Delta\phi(E_T^{\text{miss}}, p_T^{\text{miss}})$ requirements removed and the mass window criterion inverted to select only events in the mass sidebands. In this new control region, the E_T^{miss} distribution from events with $\min[\Delta\phi] < 20^\circ$ is fitted to the data with $\min[\Delta\phi] > 20^\circ$, together with other background contributions, and the resulting normalization factor is applied to the E_T^{miss} distribution from the multipjet control region. For the mono- W/Z search, the high-mass sideband is used, ranging from the upper mass window bound to 250 GeV. Since ΔR_{jj} and $\Delta\phi_{jj}$ criteria are not applied in the mono- Z' search, the event topology in the high-mass sideband is in general not close enough to the topology of the signal region. Therefore, the low-mass sideband is used for the estimate of the multijet contribution in the mono- Z' search. The sideband mass range depends on the mass of the Z' boson: the upper sideband bound is set to the lower bound of the signal region mass window and the size of the sideband is the same as the size of the mass window in the signal region. The multijet contribution is estimated to contribute up to a few percent of the total background yield depending on the signal category. The contribution from the multijet background in the one-lepton and two-lepton control regions is negligible.

For the mono- W/Z searches, all background contributions are additionally constrained by the *mass sideband regions* in the zero-lepton final state. These regions are defined by the same selection criteria as introduced in Section 6, except for the requirements on the large- R jet and dijet mass values, which are required to be above the signal mass window and below 250 GeV. Events in this region are topologically and kinematically very similar to those in the full signal region, with a similar background composition. The corresponding sideband regions are also introduced for the one-lepton and the two-lepton control regions. While there is no signal contamination expected in the one-lepton and two-lepton control regions, the signal contribution in the zero-lepton mass sideband region is not negligible. Compared to the total signal contribution in the signal region described in the previous section, about 20% of additional signal

events are expected in the sidebands in the case of the simplified vector-mediator model. For the invisible Higgs boson decays, the original signal contribution is increased by about 35% after including the sideband region, dominated by the ggH production process. No sideband regions are employed for the mono- Z' searches. Since the hypothesized mass of the Z' boson is a free parameter, the zero-lepton sideband regions cannot be considered free from signal contamination.

The final estimate of background contributions is obtained from a simultaneous fit of the expected final discriminants to data in all signal, sideband and control regions (see Section 9). The signal contributions in the mass sideband regions are taken into account in the fit.

8 Systematic uncertainties

Several experimental and theoretical systematic uncertainties affect the results of the analysis. Their impact is evaluated in each bin of an E_T^{miss} distribution. In this section, the impact of different sources of uncertainty on the expected signal and background yields is summarized, while the overall impact on the final results is discussed in the next section.

Theoretical uncertainties in the signal yield due to variations of the QCD renormalization and factorization scale, uncertainties in the parton distribution functions, and the underlying event and parton shower description, are estimated to be about 10–15% for the simplified vector-mediator model. For the invisible decays of the Higgs boson produced via VH and ggH processes, the theory uncertainties affect the signal yields by 5% and 10% respectively for the resolved event topology and are about two times larger for the merged topology. No systematic uncertainty in the VBF signal is considered, since it has a negligible impact on the final results. No theoretical uncertainty is considered for the mono- Z' signals, since it is negligible compared to the experimental uncertainties.

A number of theoretical modelling systematic uncertainties are considered for the background processes, affecting mostly the expected shape of the E_T^{miss} distribution. These uncertainties are estimated following the studies of Ref. [39] and are briefly summarized here. The uncertainties in the $V+\text{jets}$ background contribution come mainly from limited knowledge of the jet flavour composition in terms of the $V+\text{HF}$ categorization introduced in Section 5, as well as the modelling of the vector boson transverse momentum (p_T^V) and dijet mass (m_{jj}) distributions. The former are evaluated by means of scale variations in the generated **SHERPA** samples. In addition, the difference between the **SHERPA** nominal sample and an alternative **MadGraph5_aMC@NLO v2.2.2** sample produced with a different matrix-element generator is added in quadrature to yield the total uncertainty. The uncertainty in the modelling of the p_T^V and m_{jj} distributions is obtained from the comparison of simulated events with dedicated control-region data, as well as comparisons with alternative generator predictions. For $t\bar{t}$ production, uncertainties in the shapes of the top-quark transverse momentum distribution, and the m_{jj} and p_T^V distributions of the V boson candidate, are considered by comparing the nominal simulated sample to alternative samples with different parton shower, matrix element generation and tuning parameters. A similar procedure is applied for the diboson and single-top-quark backgrounds. While the overall $V+\text{jets}$ and $t\bar{t}$ normalization is determined from the fit to data, the comparison between different generators is also employed to assign a normalization uncertainty to single-top-quark and diboson production since their contributions are estimated from simulation.

An uncertainty of 100% is assigned to the multijet normalization in both the mono- W/Z and mono- Z' searches due to the statistical uncertainty in the control data, the impact of non-multijet background and

the extrapolation from multijet control regions to signal regions. The shapes of the multijet background distributions are subject to an uncertainty of the order of 10%, depending on the amount of non-multijet background in each signal region.

In both the mono- W/Z and mono- Z' searches, the largest source of experimental systematic uncertainty in the merged topology is the modelling of the large- R jet properties. The large- R jet mass scale and resolution uncertainty [72, 73, 83] has an impact of up to 5% on the expected background yields, and up to 5%, 10% and 15% on the signal yields from invisible Higgs boson decays, the simplified vector-mediator model and mono- Z' models respectively. The uncertainty in the large- R jet energy resolution affects the simplified vector-mediator signal by 3% and background by 1%. The impact on the mono- Z' signal and the signal from invisible Higgs boson decays is at the sub-percent level. The uncertainty in the scale of the $D_2^{(\beta=1)}$ substructure parameter affects the migration between the high-purity and low-purity regions, with a 5–10% (2–5%) impact on the background (mono- W/Z and mono- Z' signal) yields. The combined impact of all other large- R jet uncertainties is below a few percent. The combined impact of large- R jet uncertainties on events within the resolved-topology categories is negligible for the mono- W/Z search and below 2% for the mono- Z' searches. The small- R jet uncertainties are dominated by the energy scale and resolution uncertainties. The small- R jet energy scale uncertainty has an up to 10% (up to 6%) impact on the background (signal) yields. The uncertainty in the small- R jet energy resolution has a 2–5% impact on the signal yields. The corresponding impact of this uncertainty on the background yield is at a sub-percent level in the mass window around the W - and Z -boson mass, growing to around 1.5% for the mono- Z' search in the mass window around $m_{Z'} = 500$ GeV. The b -tagging calibration uncertainty affects the migration of signal and background events between categories with different b -tag multiplicities by up to 10%. The uncertainty in the missing transverse momentum component which is not associated with any of the selected objects with high transverse momentum affects the background (signal) yields by about 1–3% (2–10%). The uncertainties in the trigger efficiency, lepton reconstruction and identification efficiency, as well as the lepton energy scale and resolution, affect the signal and background contributions only at a sub-percent level.

The uncertainty in the combined 2015+2016 integrated luminosity is 2.1%. It is derived, following a methodology similar to that detailed in Ref. [84], from a calibration of the luminosity scale using x – y beam-separation scans performed in August 2015 and May 2016.

9 Results

9.1 Statistical interpretation

A profile likelihood fit [85] is used in the interpretation of the data to search for dark matter production. The likelihood function used to fit the data is defined as the product of conditional probabilities P over binned distributions of discriminating observables in each event category j ,

$$\mathcal{L}(\mu, \boldsymbol{\theta}) = \prod_j^{N_{\text{categories}}} \prod_i^{N_{\text{bins}}} P(N_{ij} | \mu S_{ij}(\boldsymbol{\theta}) + B_{ij}(\boldsymbol{\theta})) \prod_k^{N_{\text{nuisance}}} \mathcal{G}(\theta_k).$$

The likelihood function depends on the signal strength μ , defined as the signal yield relative to the prediction from simulation, and on the vector of nuisance parameters $\boldsymbol{\theta}$ accounting for the background normalization and systematic uncertainties introduced in Section 8. The Poisson distributions P correspond to the

observation of N_{ij} events in each bin i of the discriminating observable given the expectations for the background, $B_{ij}(\theta)$, and for the signal, $S_{ij}(\theta)$. A constraint on a nuisance parameter θ_k is represented by the Gaussian function $\mathcal{G}(\theta_k)$. The correlations between nuisance parameters across signal and background processes and categories are taken into account.

For the mono- W/Z search, the event categories include all eight zero-lepton signal regions (see Section 6), six one-lepton and six two-lepton control regions, as well as the corresponding sideband regions for each of these twenty categories (see Section 7). In comparison, no sideband regions are employed for the mono- Z' search and only categories with the resolved topology are considered for $m_{Z'} > 100$ GeV. In the zero-lepton signal and sideband regions, the E_T^{miss} distribution is used as the discriminating variable since the signal process results in relatively large E_T^{miss} values compared to the backgrounds. In order to constrain the backgrounds and the E_T^{miss} shape in the signal region, the $E_T^{\text{miss(no lepton)}}$ variables are used in the fit in the one- and two-lepton control regions. The normalizations of the $W+\text{HF}$, $W+\text{LF}$, $Z+\text{HF}$, $Z+\text{LF}$ and $t\bar{t}$ background components are treated as unconstrained parameters in the fit, independent from each other and correlated across all event categories. The uncertainties in the flavour composition of the $V+\text{HF}$ processes are taken into account following the studies outlined in Section 8. The normalization of other background components is constrained according to their theory uncertainty. A possible difference between the normalization factors in events with resolved and merged topologies for the $W+\text{jets}$, $Z+\text{jets}$ and $t\bar{t}$ processes due to systematic modelling effects is taken into account by means of two additional constrained nuisance parameters. The multijet contribution is only considered in the signal regions and the corresponding mass sidebands, with uncorrelated normalization factors in each category.

9.2 Measurement results

The normalization of the $W+\text{HF}$, $W+\text{LF}$ and $Z+\text{LF}$ background components obtained from a fit to the data under the background-only hypothesis is in a good agreement with the SM expectation, while the $Z+\text{HF}$ ($t\bar{t}$) normalization is 30% higher (20% lower) than the expected SM value. In addition to the normalization factors, the final background event yields in each event category are also affected by the systematic uncertainties discussed in Section 8. For all backgrounds other than $Z+\text{HF}$ and $t\bar{t}$, the number of background events obtained from the fit agrees well with the prediction from simulation in each event category individually. The observed number of events passing the final mono- W/Z signal selection is shown for each event category in Table 3 together with the expected background contributions obtained from the fit under the background-only hypothesis. The expectations for several signal points within the simplified vector-mediator model and for the invisible Higgs boson decays are shown in addition for comparison. Figures 5 and 6 show the corresponding distributions of the missing transverse momentum in the merged and resolved mono- W/Z signal regions, respectively. The background contributions which are illustrated here are obtained from a simultaneous fit of the expected final discriminants to data with a background-only hypothesis in all signal, sideband and control regions. In this scenario the signal regions lead to a strong constraint of the total background estimate, which is relaxed with a floating signal contribution in the final fit.

Similarly, the observed and expected numbers of events passing the final mono- Z' selection are shown in Tables 4 and 5 for mediator masses $m_{Z'}$ of 90 GeV and 350 GeV respectively. The expected and observed numbers of background events for the $m_{Z'}$ hypothesis of 90 GeV are similar to those from the mono- W/Z search in all categories, except for the $2b$ -tag category with resolved topology. There are about three times more events in that category for the mono- Z' search since no requirement on ΔR_{jj} is applied, as opposed to the strict requirement of $\Delta R_{jj} < 1.25$ employed in the mono- W/Z search. The distributions

Table 3: The expected and observed numbers of events for an integrated luminosity of 36.1 fb^{-1} and $\sqrt{s} = 13 \text{ TeV}$, shown separately in each mono- W/Z signal region category. The background yields and uncertainties are shown after the profile likelihood fit to the data (with $\mu = 0$). The quoted background uncertainties include both the statistical and systematic contributions, while the uncertainty in the signal is statistical only. The uncertainties in the total background can be smaller than those in individual components due to anti-correlations of nuisance parameters.

Process	Merged topology				
	0b-HP	0b-LP	1b-HP	1b-LP	2b
Vector-mediator model,					
$m_\chi = 1 \text{ GeV}, m_{Z'} = 200 \text{ GeV}$	814 ± 48	759 ± 45	96 ± 18	99 ± 16	49.5 ± 4.3
$m_\chi = 1 \text{ GeV}, m_{Z'} = 600 \text{ GeV}$	280.9 ± 9.0	268.5 ± 8.8	34.7 ± 3.6	33.8 ± 3.1	15.38 ± 0.84
Invisible Higgs boson decays ($m_H = 125 \text{ GeV}, \mathcal{B}_{H \rightarrow \text{inv.}} = 100\%$)					
VH	408.4 ± 2.1	299.3 ± 2.0	52.06 ± 0.85	44.06 ± 0.82	27.35 ± 0.52
ggH	184 ± 19	837 ± 35	11.7 ± 3.8	111 ± 30	12.3 ± 4.2
VBF	29.1 ± 2.5	96.0 ± 4.6	2.43 ± 0.36	5.83 ± 0.43	0.50 ± 0.07
$W+\text{jets}$	3170 ± 140	10120 ± 380	218 ± 28	890 ± 110	91 ± 12
$Z+\text{jets}$	4750 ± 200	15590 ± 590	475 ± 52	1640 ± 180	186 ± 12
$t\bar{t}$	775 ± 48	937 ± 60	629 ± 27	702 ± 34	50 ± 11
Single top-quark	159 ± 12	197 ± 13	89.7 ± 6.7	125.5 ± 8.7	16.1 ± 1.7
Diboson	770 ± 110	960 ± 140	88 ± 14	115 ± 18	54 ± 10
Multijet	12 ± 35	49 ± 140	3.7 ± 3.3	15 ± 13	9.3 ± 9.4
Total background	9642 ± 87	27850 ± 150	1502 ± 31	3490 ± 52	407 ± 15
Data	9627	27856	1502	3525	414
Resolved topology					
Process	0b		1b		2b
Vector-mediator model,					
$m_\chi = 1 \text{ GeV}, m_{Z'} = 200 \text{ GeV}$	5050 ± 130		342 ± 29		136.7 ± 6.0
$m_\chi = 1 \text{ GeV}, m_{Z'} = 600 \text{ GeV}$	840 ± 16		59.9 ± 4.6		27.86 ± 0.94
Invisible Higgs boson decays ($m_H = 125 \text{ GeV}, \mathcal{B}_{H \rightarrow \text{inv.}} = 100\%$)					
VH	2129.6 ± 6.4		171.7 ± 2.2		104.7 ± 1.2
ggH	4111 ± 78		178 ± 16		37 ± 11
VBF	514 ± 12		19.8 ± 2.3		2.33 ± 0.72
$W+\text{jets}$	117500 ± 4600		5000 ± 680		598 ± 98
$Z+\text{jets}$	135400 ± 5600		7710 ± 780		1219 ± 67
$t\bar{t}$	13800 ± 780		12070 ± 420		2046 ± 70
Single top-quark	2360 ± 140		1148 ± 71		222 ± 14
Diboson	6880 ± 950		514 ± 71		228 ± 34
Multijet	11900 ± 2300		1130 ± 370		290 ± 150
Total background	287770 ± 570		27580 ± 170		4601 ± 90
Data	287722		27586		4642

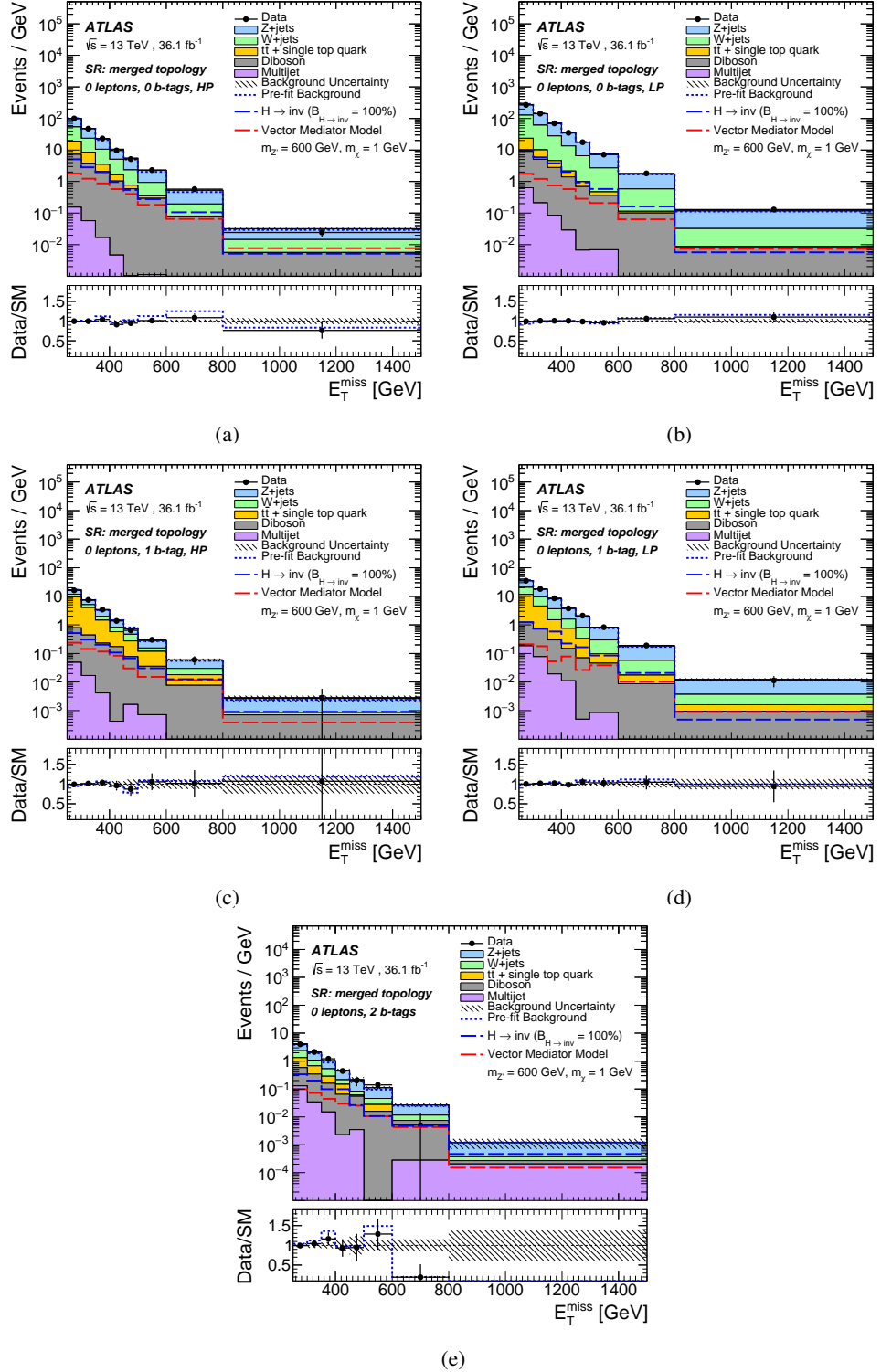


Figure 5: The observed (dots) and expected (histograms) distributions of missing transverse momentum, E_T^{miss} , obtained with 36.1 fb^{-1} of data at $\sqrt{s} = 13 \text{ TeV}$ in the mono- W/Z signal region with the merged event topology after the profile likelihood fit (with $\mu = 0$), shown separately for the (a) $0b$ -HP, (b) $0b$ -LP, (c) $1b$ -HP, (d) $1b$ -LP, and (e) $2b$ -tag event categories. The total background contribution before the fit to data is shown as a dotted blue line. The hatched area represents the total background uncertainty. The signal expectations for the simplified vector-mediator model with $m_\chi = 1 \text{ GeV}$ and $m_{Z'} = 600 \text{ GeV}$ (dashed red line) and for the invisible Higgs boson decays (dashed blue line) are shown for comparison. The inset at the bottom of each plot shows the ratio of the data to the total post-fit (dots) and pre-fit (dotted blue line) background expectation.

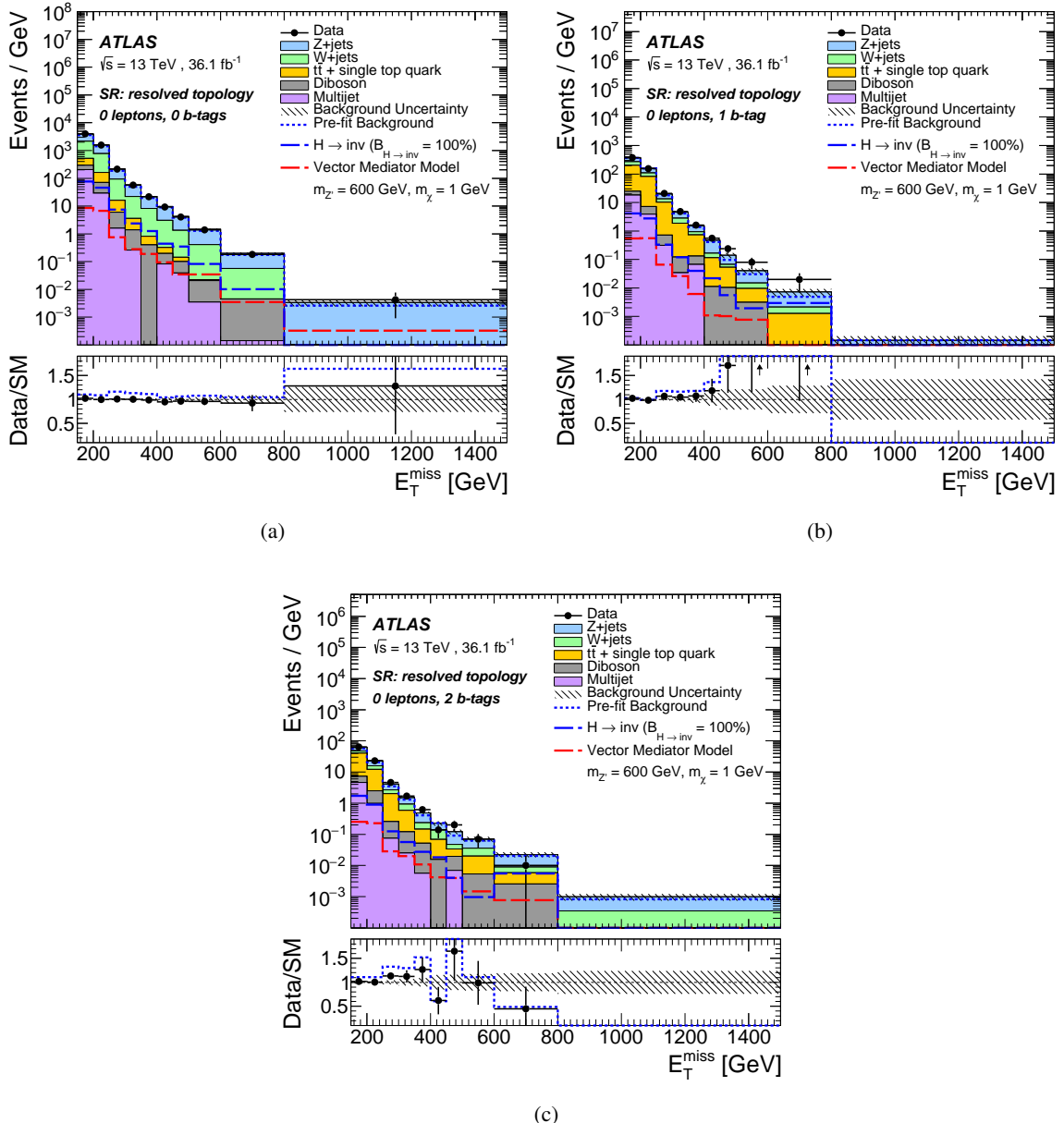


Figure 6: The observed (dots) and expected (histograms) distributions of missing transverse momentum, E_T^{miss} , obtained with 36.1 fb^{-1} of data at $\sqrt{s} = 13 \text{ TeV}$ in the mono- W/Z signal region with the resolved event topology after the profile likelihood fit (with $\mu = 0$), shown separately for the (a) $0b$ -, (b) $1b$ - and (c) $2b$ -tag categories. The total background contribution before the fit to data is shown as a dotted blue line. The hatched area represents the total background uncertainty. The signal expectations for the simplified vector-mediator model with $m_\chi = 1 \text{ GeV}$ and $m_{Z'} = 600 \text{ GeV}$ (dashed red line) and for the invisible Higgs boson decays (dashed blue line) are shown for comparison. The inset at the bottom of each plot shows the ratio of the data to the total post-fit (dots) and pre-fit (dotted blue line) background expectation.

Table 4: The expected and observed numbers of events for an integrated luminosity of 36.1 fb^{-1} and $\sqrt{s} = 13 \text{ TeV}$, shown separately in each mono- Z' signal region category assuming $m_{Z'} = 90 \text{ GeV}$. The background yields and uncertainties are shown after the profile likelihood fit to the data (with $\mu = 0$). The quoted background uncertainties include both the statistical and systematic contributions, while the uncertainty in the signal is statistical only. The uncertainties in the total background can be smaller than those in individual components due to anti-correlations of nuisance parameters.

Process	Merged topology				
	0b-HP	0b-LP	1b-HP	1b-LP	2b
Dark fermion, light sector	286 ± 54	125 ± 36	53 ± 23	26 ± 16	52 ± 23
Dark fermion, heavy sector	165 ± 18	71 ± 12	30.9 ± 7.7	18.6 ± 6.0	36.3 ± 8.4
Dark Higgs, light sector	253 ± 25	82 ± 14	37.7 ± 9.6	19.1 ± 6.9	45 ± 11
Dark Higgs, heavy sector	224 ± 14	75.9 ± 8.4	37.5 ± 5.9	21.2 ± 4.4	49.5 ± 6.8
$W + \text{jets}$	2960 ± 170	5180 ± 280	342 ± 52	680 ± 100	120 ± 120
$Z + \text{jets}$	4720 ± 190	7990 ± 310	628 ± 69	1280 ± 140	265 ± 22
$t\bar{t}$	780 ± 110	440 ± 59	646 ± 59	434 ± 49	59 ± 19
Single top-quark	161 ± 15	113 ± 14	93 ± 10	94.1 ± 8.9	17.8 ± 2.8
Diboson	830 ± 130	575 ± 95	129 ± 23	107 ± 18	61 ± 11
Multijet	48 ± 41	21 ± 66	1.2 ± 1.0	5.4 ± 5.1	0.52 ± 0.51
Total background	9498 ± 96	14310 ± 120	1840 ± 37	2600 ± 46	523 ± 19
Data	9516	14282	1845	2628	534

Process	Resolved topology		
	0b	1b	2b
Dark fermion, light sector	2060 ± 150	264 ± 52	228 ± 55
Dark fermion, heavy sector	976 ± 44	121 ± 15	164 ± 18
Dark Higgs, light sector	1206 ± 54	135 ± 18	197 ± 22
Dark Higgs, heavy sector	953 ± 30	112 ± 10	146 ± 12
$W + \text{jets}$	78400 ± 3400	4400 ± 690	1030 ± 190
$Z + \text{jets}$	91700 ± 3800	6970 ± 690	2140 ± 210
$t\bar{t}$	11170 ± 920	10590 ± 530	7760 ± 230
Single top-quark	1200 ± 170	1006 ± 74	602 ± 40
Diboson	6080 ± 930	514 ± 80	337 ± 55
Multijet	14700 ± 2500	1280 ± 540	540 ± 270
Total background	203990 ± 480	24770 ± 220	12400 ± 110
Data	203991	24783	12406

of the missing transverse momentum in each mono- Z' signal region for these mediator masses are shown in Figures 7 and 8.

The impact of the different sources of systematic uncertainty on the sensitivity of the mono- W/Z and mono- Z' searches is estimated by means of fits of the signal-plus-background model to hypothetical data comprised of these signals (with signal strength $\mu = 1$) plus expected background contributions. The resulting uncertainties on the signal strength μ serve as a measure of the analysis sensitivity and are summarized in Table 6. Tests of the background-only versus the signal-plus-background hypothesis using a profile likelihood test statistic show no significant deviation from the SM background expectation for any of the signal mass points, in both the mono- W/Z and mono- Z' searches. A modified frequentist method with the CL_s formalism [86] is used to set upper limits on the signal strength μ at 95% confidence level for all signal models.

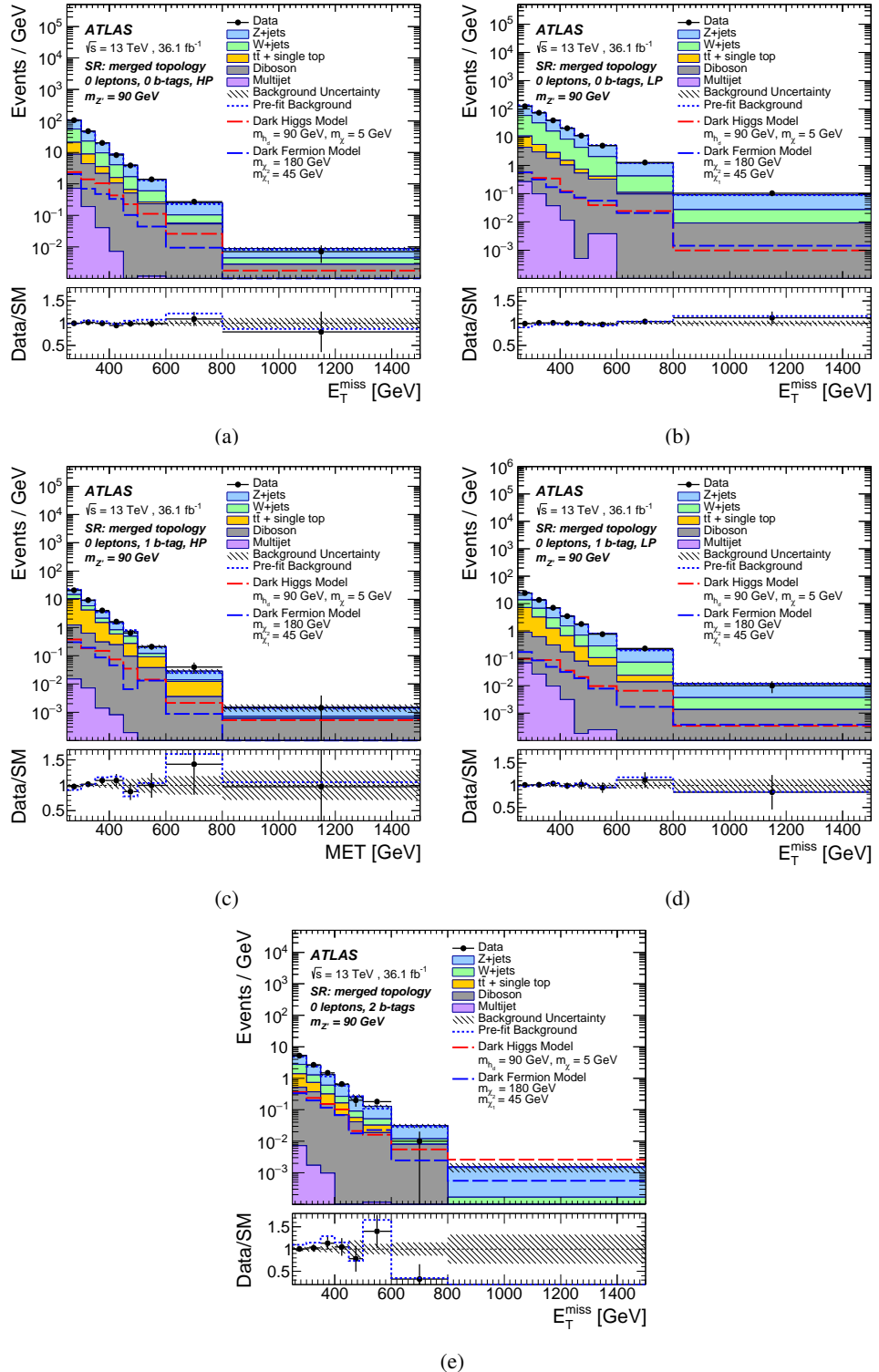


Figure 7: The observed (dots) and expected (histograms) distributions of missing transverse momentum, E_T^{miss} , obtained with 36.1 fb^{-1} of data at $\sqrt{s} = 13 \text{ TeV}$ in the mono- Z' signal region with $m_{Z'} = 90 \text{ GeV}$ and the merged event topology after the profile likelihood fit (with $\mu = 0$), shown separately for the (a) 0b-HP, (b) 0b-LP, (c) 1b-HP, (d) 1b-LP, and (e) 2b-tag event categories. The total background contribution before the fit to data is shown as a dotted blue line. The hatched area represents the total background uncertainty. The expectations for the selected dark-Higgs (dashed red line) and dark-fermion (dashed blue line) signal points are shown for comparison. The inset at the bottom of each plot shows the ratio of the data to the total post-fit (dots) and pre-fit (dotted blue line) background expectation.

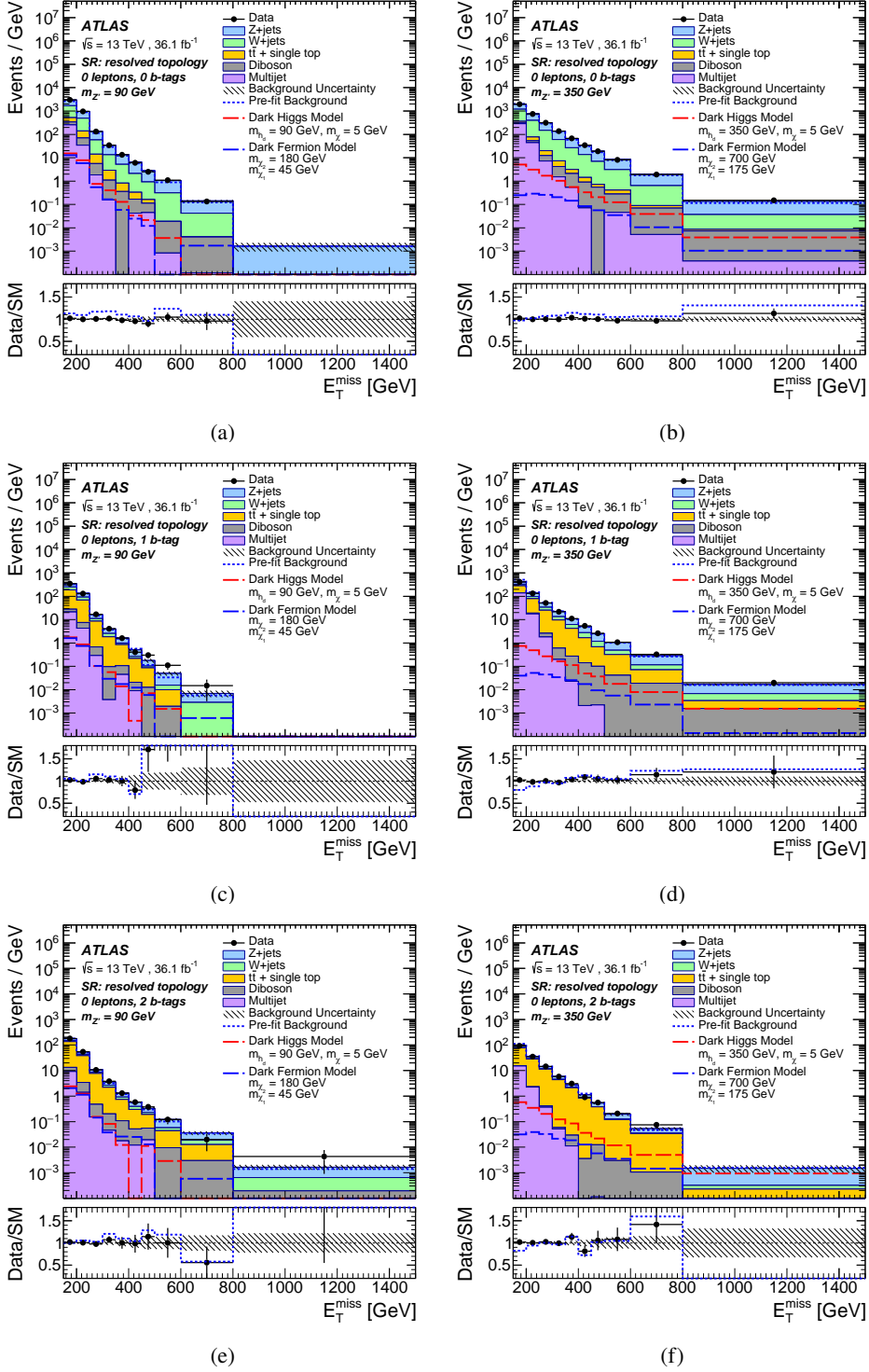


Figure 8: The observed (dots) and expected (histograms) distribution of missing transverse momentum, E_T^{miss} , obtained with 36.1 fb^{-1} of data at $\sqrt{s} = 13 \text{ TeV}$ in the mono-Z' signal region with the resolved event topology after the profile likelihood fit (with $\mu = 0$), shown separately for the (a,b) 0b, (c,d) 1b and (e,f) 2b-tag event categories. On the left-hand side, the mediator mass of 90 GeV and on the right-hand side of 350 GeV is assumed. The total background contribution before the fit to data is shown as a dotted blue line. The hatched area represents the total background uncertainty. The expectations for the selected dark-Higgs (dashed red line) and dark-fermion (dashed blue line) signal points are shown for comparison. The inset at the bottom of each plot shows the ratio of the data to the total post-fit (dots) and pre-fit (dotted blue line) background expectation.

Table 5: The expected and observed numbers of events for an integrated luminosity of 36.1 fb^{-1} and $\sqrt{s} = 13 \text{ TeV}$, shown separately in each mono- Z' signal region category assuming $m_{Z'} = 350 \text{ GeV}$. The background yields and uncertainties are shown after the profile likelihood fit to the data (with $\mu = 0$). The quoted background uncertainties include both the statistical and systematic contributions, while the uncertainty in the signal is statistical only. The uncertainties in the total background can be smaller than those in individual components due to anti-correlations of nuisance parameters.

Process	Resolved topology		
	0b	1b	2b
Dark fermion, light sector	655 ± 14	104.2 ± 5.8	89.5 ± 5.3
Dark fermion, heavy sector	70.79 ± 0.79	12.45 ± 0.33	9.04 ± 0.28
Dark Higgs, light sector	639 ± 13	96.7 ± 4.9	72.3 ± 4.3
Dark Higgs, heavy sector	118.9 ± 1.4	19.62 ± 0.58	14.24 ± 0.50
$W + \text{jets}$	68300 ± 4300	4270 ± 1100	115 ± 84
$Z + \text{jets}$	72200 ± 3000	7230 ± 800	1160 ± 110
$t\bar{t}$	3900 ± 460	10320 ± 720	4920 ± 140
Single top-quark	752 ± 69	1530 ± 110	466 ± 35
Diboson	2000 ± 340	282 ± 47	14.6 ± 2.8
Multijet	17100 ± 2300	7870 ± 390	880 ± 140
Total background	164310 ± 650	31520 ± 250	7567 ± 85
Data	164386	31465	7597

9.3 Constraints on invisible Higgs boson decays

In the search for invisible Higgs boson decays, an observed (expected) upper limit of 0.83 ($0.58^{+0.23}_{-0.16}$) is obtained at 95% CL on the branching ratio $\mathcal{B}_{H \rightarrow \text{inv.}}$, assuming the SM production cross sections and combining the contributions from VH , ggH and VBF production modes. The expected limit is a factor of about 1.5 better (while the observed is slightly worse) than the one reached by the previous analysis of Run 1 ATLAS data [6].

9.4 Constraints on the simplified vector-mediator model

In the context of the mono- W/Z simplified vector-mediator signal model, the exclusion limits on the signal strength are shown in Figure 9(a) and translated into limits on the dark matter and mediator masses (Figure 9(b)) for Dirac DM particles and couplings $g_{\text{SM}} = 0.25$ and $g_{\text{DM}} = 1$. Since only a limited number of signal points were simulated, an interpolation procedure is employed to obtain the limits on the signal strength at other mass points in the $(m_\chi, m_{Z'})$ parameter plane. All signal processes with the same mediator mass $m_{Z'}$ and different m_χ values are assumed to have the same $(\mathcal{A} \times \varepsilon)_{\text{total}}$ value as in the simulated sample with $m_\chi = 1 \text{ GeV}$. This was verified to be a reliable approximation for $m_{Z'} > 2m_\chi$. Thus, the expected signal yield at a given mass point $(m_{Z'}, m_\chi)$ only depends on the cross section $\sigma_{pp \rightarrow Z' \rightarrow \chi\chi}^{(m_{Z'}, m_\chi)}$ at that mass point. Under the narrow width approximation, this cross section can be expressed in terms of the cross section $\sigma_{pp \rightarrow Z' \rightarrow \chi\chi}^{(m_{Z'}, m_\chi=1 \text{ GeV})}$ and the branching ratio $\mathcal{B}_{Z' \rightarrow \chi\chi}^{m_\chi=1 \text{ GeV}}$ at the simulated mass point with

Table 6: Breakdown of expected signal strength uncertainties for several mono- W/Z and mono- Z' signal models, obtained for an integrated luminosity of 36.1 fb^{-1} and $\sqrt{s} = 13 \text{ TeV}$. A dark matter mass of 1 GeV is used for the two vector-mediator signals. Each systematic uncertainty contribution is determined from the quadratic difference between the total uncertainty and the uncertainty obtained by neglecting the systematic uncertainty source in question. Only the largest systematic uncertainties are shown.

Source of uncertainty	Uncertainty on $\mu = 1$ [%]				
	Vector mediator, $m_{Z'} =$		$H \rightarrow \text{invisible}$	Dark fermion, $m_{Z'} =$	
	200 GeV	600 GeV	($\mathcal{B}_{H \rightarrow \text{inv.}} = 100\%$)	90 GeV	350 GeV
Large- R jets	9	20	17	23	–
Small- R jets	3	8	7	13	7
Electrons	4	9	6	7	6
Muons	6	7	7	15	11
E_T^{miss}	1	4	3	4	3
b -tagging (track jets)	4	4	4	8	–
b -tagging (small- R jets)	2	4	2	5	5
Luminosity	3	4	3	4	4
Multijet normalization	7	11	11	13	6
Diboson normalization	5	11	6	3	1
$Z + \text{jets}$ normalization	5	9	4	15	9
$W + \text{jets}$ normalization	3	4	2	8	6
$t\bar{t}$ normalization	3	1	0.3	8	5
Signal modelling	7	9	20	–	–
$V + \text{jets}$ modelling	4	10	4	7	11
$t\bar{t}$ modelling	2	4	3	10	6
$V + \text{jets}$ flavour composition	1	3	3	4	2
Diboson modelling	1	2	2	1	0.2
Background MC stat.	10	18	14	20	12
Total syst.	21	40	38	45	29
Data stat.	7	21	5	14	12
Total	22	45	39	47	32

$m_\chi = 1$ GeV,

$$\sigma_{pp \rightarrow Z' \rightarrow \chi\chi}^{(m_{Z'}, m_\chi)} = \sigma_{pp \rightarrow Z' \rightarrow \chi\chi}^{(m_{Z'}, m_\chi = 1 \text{ GeV})} \cdot \frac{\mathcal{B}_{Z' \rightarrow \chi\chi}^{m_\chi}}{\mathcal{B}_{Z' \rightarrow \chi\chi}^{m_\chi = 1 \text{ GeV}}},$$

where the value of the branching ratio $\mathcal{B}_{Z' \rightarrow \chi\chi}^{m_\chi}$ is fully defined by the values of model parameters g_{DM} , g_{SM} , m_χ and $m_{Z'}$. For the given coupling choices, vector-mediator masses $m_{Z'}$ of up to 650 GeV are excluded at 95% CL for dark matter masses m_χ of up to 250 GeV, agreeing well with the expected exclusion of Z' masses of up to 700 GeV for m_χ of up to 230 GeV. The expected limits are improved by 15–30%, depending on the DM mass, compared to the analysis presented in Ref. [1].

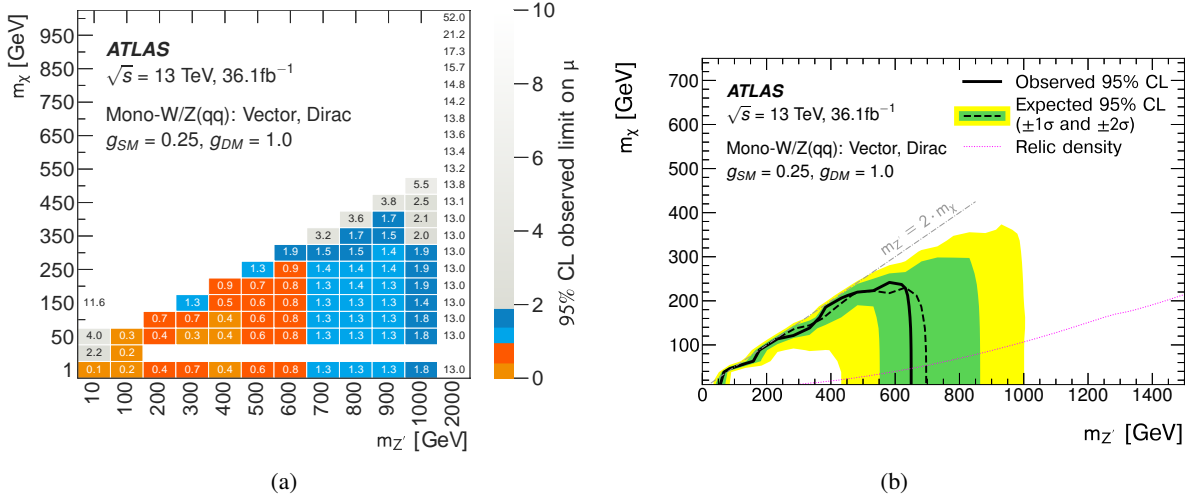


Figure 9: (a) Observed upper limits on the signal strength μ at 95% CL in the grid of the DM and mediator particle masses, $(m_\chi, m_{Z'})$, for the combined mono- W and mono- Z search in the simplified vector-mediator model with Dirac DM particles and couplings $g_{SM} = 0.25$ and $g_{DM} = 1$. There are no interpolated points and thus no limit values listed for the mass point $(m_\chi = 100 \text{ GeV}, m_{Z'} = 10 \text{ GeV})$ and in the parameter region $(m_\chi = 10 \text{ GeV}, m_{Z'} = 200\text{--}2000 \text{ GeV})$. (b) The corresponding exclusion contours at 95% CL. The black solid (dashed) curve shows the observed (expected) limit. The dotted magenta curve corresponds to the set of points for which the expected relic density is consistent with the WMAP [87] and Planck [88] measurements ($\Omega h^2 = 0.12$), as computed with MadDM [89]. The region below the curve corresponds to higher predicted relic abundance than these measurements.

9.5 Mono- W/Z constraints with reduced model dependence

In addition to the interpretation of the mono- W/Z search in terms of the simplified vector-mediator model and invisible Higgs boson decays, the analysis results are also expressed in terms of generic CLs upper limits at 95% CL on the allowed visible cross section σ_{vis} of potential $W + \text{DM}$ or $Z + \text{DM}$ production. The limits on these two processes are evaluated separately to allow more flexibility in terms of possible reinterpretations, as new models might prefer one of these two final states. While the event selection and categorization is the same as described in Section 6, i.e. including the b -tagging and mass window requirements, the exclusion limits are provided in the fiducial region that is defined by applying all signal region selection criteria except for the requirements on m_{jj} or m_J and the b -tagging multiplicity. With this definition, the exclusion limits on σ_{vis} apply to any processes which are characterized by a generic

back-to-back topology with a W/Z boson recoiling against E_T^{miss} from weakly interacting particles such as DM. The limits on σ_{vis} are given as a function of the E_T^{miss} variable in order to avoid any additional model-dependent assumptions on the E_T^{miss} distribution. Hence, the E_T^{miss} bins in the zero-lepton region are treated independently of each other in the statistical interpretation of the data. A reduced number of bins is used for $E_T^{\text{miss}} > 300$ GeV to reduce the statistical uncertainty in the per-bin analysis. In all other aspects, the approach is identical to the mono- W/Z analysis described above. The mono- W/Z vector-mediator signal samples are used as a benchmark model to estimate the residual dependence of the σ_{vis} limits on the kinematic properties of events within a given E_T^{miss} range and on the b -tagging multiplicity. For this, a wide range of (m_Z', m_χ) model parameters that yield a sizeable contribution of at least 500 simulated events in a given E_T^{miss} range is considered. Corresponding variations of 15–50% (25–50%) in the expected limits on $\sigma_{\text{vis}, W+\text{DM}}$ ($\sigma_{\text{vis}, Z+\text{DM}}$) are found. The weakest σ_{vis} limit is quoted in a given range of reconstructed E_T^{miss} in order to minimize the dependence on a benchmark model. The observed and expected limits on σ_{vis} in each E_T^{miss} range are shown in Figure 10, with the numerical values summarized in Tables 7 and 8. As a general trend, the limits on $Z + \text{DM}$ production are somewhat stronger than those on $W + \text{DM}$ since the former contributes significantly to the $2b$ category that has the highest sensitivity due to having the lowest SM background.

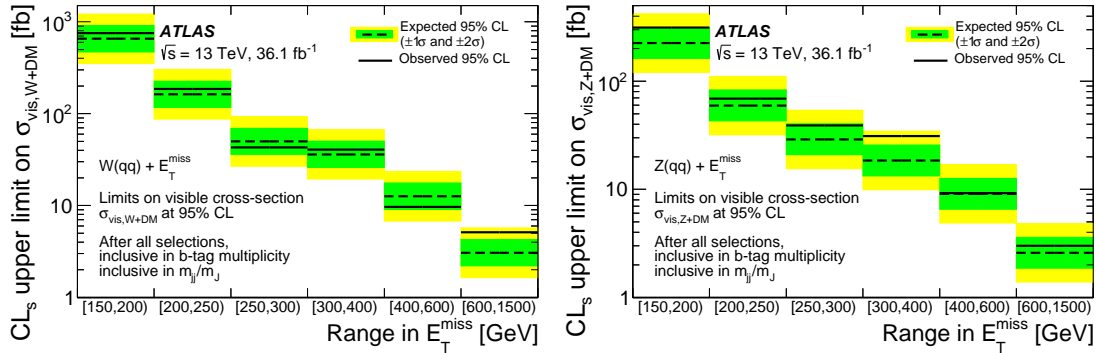


Figure 10: Upper limits at 95% CL on the visible cross section $\sigma_{\text{vis}, W+\text{DM}}$ (left) and $\sigma_{\text{vis}, Z+\text{DM}}$ (right) in the six E_T^{miss} regions, after all selection requirements, but inclusive in the b -tag multiplicity and the W/Z candidate mass m_{jj}/m_j . The observed limits (solid line) are consistent with the expectations under the SM-only hypothesis (dashed line) within uncertainties (filled bands).

Table 7: The observed and expected exclusion limit at 95% CL on σ_{vis} for $W + \text{DM}$ production for an integrated luminosity of 36.1 fb^{-1} and $\sqrt{s} = 13 \text{ TeV}$, together with the corresponding product of acceptance and efficiency ($A \times \varepsilon$) for different regions of E_T^{miss} .

E_T^{miss} range [GeV]	Upper limit at 95% CL [fb]				$A \times \varepsilon$
	$\sigma_{\text{vis}}^{\text{obs}}$	$\sigma_{\text{vis}}^{\text{exp}}$	-1σ	$+1\sigma$	
$W+\text{DM}, W \rightarrow q'q$					
[150, 200]	750	650	470	910	20%
[200, 250]	185	163	117	226	20%
[250, 300]	43	50	36	69	30%
[300, 400]	41	36	26	50	45%
[400, 600]	9.7	12.6	9.1	17.6	55%
[600, 1500]	5.1	3.1	2.2	4.3	55%

Table 8: The observed and expected exclusion limit at 95% CL on σ_{vis} for $Z + \text{DM}$ production for an integrated luminosity of 36.1 fb^{-1} and $\sqrt{s} = 13 \text{ TeV}$, together with the corresponding product of acceptance and efficiency ($A \times \varepsilon$) for different regions of E_T^{miss} .

E_T^{miss} range [GeV]	Upper limit at 95% CL [fb]				$A \times \varepsilon$
	$\sigma_{\text{vis}}^{\text{obs}}$	$\sigma_{\text{vis}}^{\text{exp}}$	-1σ	$+1\sigma$	
$Z + \text{DM}, Z \rightarrow q\bar{q}$					
[150, 200]	313	225	162	314	20%
[200, 250]	69	60	43	83	20%
[250, 300]	39	29	21	40	30%
[300, 400]	31.1	18.5	13.3	25.7	45%
[400, 600]	9.2	9.1	6.5	12.6	50%
[600, 1500]	3.0	2.6	1.9	3.6	55%

The observable σ_{vis} can be interpreted as

$$\begin{aligned}\sigma_{\text{vis}, W+\text{DM}}(E_T^{\text{miss}}) &\equiv \sigma_{W+\text{DM}}(E_T^{\text{miss}}) \times \mathcal{B}_{W \rightarrow q'q} \times (A \times \varepsilon)(E_T^{\text{miss}}) \quad \text{for } W + \text{DM} \text{ events,} \\ \sigma_{\text{vis}, Z+\text{DM}}(E_T^{\text{miss}}) &\equiv \sigma_{Z+\text{DM}}(E_T^{\text{miss}}) \times \mathcal{B}_{Z \rightarrow q\bar{q}} \times (A \times \varepsilon)(E_T^{\text{miss}}) \quad \text{for } Z + \text{DM} \text{ events,}\end{aligned}$$

where $\sigma_{W+\text{DM}}$ ($\sigma_{Z+\text{DM}}$) is the production cross section for $W + \text{DM}$ ($Z + \text{DM}$) events in a given E_T^{miss} range, $\mathcal{B}_{W \rightarrow q'q}$ ($\mathcal{B}_{Z \rightarrow q\bar{q}}$) is the branching ratio for the hadronic W (Z) boson decay, and $(A \times \varepsilon)(E_T^{\text{miss}})$ is the product of the kinematic acceptance and the experimental efficiency. This product represents the fraction of simulated $W/Z + \text{DM}$ events in a given E_T^{miss} range at parton level² that fall into the same E_T^{miss} range at detector level after reconstruction, and pass the event selection criteria applied to determine σ_{vis} . To allow a generic interpretation, the requirements on m_{jj}/m_j or b -tagging are not included in the latter. The product $(A \times \varepsilon)(E_T^{\text{miss}})$ in a given E_T^{miss} range has been evaluated for each simulated vector-mediator signal and the lowest of these values, rounded down in steps of 5%, has been taken for the limit calculation. The values obtained for each E_T^{miss} range are listed in Tables 7 and 8.

9.6 Constraints on mono- Z' models

For the mono- Z' models, the upper limits on the cross section times the branching ratio $\mathcal{B}_{Z' \rightarrow q'q}$ at 95% CL are shown in Figure 11 as a function of the mediator mass for both the dark-fermion and dark-Higgs models in the light and heavy dark-sector mass scenarios. The largest excess of the data above the expectation, corresponding to a local significance of 3σ , is observed for a hypothesized signal at $m_{Z'} = 350 \text{ GeV}$ within the dark fermion model in the heavy dark-sector scenario. Taking into account the look-elsewhere effect [90] with respect to the 19 overlapping mass windows examined in the mono- Z' search, the excess corresponds to a global significance of 2.2σ . Cross-section exclusion limits for the dark-fermion model (dark-Higgs model) in the light and the heavy dark-sector scenario are in the range of 0.68–27 pb and 0.066–9.8 pb (0.80–5.5 pb and 0.064–2.4 pb) respectively, for Z' masses between 80 and 500 GeV. The corresponding observed and expected upper limits on the coupling g_{DM} are shown in Figure 12, assuming $g_{\text{DM}} = 1$.

² At parton level, E_T^{miss} is defined as the vector sum of momenta of neutrinos and DM particles in the transverse detector plane.

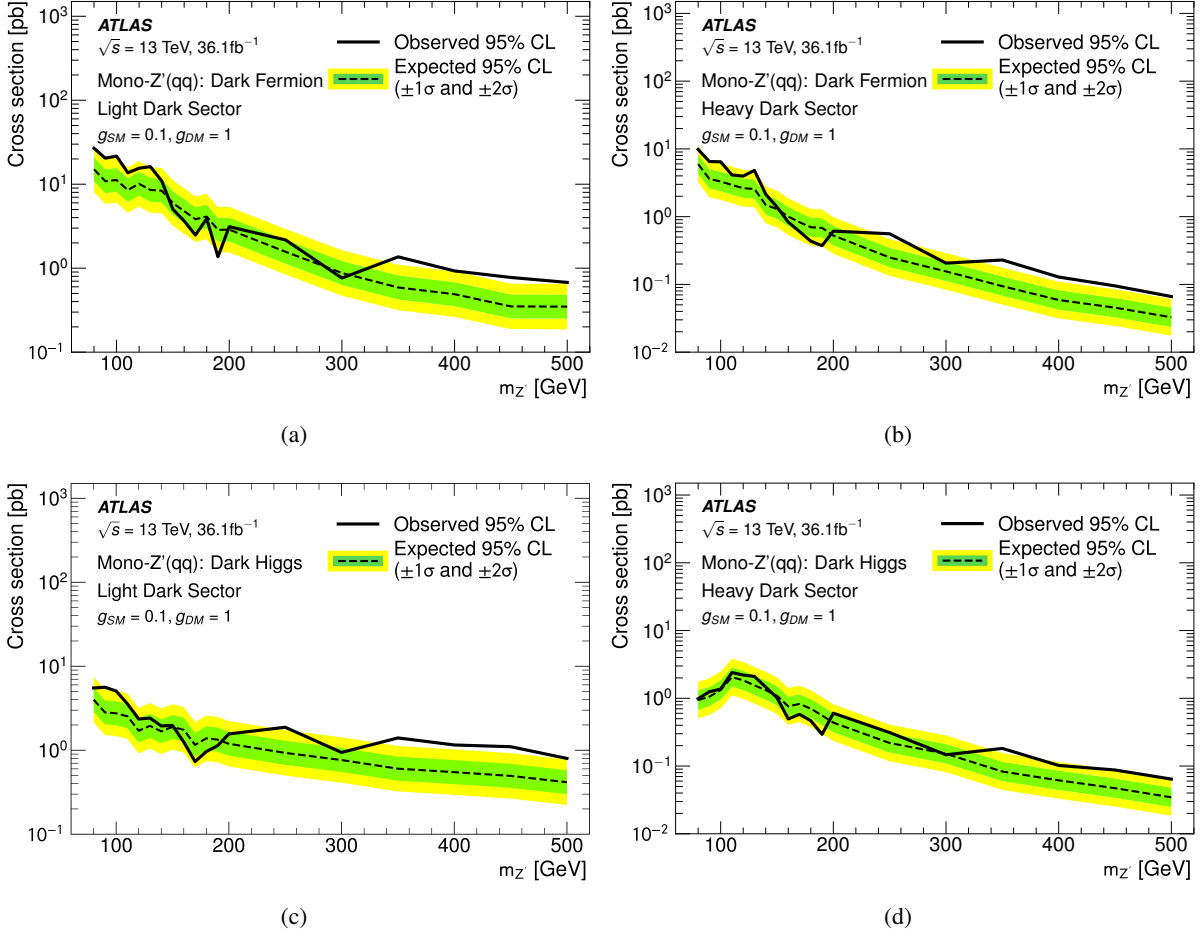


Figure 11: Upper limits at 95% CL on the cross section times the branching ratio $\mathcal{B}_{Z' \rightarrow q'q}$ in mono- Z' models as a function of the mediator mass, $m_{Z'}$, for the dark fermion model in the (a) light and (b) heavy dark-sector scenario, as well as the dark Higgs model in the (c) light and (d) heavy dark-sector scenario.

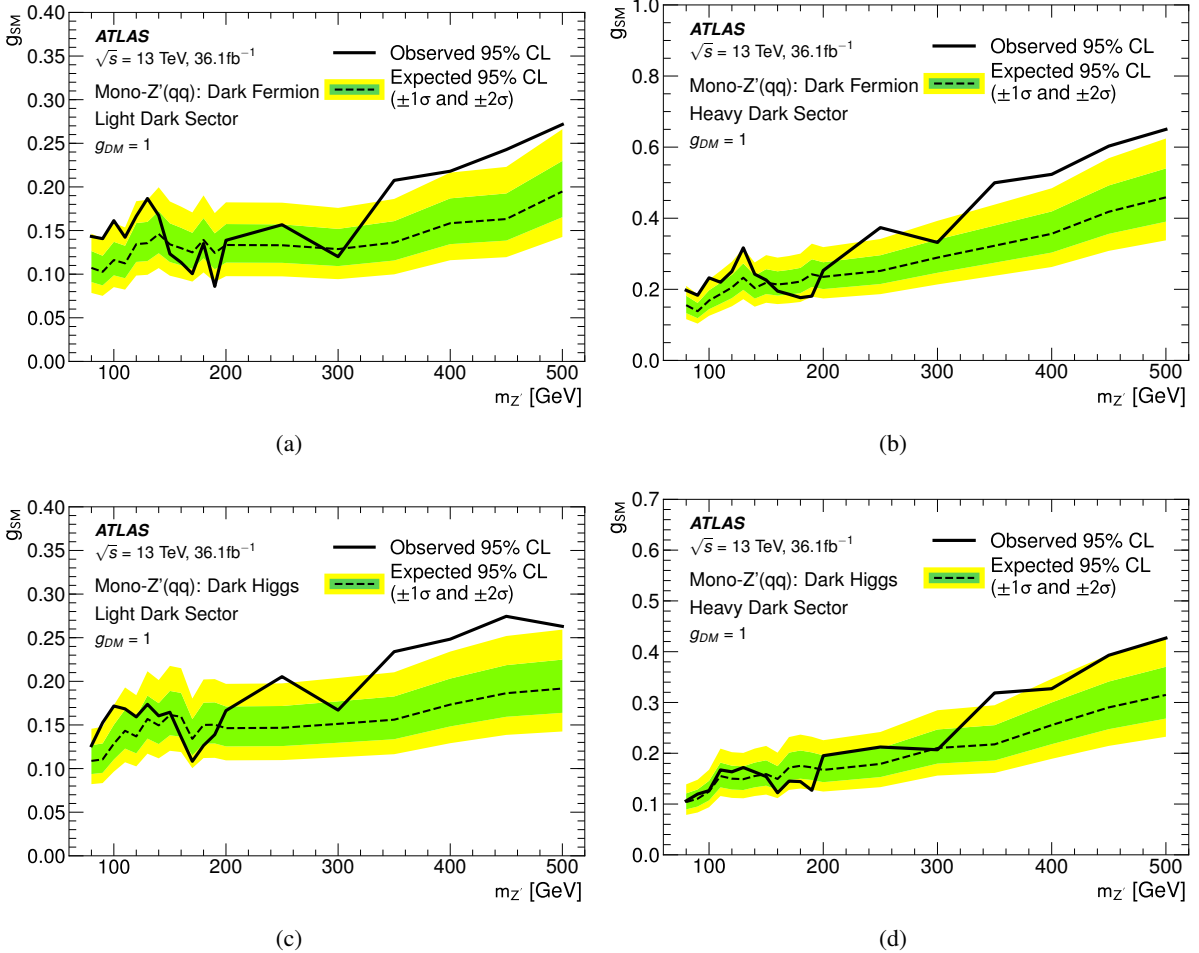


Figure 12: Upper limits at 95% CL on the product of couplings $g_{SM} g_{DM}$ in mono- Z' models as a function of the mediator mass for the dark fermion model in the (a) light and (b) heavy dark-sector scenario, as well as the dark Higgs model in the (c) light and (d) heavy dark-sector scenario.

10 Summary

A search for dark matter was performed in events having a large- R jet or a pair of small- R jets compatible with a hadronic W or Z boson decay, and large E_T^{miss} . In addition, the as of yet unexplored hypothesis of a new vector boson Z' produced in association with dark matter is considered. This search uses the ATLAS dataset corresponding to an integrated luminosity of 36.1 fb^{-1} of $\sqrt{s} = 13 \text{ TeV}$ pp collisions collected at the LHC in 2015 and 2016. It improves on previous searches by virtue of the larger dataset and further optimization of the selection criteria and signal region definitions. The results are in agreement with the SM predictions and are translated into exclusion limits on DM-pair production.

Two simplified models are considered to describe DM production in the mono- W/Z final state. For the simplified vector-mediator model in which the DM is produced via an s -channel exchange of a vector mediator Z' , masses $m_{Z'}$ of up to 650 GeV are excluded for dark matter masses m_χ of up to 250 GeV (assuming $g_{\text{SM}} = 0.25$ and $g_{\text{DM}} = 1.0$). This agrees well with the expected exclusion of $m_{Z'}$ values of up to 700 GeV for m_χ of up to 230 GeV. Limits are also placed on the visible cross section of non-SM events with large E_T^{miss} and a W or a Z boson without extra model assumptions. In the search for invisible Higgs boson decays, an upper limit of 0.83 is observed at 95% CL on the branching ratio $\mathcal{B}_{H \rightarrow \text{inv.}}$, while the corresponding expected limit is 0.58.

Two additional signal models, for DM production in association with the non-SM vector boson Z' , are considered. In the dark-fermion model, the intermediate Z' boson couples to a heavier dark-sector fermion χ_2 as well as the lighter DM candidate fermion χ_1 . In the dark-Higgs model, a dark-sector Higgs boson which decays to a $\chi\chi$ pair is radiated from the Z' boson. For coupling values of $g_{\text{SM}} = 0.1$ and $g_{\text{DM}} = 1.0$, two different choices of masses m_{χ_2} and m_{h_D} of intermediate dark-sector particles are considered. Cross-section exclusion limits for the dark-fermion model in the light and heavy dark-sector scenarios are in the range of 0.68–27 pb and 0.066–9.8 pb respectively for Z' masses between 80 and 500 GeV. The corresponding limits for the dark-Higgs model in the light and heavy dark-sector scenario are 0.80–5.5 pb and 0.064–2.4 pb, respectively.

Acknowledgements

We thank CERN for the very successful operation of the LHC, as well as the support staff from our institutions without whom ATLAS could not be operated efficiently.

We acknowledge the support of ANPCyT, Argentina; YerPhI, Armenia; ARC, Australia; BMWFW and FWF, Austria; ANAS, Azerbaijan; SSTC, Belarus; CNPq and FAPESP, Brazil; NSERC, NRC and CFI, Canada; CERN; CONICYT, Chile; CAS, MOST and NSFC, China; COLCIENCIAS, Colombia; MSMT CR, MPO CR and VSC CR, Czech Republic; DNRF and DNSRC, Denmark; IN2P3-CNRS, CEA-DRF/IRFU, France; SRNSFG, Georgia; BMBF, HGF, and MPG, Germany; GSRT, Greece; RGC, Hong Kong SAR, China; ISF, I-CORE and Benoziyo Center, Israel; INFN, Italy; MEXT and JSPS, Japan; CNRST, Morocco; NWO, Netherlands; RCN, Norway; MNiSW and NCN, Poland; FCT, Portugal; MNE/IFA, Romania; MES of Russia and NRC KI, Russian Federation; JINR; MESTD, Serbia; MSSR, Slovakia; ARRS and MIZŠ, Slovenia; DST/NRF, South Africa; MINECO, Spain; SRC and Wallenberg Foundation, Sweden; SERI, SNSF and Cantons of Bern and Geneva, Switzerland; MOST, Taiwan; TAEK, Turkey; STFC, United Kingdom; DOE and NSF, United States of America. In addition, individual groups and members have received support from BCKDF, the Canada Council, CANARIE, CRC, Compute

Canada, FQRNT, and the Ontario Innovation Trust, Canada; EPLANET, ERC, ERDF, FP7, Horizon 2020 and Marie Skłodowska-Curie Actions, European Union; Investissements d’Avenir Labex and Idex, ANR, Région Auvergne and Fondation Partager le Savoir, France; DFG and AvH Foundation, Germany; Herakleitos, Thales and Aristeia programmes co-financed by EU-ESF and the Greek NSRF; BSF, GIF and Minerva, Israel; BRF, Norway; CERCA Programme Generalitat de Catalunya, Generalitat Valenciana, Spain; the Royal Society and Leverhulme Trust, United Kingdom.

The crucial computing support from all WLCG partners is acknowledged gratefully, in particular from CERN, the ATLAS Tier-1 facilities at TRIUMF (Canada), NDGF (Denmark, Norway, Sweden), CC-IN2P3 (France), KIT/GridKA (Germany), INFN-CNAF (Italy), NL-T1 (Netherlands), PIC (Spain), ASGC (Taiwan), RAL (UK) and BNL (USA), the Tier-2 facilities worldwide and large non-WLCG resource providers. Major contributors of computing resources are listed in Ref. [91].

References

- [1] ATLAS Collaboration, *Search for dark matter produced in association with a hadronically decaying vector boson in pp collisions at $\sqrt{s} = 13$ TeV with the ATLAS detector*, *Phys. Lett. B* **763** (2016) 251, arXiv: [1608.02372 \[hep-ex\]](#).
- [2] CMS Collaboration, *Search for new physics in final states with an energetic jet or a hadronically decaying W or Z boson and transverse momentum imbalance at $\sqrt{s} = 13$ TeV*, *Phys. Rev. D* **97** (2018) 092005, arXiv: [1712.02345 \[hep-ex\]](#).
- [3] ATLAS Collaboration, *Search for dark matter in events with a hadronically decaying W or Z boson and missing transverse momentum in pp collisions at $\sqrt{s} = 8$ TeV with the ATLAS detector*, *Phys. Rev. Lett.* **112** (2014) 041802, arXiv: [1309.4017 \[hep-ex\]](#).
- [4] CMS Collaboration, *Search for dark matter in proton–proton collisions at 8 TeV with missing transverse momentum and vector boson tagged jets*, *JHEP* **12** (2016) 083, arXiv: [1607.05764 \[hep-ex\]](#).
- [5] ATLAS Collaboration, *Constraints on new phenomena via Higgs boson couplings and invisible decays with the ATLAS detector*, *JHEP* **11** (2015) 206, arXiv: [1509.00672 \[hep-ex\]](#).
- [6] ATLAS Collaboration, *Search for invisible decays of the Higgs boson produced in association with a hadronically decaying vector boson in pp collisions at $\sqrt{s} = 8$ TeV with the ATLAS detector*, *Eur. Phys. J. C* **75** (2015) 337, arXiv: [1504.04324 \[hep-ex\]](#).
- [7] CMS Collaboration, *Search for invisible decays of Higgs bosons in the vector boson fusion and associated ZH production modes*, *Eur. Phys. J. C* **74** (2014) 2980, arXiv: [1404.1344 \[hep-ex\]](#).
- [8] LHC Higgs Cross Section Working Group, D. de Florian et al., *Handbook of LHC Higgs Cross Sections: 4. Deciphering the nature of the Higgs sector*, CERN-2017-002-M (CERN, Geneva, 2016), arXiv: [1610.07922 \[hep-ph\]](#).
- [9] I. Antoniadis, M. Tuckmantel and F. Zwirner, *Phenomenology of a leptonic goldstino and invisible Higgs boson decays*, *Nucl. Phys. B* **707** (2005) 215, arXiv: [hep-ph/0410165](#).
- [10] N. Arkani-Hamed, S. Dimopoulos, G. Dvali and J. March-Russell, *Neutrino masses from large extra dimensions*, *Phys. Rev. D* **65** (2001) 024032, arXiv: [hep-ph/9811448](#).
- [11] A. Datta, K. Huitu, J. Laamanen and B. Mukhopadhyaya, *Linear collider signals of an invisible Higgs boson in theories of large extra dimensions*, *Phys. Rev. D* **70** (2004) 075003, arXiv: [hep-ph/0404056](#).
- [12] S. Kanemura, S. Matsumoto, T. Nabeshima and N. Okada, *Can WIMP dark matter overcome the nightmare scenario?*, *Phys. Rev. D* **82** (2010) 055026, arXiv: [1005.5651 \[hep-ph\]](#).
- [13] A. Djouadi, O. Lebedev, Y. Mambrini and J. Quevillon, *Implications of LHC searches for Higgs-portal dark matter*, *Phys. Lett. B* **709** (2012) 65, arXiv: [1112.3299 \[hep-ph\]](#).
- [14] CMS Collaboration, *Searches for invisible decays of the Higgs boson in pp collisions at $\sqrt{s} = 7, 8$, and 13 TeV*, *JHEP* **02** (2017) 135, arXiv: [1610.09218 \[hep-ex\]](#).

- [15] M. Autran, K. Bauer, T. Lin and D. Whiteson, *Searches for dark matter in events with a resonance and missing transverse energy*, *Phys. Rev. D* **92** (2015) 035007, arXiv: [1504.01386 \[hep-ph\]](#).
- [16] ATLAS Collaboration, *The ATLAS Experiment at the CERN Large Hadron Collider*, *JINST* **3** (2008) S08003.
- [17] ATLAS Collaboration, *ATLAS Insertable B-Layer Technical Design Report*, CERN-LHCC-2010-013, ATLAS-TDR-019, 2010, URL: <https://cds.cern.ch/record/1291633>.
- [18] ATLAS Collaboration, *ATLAS Insertable B-Layer Technical Design Report Addendum*, CERN-LHCC-2012-009, ATLAS-TDR-19-ADD-1, 2012, URL: <https://cds.cern.ch/record/1451888>.
- [19] ATLAS Collaboration, *Performance of the ATLAS Trigger System in 2015*, *Eur. Phys. J. C* **77** (2017) 317, arXiv: [1611.09661 \[hep-ex\]](#).
- [20] O. Buchmueller, M. J. Dolan, S. A. Malik and C. McCabe, *Characterising dark matter searches at colliders and direct detection experiments: Vector mediators*, *JHEP* **01** (2015) 037, arXiv: [1407.8257 \[hep-ph\]](#).
- [21] D. Abercrombie et al., *Dark Matter Benchmark Models for Early LHC Run-2 Searches: Report of the ATLAS/CMS Dark Matter Forum*, (2015), arXiv: [1507.00966 \[hep-ex\]](#).
- [22] S. Agostinelli et al., *GEANT4: A Simulation toolkit*, *Nucl. Instrum. Meth. A* **506** (2003) 250.
- [23] ATLAS Collaboration, *The ATLAS Simulation Infrastructure*, *Eur. Phys. J. C* **70** (2010) 823, arXiv: [1005.4568 \[physics.ins-det\]](#).
- [24] T. Sjöstrand, S. Mrenna and P. Z. Skands, *A Brief Introduction to PYTHIA 8.1*, *Comput. Phys. Commun.* **178** (2008) 852, arXiv: [0710.3820 \[hep-ph\]](#).
- [25] ATLAS Collaboration, *Summary of ATLAS Pythia 8 tunes*, ATL-PHYS-PUB-2012-003, 2012, URL: <https://cds.cern.ch/record/1474107>.
- [26] A. D. Martin, W. J. Stirling, R. S. Thorne and G. Watt, *Parton distributions for the LHC*, *Eur. Phys. J. C* **63** (2009) 189, arXiv: [0901.0002 \[hep-ph\]](#).
- [27] J. Alwall et al., *The automated computation of tree-level and next-to-leading order differential cross sections, and their matching to parton shower simulations*, *JHEP* **07** (2014) 079, arXiv: [1405.0301 \[hep-ph\]](#).
- [28] ATLAS Collaboration, *ATLAS Pythia 8 tunes to 7 TeV data*, ATL-PHYS-PUB-2014-021, 2014, URL: <https://cds.cern.ch/record/1966419>.
- [29] R. D. Ball et al., *Parton distributions for the LHC Run II*, *JHEP* **04** (2015) 040, arXiv: [1410.8849 \[hep-ph\]](#).
- [30] A. Albert et al., *Recommendations of the LHC Dark Matter Working Group: Comparing LHC searches for heavy mediators of dark matter production in visible and invisible decay channels*, (2017), arXiv: [1703.05703 \[hep-ex\]](#).
- [31] ATLAS Collaboration, *Search for light resonances decaying to boosted quark pairs and produced in association with a photon or a jet in proton–proton collisions at $\sqrt{s} = 13$ TeV with the ATLAS detector*, (2018), arXiv: [1801.08769 \[hep-ex\]](#).

- [32] CMS Collaboration, *Search for low mass vector resonances decaying into quark–antiquark pairs in proton–proton collisions at $\sqrt{s} = 13$ TeV*, JHEP **01** (2018) 097, arXiv: [1710.00159 \[hep-ex\]](#).
- [33] ATLAS Collaboration, *Search for new phenomena in final states with an energetic jet and large missing transverse momentum in pp collisions at $\sqrt{s} = 13$ TeV using the ATLAS detector*, Phys. Rev. D **94** (2016) 032005, arXiv: [1604.07773 \[hep-ex\]](#).
- [34] CMS Collaboration, *Search for dijet resonances in proton–proton collisions at $\sqrt{s} = 13$ TeV and constraints on dark matter and other models*, Phys. Lett. B **769** (2017) 520, arXiv: [1611.03568 \[hep-ex\]](#).
- [35] P. Nason, *A New method for combining NLO QCD with shower Monte Carlo algorithms*, JHEP **11** (2004) 040, arXiv: [hep-ph/0409146](#).
- [36] S. Frixione, P. Nason and C. Oleari, *Matching NLO QCD computations with Parton Shower simulations: the POWHEG method*, JHEP **11** (2007) 070, arXiv: [0709.2092 \[hep-ph\]](#).
- [37] S. Alioli, P. Nason, C. Oleari and E. Re, *A general framework for implementing NLO calculations in shower Monte Carlo programs: the POWHEG BOX*, JHEP **06** (2010) 043, arXiv: [1002.2581 \[hep-ph\]](#).
- [38] ATLAS Collaboration, *Measurement of inclusive and differential cross sections in the $H \rightarrow ZZ^* \rightarrow 4\ell$ decay channel in pp collisions at $\sqrt{s} = 13$ TeV with the ATLAS detector*, JHEP **10** (2017) 132, arXiv: [1708.02810 \[hep-ex\]](#).
- [39] ATLAS Collaboration, *Evidence for the $H \rightarrow b\bar{b}$ decay with the ATLAS detector*, JHEP **12** (2017) 024, arXiv: [1708.03299 \[hep-ex\]](#).
- [40] T. Gleisberg et al., *Event generation with SHERPA 1.1*, JHEP **02** (2009) 007, arXiv: [0811.4622 \[hep-ph\]](#).
- [41] T. Gleisberg and S. Höche, *Comix, a new matrix element generator*, JHEP **12** (2008) 039, arXiv: [0808.3674 \[hep-ph\]](#).
- [42] F. Cascioli, P. Maierhöfer and S. Pozzorini, *Scattering Amplitudes with Open Loops*, Phys. Rev. Lett. **108** (2012) 111601, arXiv: [1111.5206 \[hep-ph\]](#).
- [43] S. Schumann and F. Krauss, *A Parton shower algorithm based on Catani-Seymour dipole factorisation*, JHEP **03** (2008) 038, arXiv: [0709.1027 \[hep-ph\]](#).
- [44] S. Höche, F. Krauss, M. Schönherr and F. Siegert, *QCD matrix elements + parton showers: The NLO case*, JHEP **04** (2013) 027, arXiv: [1207.5030 \[hep-ph\]](#).
- [45] K. Melnikov and F. Petriello, *Electroweak gauge boson production at hadron colliders through $O(\alpha_s^2)$* , Phys. Rev. D **74** (2006) 114017, arXiv: [hep-ph/0609070](#).
- [46] H.-L. Lai et al., *New parton distributions for collider physics*, Phys. Rev. D **82** (2010) 074024, arXiv: [1007.2241 \[hep-ph\]](#).
- [47] P. Artoisenet, R. Frederix, O. Mattelaer and R. Rietkerk, *Automatic spin-entangled decays of heavy resonances in Monte Carlo simulations*, JHEP **03** (2013) 015, arXiv: [1212.3460 \[hep-ph\]](#).

- [48] T. Sjöstrand, S. Mrenna and P. Z. Skands, *PYTHIA 6.4 Physics and Manual*, JHEP **05** (2006) 026, arXiv: [hep-ph/0603175](#).
- [49] J. Pumplin et al.,
New generation of parton distributions with uncertainties from global QCD analysis, JHEP **07** (2002) 012, arXiv: [hep-ph/0201195](#).
- [50] P. Z. Skands, *Tuning Monte Carlo Generators: The Perugia Tunes*, Phys. Rev. D **82** (2010) 074018, arXiv: [1005.3457 \[hep-ph\]](#).
- [51] D. J. Lange, *The EvtGen particle decay simulation package*, Nucl. Instrum. Meth. A**462** (2001) 152.
- [52] M. Czakon, P. Fiedler and A. Mitov,
Total Top-Quark Pair-Production Cross Section at Hadron Colliders Through $O(\alpha_S^4)$, Phys. Rev. Lett. **110** (2013) 252004, arXiv: [1303.6254 \[hep-ph\]](#).
- [53] T. Stelzer, Z. Sullivan and S. Willenbrock,
Single top quark production via W - gluon fusion at next-to-leading order, Phys. Rev. D **56** (1997) 5919, arXiv: [hep-ph/9705398 \[hep-ph\]](#).
- [54] T. Stelzer, Z. Sullivan and S. S. Willenbrock, *Single top quark production at hadron colliders*, Phys. Rev. D **58** (1998) 094021, arXiv: [hep-ph/9807340](#).
- [55] M. C. Smith and S. S. Willenbrock,
QCD and Yukawa corrections to single top quark production via $q\bar{q} \rightarrow t\bar{b}$, Phys. Rev. D **54** (1996) 6696, arXiv: [hep-ph/9604223](#).
- [56] Kidonakis, Nikolaos, *Top Quark Production*, DESY-PROC-2013-03, arXiv: [1311.0283 \[hep-ph\]](#).
- [57] ATLAS Collaboration,
Topological cell clustering in the ATLAS calorimeters and its performance in LHC Run 1, Eur. Phys. J. C **77** (2017) 490, arXiv: [1603.02934 \[hep-ex\]](#).
- [58] M. Cacciari, G. P. Salam and G. Soyez, *The anti- k_t jet clustering algorithm*, JHEP **04** (2008) 063, arXiv: [0802.1189 \[hep-ph\]](#).
- [59] M. Cacciari, G. P. Salam and G. Soyez, *FastJet User Manual*, Eur. Phys. J. C **72** (2012) 1896, arXiv: [1111.6097 \[hep-ph\]](#).
- [60] ATLAS Collaboration, *Tagging and suppression of pileup jets with the ATLAS detector*, ATLAS-CONF-2014-018, 2014, URL: <https://cds.cern.ch/record/1700870>.
- [61] ATLAS Collaboration, *Jet energy scale measurements and their systematic uncertainties in proton–proton collisions at $\sqrt{s} = 13$ TeV with the ATLAS detector*, Phys. Rev. D **96** (2017) 072002, arXiv: [1703.09665 \[hep-ex\]](#).
- [62] ATLAS Collaboration, *Data-driven determination of the energy scale and resolution of jets reconstructed in the ATLAS calorimeters using dijet and multijet events at $\sqrt{s} = 8$ TeV*, ATLAS-CONF-2015-017, 2015, URL: <https://cds.cern.ch/record/2008678>.
- [63] ATLAS Collaboration, *Performance of b-jet identification in the ATLAS experiment*, JINST **11** (2016) P04008, arXiv: [1512.01094 \[hep-ex\]](#).
- [64] ATLAS Collaboration, *Optimisation of the ATLAS b-tagging performance for the 2016 LHC Run*, ATL-PHYS-PUB-2016-012, 2016, URL: <https://cds.cern.ch/record/2160731>.

- [65] ATLAS Collaboration, *Commissioning of the ATLAS b-tagging algorithms using $t\bar{t}$ events in early Run 2 data*, ATL-PHYS-PUB-2015-039, 2015, URL: <https://cds.cern.ch/record/2047871>.
- [66] ATLAS Collaboration, *Identification of Boosted, Hadronically Decaying W Bosons and Comparisons with ATLAS Data Taken at $\sqrt{s} = 8$ TeV*, *Eur. Phys. J. C* **76** (2016) 154, arXiv: [1510.05821 \[hep-ex\]](https://arxiv.org/abs/1510.05821).
- [67] ATLAS Collaboration, *Identification of Boosted, Hadronically-Decaying W and Z Bosons in $\sqrt{s} = 13$ TeV Monte Carlo Simulations for ATLAS*, ATL-PHYS-PUB-2015-033, 2015, URL: <https://cds.cern.ch/record/2041461>.
- [68] D. Krohn, J. Thaler and L.-T. Wang, *Jet Trimming*, *JHEP* **02** (2010) 084, arXiv: [0912.1342 \[hep-ph\]](https://arxiv.org/abs/0912.1342).
- [69] ATLAS Collaboration, *Jet mass reconstruction with the ATLAS Detector in early Run 2 data*, ATLAS-CONF-2016-035, 2016, URL: <https://cds.cern.ch/record/2200211>.
- [70] A. J. Larkoski, I. Moult and D. Neill, *Power Counting to Better Jet Observables*, *JHEP* **12** (2014) 009, arXiv: [1409.6298 \[hep-ph\]](https://arxiv.org/abs/1409.6298).
- [71] A. J. Larkoski, G. P. Salam and J. Thaler, *Energy Correlation Functions for Jet Substructure*, *JHEP* **06** (2013) 108, arXiv: [1305.0007 \[hep-ph\]](https://arxiv.org/abs/1305.0007).
- [72] ATLAS Collaboration, *Performance of jet substructure techniques for large- R jets in proton–proton collisions at $\sqrt{s} = 7$ TeV using the ATLAS detector*, *JHEP* **09** (2013) 076, arXiv: [1306.4945 \[hep-ex\]](https://arxiv.org/abs/1306.4945).
- [73] ATLAS Collaboration, *Performance of jet substructure techniques in early $\sqrt{s} = 13$ TeV pp collisions with the ATLAS detector*, ATLAS-CONF-2015-035, 2015, URL: <https://cds.cern.ch/record/2041462>.
- [74] ATLAS Collaboration, *Flavor Tagging with Track-Jets in Boosted Topologies with the ATLAS Detector*, ATL-PHYS-PUB-2014-013, 2014, URL: <https://cds.cern.ch/record/1750681>.
- [75] ATLAS Collaboration, *Boosted Higgs ($\rightarrow b\bar{b}$) Boson Identification with the ATLAS Detector at $\sqrt{s} = 13$ TeV*, ATLAS-CONF-2016-039, 2016, URL: <https://cds.cern.ch/record/2206038>.
- [76] M. Cacciari, G. P. Salam and G. Soyez, *The Catchment Area of Jets*, *JHEP* **04** (2008) 005, arXiv: [0802.1188 \[hep-ph\]](https://arxiv.org/abs/0802.1188).
- [77] ATLAS Collaboration, *Electron efficiency measurements with the ATLAS detector using 2012 LHC proton–proton collision data*, *Eur. Phys. J. C* **77** (2017) 195, arXiv: [1612.01456 \[hep-ex\]](https://arxiv.org/abs/1612.01456).
- [78] ATLAS Collaboration, *Electron efficiency measurements with the ATLAS detector using the 2015 LHC proton–proton collision data*, ATLAS-CONF-2016-024, 2016, URL: <https://cds.cern.ch/record/2157687>.
- [79] ATLAS Collaboration, *Electron and photon energy calibration with the ATLAS detector using LHC Run 1 data*, *Eur. Phys. J. C* **74** (2014) 3071, arXiv: [1407.5063 \[hep-ex\]](https://arxiv.org/abs/1407.5063).
- [80] ATLAS Collaboration, *Electron and photon energy calibration with the ATLAS detector using data collected in 2015 at $\sqrt{s} = 13$ TeV*, ATL-PHYS-PUB-2016-015, 2016, URL: <https://cds.cern.ch/record/2203514>.

- [81] ATLAS Collaboration, *Muon reconstruction performance of the ATLAS detector in proton–proton collision data at $\sqrt{s} = 13$ TeV*, *Eur. Phys. J. C* **76** (2016) 292, arXiv: [1603.05598 \[hep-ex\]](#).
- [82] ATLAS Collaboration, *Performance of missing transverse momentum reconstruction with the ATLAS detector using proton-proton collisions at $\sqrt{s} = 13$ TeV*, (2018), arXiv: [1802.08168 \[hep-ex\]](#).
- [83] ATLAS Collaboration, *Performance of Top Quark and W Boson Tagging in Run 2 with ATLAS*, ATLAS-CONF-2017-064, 2017, URL: <https://cds.cern.ch/record/2281054>.
- [84] ATLAS Collaboration, *Luminosity determination in pp collisions at $\sqrt{s} = 8$ TeV using the ATLAS detector at the LHC*, *Eur. Phys. J. C* **76** (2016) 653, arXiv: [1608.03953 \[hep-ex\]](#).
- [85] G. Cowan, K. Cranmer, E. Gross and O. Vitells, *Asymptotic formulae for likelihood-based tests of new physics*, *Eur. Phys. J. C* **71** (2011) 1554, arXiv: [1007.1727 \[physics.data-an\]](#).
- [86] A. L. Read, *Presentation of search results: The $CL(s)$ technique*, *J. Phys. G* **28** (2002) 2693.
- [87] WMAP Collaboration, *Nine-Year Wilkinson Microwave Anisotropy Probe (WMAP) Observations: Cosmological Parameter Results*, *Astrophys. J. Suppl.* **208** (2013) 19, arXiv: [1212.5226 \[astro-ph.CO\]](#).
- [88] Planck Collaboration, *Planck 2015 results. I. Overview of products and scientific results*, *Astron. Astrophys.* **594** (2016) A1, arXiv: [1502.01582 \[astro-ph.CO\]](#).
- [89] M. Backović, A. Martini, O. Mattelaer, K. Kong and G. Mohlabeng, *Direct Detection of Dark Matter with MadDM v.2.0*, *Phys. Dark Univ.* **9-10** (2015) 37, arXiv: [1505.04190 \[hep-ph\]](#).
- [90] E. Gross and O. Vitells, *Trial factors or the look elsewhere effect in high energy physics*, *Eur. Phys. J. C* **70** (2010) 525, arXiv: [1005.1891 \[physics.data-an\]](#).
- [91] ATLAS Collaboration, *ATLAS Computing Acknowledgements*, ATL-GEN-PUB-2016-002, URL: <https://cds.cern.ch/record/2202407>.

The ATLAS Collaboration

M. Aaboud^{34d}, G. Aad⁹⁹, B. Abbott¹²⁴, O. Abdinov^{13,*}, B. Abelos¹²⁸, D.K. Abhayasinghe⁹¹, S.H. Abidi¹⁶⁴, O.S. AbouZeid³⁹, N.L. Abraham¹⁵³, H. Abramowicz¹⁵⁸, H. Abreu¹⁵⁷, Y. Abulaiti⁶, B.S. Acharya^{64a,64b,n}, S. Adachi¹⁶⁰, L. Adamczyk^{81a}, J. Adelman¹¹⁹, M. Adersberger¹¹², A. Adiguzel^{12c}, T. Adye¹⁴¹, A.A. Affolder¹⁴³, Y. Afik¹⁵⁷, C. Agheorghiesei^{27c}, J.A. Aguilar-Saavedra^{136f,136a}, F. Ahmadov^{77,ad}, G. Aielli^{71a,71b}, S. Akatsuka⁸³, T.P.A. Åkesson⁹⁴, E. Akilli⁵², A.V. Akimov¹⁰⁸, G.L. Alberghi^{23b,23a}, J. Albert¹⁷³, P. Albicocco⁴⁹, M.J. Alconada Verzini⁸⁶, S. Alderweireldt¹¹⁷, M. Aleksa³⁵, I.N. Aleksandrov⁷⁷, C. Alexa^{27b}, T. Alexopoulos¹⁰, M. Alhroob¹²⁴, B. Ali¹³⁸, G. Alimonti^{66a}, J. Alison³⁶, S.P. Alkire¹⁴⁵, C. Allaire¹²⁸, B.M.M. Allbrooke¹⁵³, B.W. Allen¹²⁷, P.P. Allport²¹, A. Aloisio^{67a,67b}, A. Alonso³⁹, F. Alonso⁸⁶, C. Alpigiani¹⁴⁵, A.A. Alshehri⁵⁵, M.I. Alstaty⁹⁹, B. Alvarez Gonzalez³⁵, D. Álvarez Piqueras¹⁷¹, M.G. Alvaggi^{67a,67b}, B.T. Amadio¹⁸, Y. Amaral Coutinho^{78b}, L. Ambroz¹³¹, C. Amelung²⁶, D. Amidei¹⁰³, S.P. Amor Dos Santos^{136a,136c}, S. Amoroso⁴⁴, C.S. Amrouche⁵², C. Anastopoulos¹⁴⁶, L.S. Ancu⁵², N. Andari²¹, T. Andeen¹¹, C.F. Anders^{59b}, J.K. Anders²⁰, K.J. Anderson³⁶, A. Andreazza^{66a,66b}, V. Andrei^{59a}, C.R. Anelli¹⁷³, S. Angelidakis³⁷, I. Angelozzi¹¹⁸, A. Angerami³⁸, A.V. Anisenkov^{120b,120a}, A. Annovi^{69a}, C. Antel^{59a}, M.T. Anthony¹⁴⁶, M. Antonelli⁴⁹, D.J.A. Antrim¹⁶⁸, F. Anulli^{70a}, M. Aoki⁷⁹, L. Aperio Bella³⁵, G. Arabidze¹⁰⁴, J.P. Araque^{136a}, V. Araujo Ferraz^{78b}, R. Araujo Pereira^{78b}, A.T.H. Arce⁴⁷, R.E. Ardell⁹¹, F.A. Arduh⁸⁶, J-F. Arguin¹⁰⁷, S. Argyropoulos⁷⁵, A.J. Armbruster³⁵, L.J. Armitage⁹⁰, A.iii. Armstrong¹⁶⁸, O. Arnaez¹⁶⁴, H. Arnold¹¹⁸, M. Arratia³¹, O. Arslan²⁴, A. Artamonov^{109,*}, G. Artoni¹³¹, S. Artz⁹⁷, S. Asai¹⁶⁰, N. Asbah⁴⁴, A. Ashkenazi¹⁵⁸, E.M. Asimakopoulou¹⁶⁹, L. Asquith¹⁵³, K. Assamagan²⁹, R. Astalos^{28a}, R.J. Atkin^{32a}, M. Atkinson¹⁷⁰, N.B. Atlay¹⁴⁸, K. Augsten¹³⁸, G. Avolio³⁵, R. Avramidou^{58a}, M.K. Ayoub^{15a}, G. Azuelos^{107,aq}, A.E. Baas^{59a}, M.J. Baca²¹, H. Bachacou¹⁴², K. Bachas^{65a,65b}, M. Backes¹³¹, P. Bagnaia^{70a,70b}, M. Bahmani⁸², H. Bahrasemani¹⁴⁹, A.J. Bailey¹⁷¹, J.T. Baines¹⁴¹, M. Bajic³⁹, C. Bakalis¹⁰, O.K. Baker¹⁸⁰, P.J. Bakker¹¹⁸, D. Bakshi Gupta⁹³, E.M. Baldin^{120b,120a}, P. Balek¹⁷⁷, F. Balli¹⁴², W.K. Balunas¹³³, J. Balz⁹⁷, E. Banas⁸², A. Bandyopadhyay²⁴, S. Banerjee^{178,j}, A.A.E. Bannoura¹⁷⁹, L. Barak¹⁵⁸, W.M. Barbe³⁷, E.L. Barberio¹⁰², D. Barberis^{53b,53a}, M. Barbero⁹⁹, T. Barillari¹¹³, M-S. Barisits³⁵, J. Barkeloo¹²⁷, T. Barklow¹⁵⁰, N. Barlow³¹, R. Barnea¹⁵⁷, S.L. Barnes^{58c}, B.M. Barnett¹⁴¹, R.M. Barnett¹⁸, Z. Barnovska-Blenessy^{58a}, A. Baroncelli^{72a}, G. Barone²⁶, A.J. Barr¹³¹, L. Barranco Navarro¹⁷¹, F. Barreiro⁹⁶, J. Barreiro Guimaraes da Costa^{15a}, R. Bartoldus¹⁵⁰, A.E. Barton⁸⁷, P. Bartos^{28a}, A. Basalaev¹³⁴, A. Bassalat¹²⁸, R.L. Bates⁵⁵, S.J. Batista¹⁶⁴, S. Batlamous^{34e}, J.R. Batley³¹, M. Battaglia¹⁴³, M. Bauce^{70a,70b}, F. Bauer¹⁴², K.T. Bauer¹⁶⁸, H.S. Bawa^{150,1}, J.B. Beacham¹²², M.D. Beattie⁸⁷, T. Beau¹³², P.H. Beauchemin¹⁶⁷, P. Bechtle²⁴, H.C. Beck⁵¹, H.P. Beck^{20,p}, K. Becker⁵⁰, M. Becker⁹⁷, C. Becot⁴⁴, A. Beddall^{12d}, A.J. Beddall^{12a}, V.A. Bednyakov⁷⁷, M. Bedognetti¹¹⁸, C.P. Bee¹⁵², T.A. Beermann³⁵, M. Begalli^{78b}, M. Begel²⁹, A. Behera¹⁵², J.K. Behr⁴⁴, A.S. Bell⁹², G. Bella¹⁵⁸, L. Bellagamba^{23b}, A. Bellerive³³, M. Bellomo¹⁵⁷, P. Bellos⁹, K. Belotskiy¹¹⁰, N.L. Belyaev¹¹⁰, O. Benary^{158,*}, D. Benchekroun^{34a}, M. Bender¹¹², N. Benekos¹⁰, Y. Benhammou¹⁵⁸, E. Benhar Noccioli¹⁸⁰, J. Benitez⁷⁵, D.P. Benjamin⁴⁷, M. Benoit⁵², J.R. Bensinger²⁶, S. Bentvelsen¹¹⁸, L. Beresford¹³¹, M. Beretta⁴⁹, D. Berge⁴⁴, E. Bergeaas Kuutmann¹⁶⁹, N. Berger⁵, L.J. Bergsten²⁶, J. Beringer¹⁸, S. Berlendis⁷, N.R. Bernard¹⁰⁰, G. Bernardi¹³², C. Bernius¹⁵⁰, F.U. Bernlochner²⁴, T. Berry⁹¹, P. Berta⁹⁷, C. Bertella^{15a}, G. Bertoli^{43a,43b}, I.A. Bertram⁸⁷, G.J. Besjes³⁹, O. Bessidskaia Bylund^{43a,43b}, M. Bessner⁴⁴, N. Besson¹⁴², A. Bethani⁹⁸, S. Bethke¹¹³, A. Betti²⁴, A.J. Bevan⁹⁰, J. Beyer¹¹³, R.M.B. Bianchi¹³⁵, O. Biebel¹¹², D. Biedermann¹⁹, R. Bielski⁹⁸, K. Bierwagen⁹⁷, N.V. Biesuz^{69a,69b}, M. Biglietti^{72a}, T.R.V. Billoud¹⁰⁷, M. Bindi⁵¹, A. Bingul^{12d}, C. Bini^{70a,70b}, S. Biondi^{23b,23a}, M. Birman¹⁷⁷, T. Bisanz⁵¹, J.P. Biswal¹⁵⁸, C. Bittrich⁴⁶,

D.M. Bjergaard⁴⁷, J.E. Black¹⁵⁰, K.M. Black²⁵, T. Blazek^{28a}, I. Bloch⁴⁴, C. Blocker²⁶, A. Blue⁵⁵, U. Blumenschein⁹⁰, Dr. Blunier^{144a}, G.J. Bobbink¹¹⁸, V.S. Bobrovnikov^{120b,120a}, S.S. Bocchetta⁹⁴, A. Bocci⁴⁷, D. Boerner¹⁷⁹, D. Bogavac¹¹², A.G. Bogdanchikov^{120b,120a}, C. Bohm^{43a}, V. Boisvert⁹¹, P. Bokan^{169,w}, T. Bold^{81a}, A.S. Boldyrev¹¹¹, A.E. Bolz^{59b}, M. Bomben¹³², M. Bona⁹⁰, J.S. Bonilla¹²⁷, M. Boonekamp¹⁴², A. Borisov¹⁴⁰, G. Borissov⁸⁷, J. Bortfeldt³⁵, D. Bortoletto¹³¹, V. Bortolotto^{71a,61b,61c,71b}, D. Boscherini^{23b}, M. Bosman¹⁴, J.D. Bossio Sola³⁰, K. Bouaouda^{34a}, J. Boudreau¹³⁵, E.V. Bouhova-Thacker⁸⁷, D. Boumediene³⁷, C. Bourdarios¹²⁸, S.K. Boutle⁵⁵, A. Boveia¹²², J. Boyd³⁵, I.R. Boyko⁷⁷, A.J. Bozson⁹¹, J. Bracinik²¹, N. Brahimi⁹⁹, A. Brandt⁸, G. Brandt¹⁷⁹, O. Brandt^{59a}, F. Braren⁴⁴, U. Bratzler¹⁶¹, B. Brau¹⁰⁰, J.E. Brau¹²⁷, W.D. Breaden Madden⁵⁵, K. Brendlinger⁴⁴, A.J. Brennan¹⁰², L. Brenner⁴⁴, R. Brenner¹⁶⁹, S. Bressler¹⁷⁷, B. Brickwedde⁹⁷, D.L. Briglin²¹, D. Britton⁵⁵, D. Britzger^{59b}, I. Brock²⁴, R. Brock¹⁰⁴, G. Brooijmans³⁸, T. Brooks⁹¹, W.K. Brooks^{144b}, E. Brost¹¹⁹, J.H. Broughton²¹, P.A. Bruckman de Renstrom⁸², D. Bruncko^{28b}, A. Bruni^{23b}, G. Bruni^{23b}, L.S. Bruni¹¹⁸, S. Bruno^{71a,71b}, B.H. Brunt³¹, M. Bruschi^{23b}, N. Bruscino¹³⁵, P. Bryant³⁶, L. Bryngemark⁴⁴, T. Buanes¹⁷, Q. Buat³⁵, P. Buchholz¹⁴⁸, A.G. Buckley⁵⁵, I.A. Budagov⁷⁷, F. Buehrer⁵⁰, M.K. Bugge¹³⁰, O. Bulekov¹¹⁰, D. Bullock⁸, T.J. Burch¹¹⁹, S. Burdin⁸⁸, C.D. Burgard¹¹⁸, A.M. Burger⁵, B. Burghgrave¹¹⁹, K. Burka⁸², S. Burke¹⁴¹, I. Burmeister⁴⁵, J.T.P. Burr¹³¹, D. Büscher⁵⁰, V. Büscher⁹⁷, E. Buschmann⁵¹, P. Bussey⁵⁵, J.M. Butler²⁵, C.M. Buttar⁵⁵, J.M. Butterworth⁹², P. Butti³⁵, W. Buttinger³⁵, A. Buzatu¹⁵⁵, A.R. Buzykaev^{120b,120a}, G. Cabras^{23b,23a}, S. Cabrera Urbán¹⁷¹, D. Caforio¹³⁸, H. Cai¹⁷⁰, V.M.M. Cairo², O. Cakir^{4a}, N. Calace⁵², P. Calafiura¹⁸, A. Calandri⁹⁹, G. Calderini¹³², P. Calfayan⁶³, G. Callea^{40b,40a}, L.P. Caloba^{78b}, S. Calvente Lopez⁹⁶, D. Calvet³⁷, S. Calvet³⁷, T.P. Calvet¹⁵², M. Calvetti^{69a,69b}, R. Camacho Toro¹³², S. Camarda³⁵, P. Camarri^{71a,71b}, D. Cameron¹³⁰, R. Caminal Armadans¹⁰⁰, C. Camincher³⁵, S. Campana³⁵, M. Campanelli⁹², A. Camplani³⁹, A. Campoverde¹⁴⁸, V. Canale^{67a,67b}, M. Cano Bret^{58c}, J. Cantero¹²⁵, T. Cao¹⁵⁸, Y. Cao¹⁷⁰, M.D.M. Capeans Garrido³⁵, I. Caprini^{27b}, M. Caprini^{27b}, M. Capua^{40b,40a}, R.M. Carbone³⁸, R. Cardarelli^{71a}, F. Cardillo⁵⁰, I. Carli¹³⁹, T. Carli³⁵, G. Carlino^{67a}, B.T. Carlson¹³⁵, L. Carminati^{66a,66b}, R.M.D. Carney^{43a,43b}, S. Caron¹¹⁷, E. Carquin^{144b}, S. Carrá^{66a,66b}, G.D. Carrillo-Montoya³⁵, D. Casadei^{32b}, M.P. Casado^{14,f}, A.F. Casha¹⁶⁴, M. Casolino¹⁴, D.W. Casper¹⁶⁸, R. Castelijn¹¹⁸, F.L. Castillo¹⁷¹, V. Castillo Gimenez¹⁷¹, N.F. Castro^{136a,136e}, A. Catinaccio³⁵, J.R. Catmore¹³⁰, A. Cattai³⁵, J. Caudron²⁴, V. Cavaliere²⁹, E. Cavallaro¹⁴, D. Cavalli^{66a}, M. Cavalli-Sforza¹⁴, V. Cavasinni^{69a,69b}, E. Celebi^{12b}, F. Ceradini^{72a,72b}, L. Cerdà Alberich¹⁷¹, A.S. Cerqueira^{78a}, A. Cerri¹⁵³, L. Cerrito^{71a,71b}, F. Cerutti¹⁸, A. Cervelli^{23b,23a}, S.A. Cetin^{12b}, A. Chafaq^{34a}, D. Chakraborty¹¹⁹, S.K. Chan⁵⁷, W.S. Chan¹¹⁸, Y.L. Chan^{61a}, J.D. Chapman³¹, D.G. Charlton²¹, C.C. Chau³³, C.A. Chavez Barajas¹⁵³, S. Che¹²², A. Chegwidden¹⁰⁴, S. Chekanov⁶, S.V. Chekulaev^{165a}, G.A. Chelkov^{77,ap}, M.A. Chelstowska³⁵, C. Chen^{58a}, C.H. Chen⁷⁶, H. Chen²⁹, J. Chen^{58a}, J. Chen³⁸, S. Chen¹³³, S.J. Chen^{15b}, X. Chen^{15c,ao}, Y. Chen⁸⁰, Y-H. Chen⁴⁴, H.C. Cheng¹⁰³, H.J. Cheng^{15d}, A. Cheplakov⁷⁷, E. Cheremushkina¹⁴⁰, R. Cherkaoui El Moursli^{34e}, E. Cheu⁷, K. Cheung⁶², L. Chevalier¹⁴², V. Chiarella⁴⁹, G. Chiarelli^{69a}, G. Chiodini^{65a}, A.S. Chisholm³⁵, A. Chitan^{27b}, I. Chiu¹⁶⁰, Y.H. Chiu¹⁷³, M.V. Chizhov⁷⁷, K. Choi⁶³, A.R. Chomont¹²⁸, S. Chouridou¹⁵⁹, Y.S. Chow¹¹⁸, V. Christodoulou⁹², M.C. Chu^{61a}, J. Chudoba¹³⁷, A.J. Chuinard¹⁰¹, J.J. Chwastowski⁸², L. Chytka¹²⁶, D. Cinca⁴⁵, V. Cindro⁸⁹, I.A. Cioara²⁴, A. Ciocio¹⁸, F. Cirotto^{67a,67b}, Z.H. Citron¹⁷⁷, M. Citterio^{66a}, A. Clark⁵², M.R. Clark³⁸, P.J. Clark⁴⁸, C. Clement^{43a,43b}, Y. Coadou⁹⁹, M. Cobal^{64a,64c}, A. Coccaro^{53b,53a}, J. Cochran⁷⁶, A.E.C. Coimbra¹⁷⁷, L. Colasurdo¹¹⁷, B. Cole³⁸, A.P. Colijn¹¹⁸, J. Collot⁵⁶, P. Conde Muñoz^{136a,136b}, E. Coniavitis⁵⁰, S.H. Connell^{32b}, I.A. Connolly⁹⁸, S. Constantinescu^{27b}, F. Conventi^{67a,ar}, A.M. Cooper-Sarkar¹³¹, F. Cormier¹⁷², K.J.R. Cormier¹⁶⁴, M. Corradi^{70a,70b}, E.E. Corrigan⁹⁴, F. Corriveau^{101,ab}, A. Cortes-Gonzalez³⁵, M.J. Costa¹⁷¹, D. Costanzo¹⁴⁶, G. Cottin³¹, G. Cowan⁹¹, B.E. Cox⁹⁸, J. Crane⁹⁸, K. Cranmer¹²¹, S.J. Crawley⁵⁵, R.A. Creager¹³³, G. Cree³³, S. Crépé-Renaudin⁵⁶, F. Crescioli¹³², M. Cristinziani²⁴, V. Croft¹²¹,

G. Crosetti^{40b,40a}, A. Cueto⁹⁶, T. Cuhadar Donszelmann¹⁴⁶, A.R. Cukierman¹⁵⁰, J. Cúth⁹⁷,
 S. Czekierda⁸², P. Czodrowski³⁵, M.J. Da Cunha Sargedas De Sousa^{58b,136b}, C. Da Via⁹⁸,
 W. Dabrowski^{81a}, T. Dado^{28a,w}, S. Dahbi^{34e}, T. Dai¹⁰³, F. Dallaire¹⁰⁷, C. Dallapiccola¹⁰⁰, M. Dam³⁹,
 G. D'amen^{23b,23a}, J. Damp⁹⁷, J.R. Dandoy¹³³, M.F. Daneri³⁰, N.P. Dang^{178,j}, N.D Dann⁹⁸,
 M. Dannerger¹⁷², V. Dao³⁵, G. Darbo^{53b}, S. Darmora⁸, O. Dartsi⁵, A. Dattagupta¹²⁷, T. Daubney⁴⁴,
 S. D'Auria⁵⁵, W. Davey²⁴, C. David⁴⁴, T. Davidek¹³⁹, D.R. Davis⁴⁷, E. Dawe¹⁰², I. Dawson¹⁴⁶, K. De⁸,
 R. De Asmundis^{67a}, A. De Benedetti¹²⁴, M. De Beurs¹¹⁸, S. De Castro^{23b,23a}, S. De Cecco^{70a,70b},
 N. De Groot¹¹⁷, P. de Jong¹¹⁸, H. De la Torre¹⁰⁴, F. De Lorenzi⁷⁶, A. De Maria^{51,r}, D. De Pedis^{70a},
 A. De Salvo^{70a}, U. De Sanctis^{71a,71b}, A. De Santo¹⁵³, K. De Vasconcelos Corga⁹⁹,
 J.B. De Vivie De Regie¹²⁸, C. Debenedetti¹⁴³, D.V. Dedovich⁷⁷, N. Dehghanian³, M. Del Gaudio^{40b,40a},
 J. Del Peso⁹⁶, Y. Delabat Diaz⁴⁴, D. Delgove¹²⁸, F. Deliot¹⁴², C.M. Delitzsch⁷, M. Della Pietra^{67a,67b},
 D. Della Volpe⁵², A. Dell'Acqua³⁵, L. Dell'Asta²⁵, M. Delmastro⁵, C. Delporte¹²⁸, P.A. Delsart⁵⁶,
 D.A. DeMarco¹⁶⁴, S. Demers¹⁸⁰, M. Demichev⁷⁷, S.P. Denisov¹⁴⁰, D. Denysiuk¹¹⁸, L. D'Eramo¹³²,
 D. Derendarz⁸², J.E. Derkaoui^{34d}, F. Derue¹³², P. Dervan⁸⁸, K. Desch²⁴, C. Deterre⁴⁴, K. Dette¹⁶⁴,
 M.R. Devesa³⁰, P.O. Deviveiros³⁵, A. Dewhurst¹⁴¹, S. Dhaliwal²⁶, F.A. Di Bello⁵², A. Di Ciaccio^{71a,71b},
 L. Di Ciaccio⁵, W.K. Di Clemente¹³³, C. Di Donato^{67a,67b}, A. Di Girolamo³⁵, B. Di Micco^{72a,72b},
 R. Di Nardo¹⁰⁰, K.F. Di Petrillo⁵⁷, A. Di Simone⁵⁰, R. Di Sipio¹⁶⁴, D. Di Valentino³³, C. Diaconu⁹⁹,
 M. Diamond¹⁶⁴, F.A. Dias³⁹, T. Dias Do Vale^{136a}, M.A. Diaz^{144a}, J. Dickinson¹⁸, E.B. Diehl¹⁰³,
 J. Dietrich¹⁹, S. Díez Cornell⁴⁴, A. Dimitrievska¹⁸, J. Dingfelder²⁴, F. Dittus³⁵, F. Djama⁹⁹,
 T. Djobava^{156b}, J.I. Djuvsland^{59a}, M.A.B. Do Vale^{78c}, M. Dobre^{27b}, D. Dodsworth²⁶, C. Doglioni⁹⁴,
 J. Dolejsi¹³⁹, Z. Dolezal¹³⁹, M. Donadelli^{78d}, J. Donini³⁷, A. D'onofrio⁹⁰, M. D'Onofrio⁸⁸, J. Dopke¹⁴¹,
 A. Doria^{67a}, M.T. Dova⁸⁶, A.T. Doyle⁵⁵, E. Drechsler⁵¹, E. Dreyer¹⁴⁹, T. Dreyer⁵¹, Y. Du^{58b},
 J. Duarte-Campderros¹⁵⁸, F. Dubinin¹⁰⁸, M. Dubovsky^{28a}, A. Dubreuil⁵², E. Duchovni¹⁷⁷,
 G. Duckeck¹¹², A. Ducourthial¹³², O.A. Ducu^{107,v}, D. Duda¹¹³, A. Dudarev³⁵, A.C. Dudder⁹⁷,
 E.M. Duffield¹⁸, L. Duflot¹²⁸, M. Dührssen³⁵, C. Dülsen¹⁷⁹, M. Dumancic¹⁷⁷, A.E. Dumitriu^{27b,d},
 A.K. Duncan⁵⁵, M. Dunford^{59a}, A. Duperrin⁹⁹, H. Duran Yildiz^{4a}, M. Düren⁵⁴, A. Durglishvili^{156b},
 D. Duschinger⁴⁶, B. Dutta⁴⁴, D. Duvnjak¹, M. Dyndal⁴⁴, S. Dysch⁹⁸, B.S. Dziedzic⁸², C. Eckardt⁴⁴,
 K.M. Ecker¹¹³, R.C. Edgar¹⁰³, T. Eifert³⁵, G. Eigen¹⁷, K. Einsweiler¹⁸, T. Ekelof¹⁶⁹, M. El Kacimi^{34c},
 R. El Kosseifi⁹⁹, V. Ellajosyula⁹⁹, M. Ellert¹⁶⁹, F. Ellinghaus¹⁷⁹, A.A. Elliot⁹⁰, N. Ellis³⁵,
 J. Elmsheuser²⁹, M. Elsing³⁵, D. Emeliyanov¹⁴¹, Y. Enari¹⁶⁰, J.S. Ennis¹⁷⁵, M.B. Epland⁴⁷,
 J. Erdmann⁴⁵, A. Ereditato²⁰, S. Errede¹⁷⁰, M. Escalier¹²⁸, C. Escobar¹⁷¹, O. Estrada Pastor¹⁷¹,
 A.I. Etienne¹⁴², E. Etzion¹⁵⁸, H. Evans⁶³, A. Ezhilov¹³⁴, M. Ezzi^{34e}, F. Fabbri⁵⁵, L. Fabbri^{23b,23a},
 V. Fabiani¹¹⁷, G. Facini⁹², R.M. Faisca Rodrigues Pereira^{136a}, R.M. Fakhrutdinov¹⁴⁰, S. Falciano^{70a},
 P.J. Falke⁵, S. Falke⁵, J. Faltova¹³⁹, Y. Fang^{15a}, M. Fanti^{66a,66b}, A. Farbin⁸, A. Farilla^{72a},
 E.M. Farina^{68a,68b}, T. Farooque¹⁰⁴, S. Farrell¹⁸, S.M. Farrington¹⁷⁵, P. Farthouat³⁵, F. Fassi^{34e},
 P. Fassnacht³⁵, D. Fassouliotis⁹, M. Fucci Giannelli⁴⁸, A. Favareto^{53b,53a}, W.J. Fawcett⁵², L. Fayard¹²⁸,
 O.L. Fedin^{134,o}, W. Fedorko¹⁷², M. Feickert⁴¹, S. Feigl¹³⁰, L. Feligioni⁹⁹, C. Feng^{58b}, E.J. Feng³⁵,
 M. Feng⁴⁷, M.J. Fenton⁵⁵, A.B. Fenyuk¹⁴⁰, L. Feremenga⁸, J. Ferrando⁴⁴, A. Ferrari¹⁶⁹, P. Ferrari¹¹⁸,
 R. Ferrari^{68a}, D.E. Ferreira de Lima^{59b}, A. Ferrer¹⁷¹, D. Ferrere⁵², C. Ferretti¹⁰³, F. Fiedler⁹⁷,
 A. Filipčić⁸⁹, F. Filthaut¹¹⁷, K.D. Finelli²⁵, M.C.N. Fiolhais^{136a,136c,a}, L. Fiorini¹⁷¹, C. Fischer¹⁴,
 W.C. Fisher¹⁰⁴, N. Flaschel⁴⁴, I. Fleck¹⁴⁸, P. Fleischmann¹⁰³, R.R.M. Fletcher¹³³, T. Flick¹⁷⁹,
 B.M. Flierl¹¹², L.M. Flores¹³³, L.R. Flores Castillo^{61a}, N. Fomin¹⁷, G.T. Forcolin⁹⁸, A. Formica¹⁴²,
 F.A. Förster¹⁴, A.C. Forti⁹⁸, A.G. Foster²¹, D. Fournier¹²⁸, H. Fox⁸⁷, S. Fracchia¹⁴⁶, P. Francavilla^{69a,69b},
 M. Franchini^{23b,23a}, S. Franchino^{59a}, D. Francis³⁵, L. Franconi¹³⁰, M. Franklin⁵⁷, M. Frate¹⁶⁸,
 M. Fraternali^{68a,68b}, D. Freeborn⁹², S.M. Fressard-Batraneanu³⁵, B. Freund¹⁰⁷, W.S. Freund^{78b},
 D. Froidevaux³⁵, J.A. Frost¹³¹, C. Fukunaga¹⁶¹, E. Fullana Torregrosa¹⁷¹, T. Fusayasu¹¹⁴, J. Fuster¹⁷¹,
 O. Gabizon¹⁵⁷, A. Gabrielli^{23b,23a}, A. Gabrielli¹⁸, G.P. Gach^{81a}, S. Gadatsch⁵², P. Gadow¹¹³,

G. Gagliardi^{53b,53a}, L.G. Gagnon¹⁰⁷, C. Galea^{27b}, B. Galhardo^{136a,136c}, E.J. Gallas¹³¹, B.J. Gallop¹⁴¹, P. Gallus¹³⁸, G. Galster³⁹, R. Gamboa Goni⁹⁰, K.K. Gan¹²², S. Ganguly¹⁷⁷, Y. Gao⁸⁸, Y.S. Gao^{150,1}, C. García¹⁷¹, J.E. García Navarro¹⁷¹, J.A. García Pascual^{15a}, M. Garcia-Sciveres¹⁸, R.W. Gardner³⁶, N. Garelli¹⁵⁰, V. Garonne¹³⁰, K. Gasnikova⁴⁴, A. Gaudiello^{53b,53a}, G. Gaudio^{68a}, I.L. Gavrilenko¹⁰⁸, A. Gavrilyuk¹⁰⁹, C. Gay¹⁷², G. Gaycken²⁴, E.N. Gazis¹⁰, C.N.P. Gee¹⁴¹, J. Geisen⁵¹, M. Geisen⁹⁷, M.P. Geisler^{59a}, K. Gellerstedt^{43a,43b}, C. Gemme^{53b}, M.H. Genest⁵⁶, C. Geng¹⁰³, S. Gentile^{70a,70b}, C. Gentsos¹⁵⁹, S. George⁹¹, D. Gerbaudo¹⁴, G. Gessner⁴⁵, S. Ghasemi¹⁴⁸, M. Ghasemi Bostanabad¹⁷³, M. Ghneimat²⁴, B. Giacobbe^{23b}, S. Giagu^{70a,70b}, N. Giangiocomi^{23b,23a}, P. Giannetti^{69a}, A. Giannini^{67a,67b}, S.M. Gibson⁹¹, M. Gignac¹⁴³, D. Gillberg³³, G. Gilles¹⁷⁹, D.M. Gingrich^{3,aq}, M.P. Giordani^{64a,64c}, F.M. Giorgi^{23b}, P.F. Giraud¹⁴², P. Giromini⁵⁷, G. Giugliarelli^{64a,64c}, D. Giugni^{66a}, F. Juli¹³¹, M. Giulini^{59b}, S. Gkaitatzis¹⁵⁹, I. Gkialas^{9,i}, E.L. Gkougkousis¹⁴, P. Gkountoumis¹⁰, L.K. Gladilin¹¹¹, C. Glasman⁹⁶, J. Glatzer¹⁴, P.C.F. Glaysher⁴⁴, A. Glazov⁴⁴, M. Goblirsch-Kolb²⁶, J. Godlewski⁸², S. Goldfarb¹⁰², T. Golling⁵², D. Golubkov¹⁴⁰, A. Gomes^{136a,136b,136d}, R. Goncalves Gama^{78a}, R. Gonçalo^{136a}, G. Gonella⁵⁰, L. Gonella²¹, A. Gongadze⁷⁷, F. Gonnella²¹, J.L. Gonski⁵⁷, S. González de la Hoz¹⁷¹, S. Gonzalez-Sevilla⁵², L. Goossens³⁵, P.A. Gorbounov¹⁰⁹, H.A. Gordon²⁹, B. Gorini³⁵, E. Gorini^{65a,65b}, A. Gorišek⁸⁹, A.T. Goshaw⁴⁷, C. Gössling⁴⁵, M.I. Gostkin⁷⁷, C.A. Gottardo²⁴, C.R. Goudet¹²⁸, D. Goujami^{34c}, A.G. Goussiou¹⁴⁵, N. Govender^{32b,b}, C. Goy⁵, E. Gozani¹⁵⁷, I. Grabowska-Bold^{81a}, P.O.J. Gradin¹⁶⁹, E.C. Graham⁸⁸, J. Gramling¹⁶⁸, E. Gramstad¹³⁰, S. Grancagnolo¹⁹, V. Gratchev¹³⁴, P.M. Gravila^{27f}, C. Gray⁵⁵, H.M. Gray¹⁸, Z.D. Greenwood^{93,ag}, C. Grefe²⁴, K. Gregersen⁹², I.M. Gregor⁴⁴, P. Grenier¹⁵⁰, K. Grevtsov⁴⁴, J. Griffiths⁸, A.A. Grillo¹⁴³, K. Grimm¹⁵⁰, S. Grinstein^{14,x}, Ph. Gris³⁷, J.-F. Grivaz¹²⁸, S. Groh⁹⁷, E. Gross¹⁷⁷, J. Grosse-Knetter⁵¹, G.C. Grossi⁹³, Z.J. Grout⁹², C. Grud¹⁰³, A. Grummer¹¹⁶, L. Guan¹⁰³, W. Guan¹⁷⁸, J. Guenther³⁵, A. Guerguichon¹²⁸, F. Guescini^{165a}, D. Guest¹⁶⁸, R. Gugej⁵⁰, B. Gui¹²², T. Guillemin⁵, S. Guindon³⁵, U. Gul⁵⁵, C. Gumpert³⁵, J. Guo^{58c}, W. Guo¹⁰³, Y. Guo^{58a,q}, Z. Guo⁹⁹, R. Gupta⁴¹, S. Gurbuz^{12c}, G. Gustavino¹²⁴, B.J. Gutelman¹⁵⁷, P. Gutierrez¹²⁴, C. Gutschow⁹², C. Guyot¹⁴², M.P. Guzik^{81a}, C. Gwenlan¹³¹, C.B. Gwilliam⁸⁸, A. Haas¹²¹, C. Haber¹⁸, H.K. Hadavand⁸, N. Haddad^{34e}, A. Hadef^{58a}, S. Hageböck²⁴, M. Hagihara¹⁶⁶, H. Hakobyan^{181,*}, M. Haleem¹⁷⁴, J. Haley¹²⁵, G. Halladjian¹⁰⁴, G.D. Hallewell⁹⁹, K. Hamacher¹⁷⁹, P. Hamal¹²⁶, K. Hamano¹⁷³, A. Hamilton^{32a}, G.N. Hamity¹⁴⁶, K. Han^{58a,af}, L. Han^{58a}, S. Han^{15d}, K. Hanagaki^{79,t}, M. Hance¹⁴³, D.M. Handl¹¹², B. Haney¹³³, R. Hankache¹³², P. Hanke^{59a}, E. Hansen⁹⁴, J.B. Hansen³⁹, J.D. Hansen³⁹, M.C. Hansen²⁴, P.H. Hansen³⁹, K. Hara¹⁶⁶, A.S. Hard¹⁷⁸, T. Harenberg¹⁷⁹, S. Harkusha¹⁰⁵, P.F. Harrison¹⁷⁵, N.M. Hartmann¹¹², Y. Hasegawa¹⁴⁷, A. Hasib⁴⁸, S. Hassani¹⁴², S. Haug²⁰, R. Hauser¹⁰⁴, L. Hauswald⁴⁶, L.B. Havener³⁸, M. Havranek¹³⁸, C.M. Hawkes²¹, R.J. Hawkings³⁵, D. Hayden¹⁰⁴, C. Hayes¹⁵², C.P. Hays¹³¹, J.M. Hays⁹⁰, H.S. Hayward⁸⁸, S.J. Haywood¹⁴¹, M.P. Heath⁴⁸, V. Hedberg⁹⁴, L. Heelan⁸, S. Heer²⁴, K.K. Heidegger⁵⁰, J. Heilman³³, S. Heim⁴⁴, T. Heim¹⁸, B. Heinemann^{44,al}, J.J. Heinrich¹¹², L. Heinrich¹²¹, C. Heinz⁵⁴, J. Hejbal¹³⁷, L. Helary³⁵, A. Held¹⁷², S. Hellesund¹³⁰, S. Hellman^{43a,43b}, C. Helsens³⁵, R.C.W. Henderson⁸⁷, Y. Heng¹⁷⁸, S. Henkelmann¹⁷², A.M. Henriques Correia³⁵, G.H. Herbert¹⁹, H. Herde²⁶, V. Herget¹⁷⁴, Y. Hernández Jiménez^{32c}, H. Herr⁹⁷, M.G. Herrmann¹¹², G. Herten⁵⁰, R. Hertenberger¹¹², L. Hervas³⁵, T.C. Herwig¹³³, G.G. Hesketh⁹², N.P. Hessey^{165a}, J.W. Hetherly⁴¹, S. Higashino⁷⁹, E. Higón-Rodriguez¹⁷¹, K. Hildebrand³⁶, E. Hill¹⁷³, J.C. Hill³¹, K.K. Hill²⁹, K.H. Hiller⁴⁴, S.J. Hillier²¹, M. Hils⁴⁶, I. Hinchliffe¹⁸, M. Hirose¹²⁹, D. Hirschbuehl¹⁷⁹, B. Hiti⁸⁹, O. Hladik¹³⁷, D.R. Hlaluku^{32c}, X. Hoad⁴⁸, J. Hobbs¹⁵², N. Hod^{165a}, M.C. Hodgkinson¹⁴⁶, A. Hoecker³⁵, M.R. Hoeferkamp¹¹⁶, F. Hoenig¹¹², D. Hohn²⁴, D. Hohov¹²⁸, T.R. Holmes³⁶, M. Holzbock¹¹², M. Homann⁴⁵, S. Honda¹⁶⁶, T. Honda⁷⁹, T.M. Hong¹³⁵, A. Hönle¹¹³, B.H. Hooberman¹⁷⁰, W.H. Hopkins¹²⁷, Y. Horii¹¹⁵, P. Horn⁴⁶, A.J. Horton¹⁴⁹, L.A. Horyn³⁶, J-Y. Hostachy⁵⁶, A. Hostiuc¹⁴⁵, S. Hou¹⁵⁵, A. Hoummada^{34a}, J. Howarth⁹⁸, J. Hoya⁸⁶, M. Hrabovsky¹²⁶, J. Hrdinka³⁵, I. Hristova¹⁹, J. Hrvnac¹²⁸, A. Hrynevich¹⁰⁶,

T. Hryna'ova⁵, P.J. Hsu⁶², S.-C. Hsu¹⁴⁵, Q. Hu²⁹, S. Hu^{58c}, Y. Huang^{15a}, Z. Hubacek¹³⁸, F. Hubaut⁹⁹, M. Huebner²⁴, F. Huegging²⁴, T.B. Huffman¹³¹, E.W. Hughes³⁸, M. Huhtinen³⁵, R.F.H. Hunter³³, P. Huo¹⁵², A.M. Hupe³³, N. Huseynov^{77,ad}, J. Huston¹⁰⁴, J. Huth⁵⁷, R. Hyneman¹⁰³, G. Iacobucci⁵², G. Iakovidis²⁹, I. Ibragimov¹⁴⁸, L. Iconomidou-Fayard¹²⁸, Z. Idrissi^{34e}, P. Iengo³⁵, R. Ignazzi³⁹, O. Igonkina^{118,z}, R. Iguchi¹⁶⁰, T. Iizawa⁵², Y. Ikegami⁷⁹, M. Ikeno⁷⁹, D. Iliadis¹⁵⁹, N. Ilic¹⁵⁰, F. Iltzsche⁴⁶, G. Introzzi^{68a,68b}, M. Iodice^{72a}, K. Iordanidou³⁸, V. Ippolito^{70a,70b}, M.F. Isacson¹⁶⁹, N. Ishijima¹²⁹, M. Ishino¹⁶⁰, M. Ishitsuka¹⁶², W. Islam¹²⁵, C. Issever¹³¹, S. Istin^{12c,ak}, F. Ito¹⁶⁶, J.M. Iturbe Ponce^{61a}, R. Iuppa^{73a,73b}, A. Ivina¹⁷⁷, H. Iwasaki⁷⁹, J.M. Izen⁴², V. Izzo^{67a}, S. Jabbar³, P. Jacka¹³⁷, P. Jackson¹, R.M. Jacobs²⁴, V. Jain², G. Jäkel¹⁷⁹, K.B. Jakobi⁹⁷, K. Jakobs⁵⁰, S. Jakobsen⁷⁴, T. Jakoubek¹³⁷, D.O. Jamin¹²⁵, D.K. Jana⁹³, R. Jansky⁵², J. Janssen²⁴, M. Janus⁵¹, P.A. Janus^{81a}, G. Jarlskog⁹⁴, N. Javadov^{77,ad}, T. Javůrek⁵⁰, M. Javurkova⁵⁰, F. Jeanneau¹⁴², L. Jeanty¹⁸, J. Jejelava^{156a,ae}, A. Jelinskas¹⁷⁵, P. Jenni^{50,c}, J. Jeong⁴⁴, S. Jézéquel⁵, H. Ji¹⁷⁸, J. Jia¹⁵², H. Jiang⁷⁶, Y. Jiang^{58a}, Z. Jiang¹⁵⁰, S. Jiggins⁵⁰, F.A. Jimenez Morales³⁷, J. Jimenez Pena¹⁷¹, S. Jin^{15b}, A. Jinaru^{27b}, O. Jinnouchi¹⁶², H. Jivan^{32c}, P. Johansson¹⁴⁶, K.A. Johns⁷, C.A. Johnson⁶³, W.J. Johnson¹⁴⁵, K. Jon-And^{43a,43b}, R.W.L. Jones⁸⁷, S.D. Jones¹⁵³, S. Jones⁷, T.J. Jones⁸⁸, J. Jongmanns^{59a}, P.M. Jorge^{136a,136b}, J. Jovicevic^{165a}, X. Ju¹⁷⁸, J.J. Junggeburth¹¹³, A. Juste Rozas^{14,x}, A. Kaczmarska⁸², M. Kado¹²⁸, H. Kagan¹²², M. Kagan¹⁵⁰, T. Kaji¹⁷⁶, E. Kajomovitz¹⁵⁷, C.W. Kalderon⁹⁴, A. Kaluza⁹⁷, S. Kama⁴¹, A. Kamenshchikov¹⁴⁰, L. Kanjir⁸⁹, Y. Kano¹⁶⁰, V.A. Kantserov¹¹⁰, J. Kanzaki⁷⁹, B. Kaplan¹²¹, L.S. Kaplan¹⁷⁸, D. Kar^{32c}, M.J. Kareem^{165b}, E. Karentzos¹⁰, S.N. Karpov⁷⁷, Z.M. Karpova⁷⁷, V. Kartvelishvili⁸⁷, A.N. Karyukhin¹⁴⁰, K. Kasahara¹⁶⁶, L. Kashif¹⁷⁸, R.D. Kass¹²², A. Kastanas¹⁵¹, Y. Kataoka¹⁶⁰, C. Kato¹⁶⁰, J. Katzy⁴⁴, K. Kawade⁸⁰, K. Kawagoe⁸⁵, T. Kawamoto¹⁶⁰, G. Kawamura⁵¹, E.F. Kay⁸⁸, V.F. Kazanin^{120b,120a}, R. Keeler¹⁷³, R. Kehoe⁴¹, J.S. Keller³³, E. Kellermann⁹⁴, J.J. Kempster²¹, J. Kendrick²¹, O. Kepka¹³⁷, S. Kersten¹⁷⁹, B.P. Kerševan⁸⁹, R.A. Keyes¹⁰¹, M. Khader¹⁷⁰, F. Khalil-Zada¹³, A. Khanov¹²⁵, A.G. Kharlamov^{120b,120a}, T. Kharlamova^{120b,120a}, A. Khodinov¹⁶³, T.J. Khoo⁵², E. Khramov⁷⁷, J. Khubua^{156b}, S. Kido⁸⁰, M. Kiehn⁵², C.R. Kilby⁹¹, S.H. Kim¹⁶⁶, Y.K. Kim³⁶, N. Kimura^{64a,64c}, O.M. Kind¹⁹, B.T. King⁸⁸, D. Kirchmeier⁴⁶, J. Kirk¹⁴¹, A.E. Kiryunin¹¹³, T. Kishimoto¹⁶⁰, D. Kisielewska^{81a}, V. Kitali⁴⁴, O. Kiverny⁵, E. Kladiva^{28b}, T. Klapdor-Kleingrothaus⁵⁰, M.H. Klein¹⁰³, M. Klein⁸⁸, U. Klein⁸⁸, K. Kleinknecht⁹⁷, P. Klimek¹¹⁹, A. Klimentov²⁹, R. Klingenberg^{45,*}, T. Klingl²⁴, T. Klioutchnikova³⁵, F.F. Klitzner¹¹², P. Kluit¹¹⁸, S. Kluth¹¹³, E. Kneringer⁷⁴, E.B.F.G. Knoops⁹⁹, A. Knue⁵⁰, A. Kobayashi¹⁶⁰, D. Kobayashi⁸⁵, T. Kobayashi¹⁶⁰, M. Kobel⁴⁶, M. Kocian¹⁵⁰, P. Kodys¹³⁹, T. Koffas³³, E. Koffeman¹¹⁸, N.M. Köhler¹¹³, T. Koi¹⁵⁰, M. Kolb^{59b}, I. Koletsou⁵, T. Kondo⁷⁹, N. Kondrashova^{58c}, K. Köneke⁵⁰, A.C. König¹¹⁷, T. Kono⁷⁹, R. Konoplich^{121,ah}, V. Konstantinides⁹², N. Konstantinidis⁹², B. Konya⁹⁴, R. Kopeliansky⁶³, S. Koperny^{81a}, K. Korcyl⁸², K. Kordas¹⁵⁹, A. Korn⁹², I. Korolkov¹⁴, E.V. Korolkova¹⁴⁶, O. Kortner¹¹³, S. Kortner¹¹³, T. Kosek¹³⁹, V.V. Kostyukhin²⁴, A. Kotwal⁴⁷, A. Koulouris¹⁰, A. Kourkoumeli-Charalampidi^{68a,68b}, C. Kourkoumelis⁹, E. Kourlitis¹⁴⁶, V. Kouskoura²⁹, A.B. Kowalewska⁸², R. Kowalewski¹⁷³, T.Z. Kowalski^{81a}, C. Kozakai¹⁶⁰, W. Kozanecki¹⁴², A.S. Kozhin¹⁴⁰, V.A. Kramarenko¹¹¹, G. Kramberger⁸⁹, D. Krasnopervtsev¹¹⁰, M.W. Krasny¹³², A. Krasznahorkay³⁵, D. Krauss¹¹³, J.A. Kremer^{81a}, J. Kretzschmar⁸⁸, P. Krieger¹⁶⁴, K. Krizka¹⁸, K. Kroeninger⁴⁵, H. Kroha¹¹³, J. Kroll¹³⁷, J. Kroll¹³³, J. Krstic¹⁶, U. Kruchonak⁷⁷, H. Krüger²⁴, N. Krumnack⁷⁶, M.C. Kruse⁴⁷, T. Kubota¹⁰², S. Kuday^{4b}, J.T. Kuechler¹⁷⁹, S. Kuehn³⁵, A. Kugel^{59a}, F. Kuger¹⁷⁴, T. Kuhl⁴⁴, V. Kukhtin⁷⁷, R. Kukla⁹⁹, Y. Kulchitsky¹⁰⁵, S. Kuleshov^{144b}, Y.P. Kulinich¹⁷⁰, M. Kuna⁵⁶, T. Kunigo⁸³, A. Kupco¹³⁷, T. Kupfer⁴⁵, O. Kuprash¹⁵⁸, H. Kurashige⁸⁰, L.L. Kurchaninov^{165a}, Y.A. Kurochkin¹⁰⁵, M.G. Kurth^{15d}, E.S. Kuwertz¹⁷³, M. Kuze¹⁶², J. Kvita¹²⁶, T. Kwan¹⁰¹, A. La Rosa¹¹³, J.L. La Rosa Navarro^{78d}, L. La Rotonda^{40b,40a}, F. La Ruffa^{40b,40a}, C. Lacasta¹⁷¹, F. Lacava^{70a,70b}, J. Lacey⁴⁴, D.P.J. Lack⁹⁸, H. Lacker¹⁹, D. Lacour¹³², E. Ladygin⁷⁷, R. Lafaye⁵, B. Laforge¹³², T. Lagouri^{32c}, S. Lai⁵¹, S. Lammers⁶³, W. Lampl⁷, E. Lançon²⁹,

U. Landgraf⁵⁰, M.P.J. Landon⁹⁰, M.C. Lanfermann⁵², V.S. Lang⁴⁴, J.C. Lange¹⁴, R.J. Langenberg³⁵,
 A.J. Lankford¹⁶⁸, F. Lanni²⁹, K. Lantzsch²⁴, A. Lanza^{68a}, A. Lapertosa^{53b,53a}, S. Laplace¹³²,
 J.F. Laporte¹⁴², T. Lari^{66a}, F. Lasagni Manghi^{23b,23a}, M. Lassnig³⁵, T.S. Lau^{61a}, A. Laudrain¹²⁸,
 M. Lavorgna^{67a,67b}, A.T. Law¹⁴³, P. Laycock⁸⁸, M. Lazzaroni^{66a,66b}, B. Le¹⁰², O. Le Dertz¹³²,
 E. Le Guiriec⁹⁹, E.P. Le Quilleuc¹⁴², M. LeBlanc⁷, T. LeCompte⁶, F. Ledroit-Guillon⁵⁶, C.A. Lee²⁹,
 G.R. Lee^{144a}, L. Lee⁵⁷, S.C. Lee¹⁵⁵, B. Lefebvre¹⁰¹, M. Lefebvre¹⁷³, F. Legger¹¹², C. Leggett¹⁸,
 N. Lehmann¹⁷⁹, G. Lehmann Miotto³⁵, W.A. Leight⁴⁴, A. Leisos^{159,u}, M.A.L. Leite^{78d}, R. Leitner¹³⁹,
 D. Lellouch¹⁷⁷, B. Lemmer⁵¹, K.J.C. Leney⁹², T. Lenz²⁴, B. Lenzi³⁵, R. Leone⁷, S. Leone^{69a},
 C. Leonidopoulos⁴⁸, G. Lerner¹⁵³, C. Leroy¹⁰⁷, R. Les¹⁶⁴, A.A.J. Lesage¹⁴², C.G. Lester³¹,
 M. Levchenko¹³⁴, J. Levêque⁵, D. Levin¹⁰³, L.J. Levinson¹⁷⁷, D. Lewis⁹⁰, B. Li¹⁰³, C-Q. Li^{58a}, H. Li^{58b},
 L. Li^{58c}, Q. Li^{15d}, Q.Y. Li^{58a}, S. Li^{58d,58c}, X. Li^{58c}, Y. Li¹⁴⁸, Z. Liang^{15a}, B. Liberti^{71a}, A. Liblong¹⁶⁴,
 K. Lie^{61c}, S. Liem¹¹⁸, A. Limosani¹⁵⁴, C.Y. Lin³¹, K. Lin¹⁰⁴, T.H. Lin⁹⁷, R.A. Linck⁶³,
 B.E. Lindquist¹⁵², A.L. Lioni⁵², E. Lipeles¹³³, A. Lipniacka¹⁷, M. Lisovyi^{59b}, T.M. Liss^{170,an},
 A. Lister¹⁷², A.M. Litke¹⁴³, J.D. Little⁸, B. Liu⁷⁶, B.L. Liu⁶, H.B. Liu²⁹, H. Liu¹⁰³, J.B. Liu^{58a},
 J.K.K. Liu¹³¹, K. Liu¹³², M. Liu^{58a}, P. Liu¹⁸, Y. Liu^{15a}, Y.L. Liu^{58a}, Y.W. Liu^{58a}, M. Livan^{68a,68b},
 A. Lleres⁵⁶, J. Llorente Merino^{15a}, S.L. Lloyd⁹⁰, C.Y. Lo^{61b}, F. Lo Sterzo⁴¹, E.M. Lobodzinska⁴⁴,
 P. Loch⁷, A. Loesle⁵⁰, K.M. Loew²⁶, T. Lohse¹⁹, K. Lohwasser¹⁴⁶, M. Lokajicek¹³⁷, B.A. Long²⁵,
 J.D. Long¹⁷⁰, R.E. Long⁸⁷, L. Longo^{65a,65b}, K.A.Looper¹²², J.A. Lopez^{144b}, I. Lopez Paz¹⁴,
 A. Lopez Solis¹⁴⁶, J. Lorenz¹¹², N. Lorenzo Martinez⁵, M. Losada²², P.J. Lösel¹¹², X. Lou⁴⁴, X. Lou^{15a},
 A. Lounis¹²⁸, J. Love⁶, P.A. Love⁸⁷, J.J. Lozano Bahilo¹⁷¹, H. Lu^{61a}, M. Lu^{58a}, N. Lu¹⁰³, Y.J. Lu⁶²,
 H.J. Lubatti¹⁴⁵, C. Luci^{70a,70b}, A. Lucotte⁵⁶, C. Luedtke⁵⁰, F. Luehring⁶³, I. Luise¹³², W. Lukas⁷⁴,
 L. Luminari^{70a}, B. Lund-Jensen¹⁵¹, M.S. Lutz¹⁰⁰, P.M. Luzi¹³², D. Lynn²⁹, R. Lysak¹³⁷, E. Lytken⁹⁴,
 F. Lyu^{15a}, V. Lyubushkin⁷⁷, H. Ma²⁹, L.L. Ma^{58b}, Y. Ma^{58b}, G. Maccarrone⁴⁹, A. Macchiolo¹¹³,
 C.M. Macdonald¹⁴⁶, J. Machado Miguens^{133,136b}, D. Madaffari¹⁷¹, R. Madar³⁷, W.F. Mader⁴⁶,
 A. Madsen⁴⁴, N. Madysa⁴⁶, J. Maeda⁸⁰, K. Maekawa¹⁶⁰, S. Maeland¹⁷, T. Maeno²⁹, A.S. Maevskiy¹¹¹,
 V. Magerl⁵⁰, C. Maidantchik^{78b}, T. Maier¹¹², A. Maio^{136a,136b,136d}, O. Majersky^{28a}, S. Majewski¹²⁷,
 Y. Makida⁷⁹, N. Makovec¹²⁸, B. Malaescu¹³², Pa. Malecki⁸², V.P. Maleev¹³⁴, F. Malek⁵⁶, U. Mallik⁷⁵,
 D. Malon⁶, C. Malone³¹, S. Maltezos¹⁰, S. Malyukov³⁵, J. Mamuzic¹⁷¹, G. Mancini⁴⁹, I. Mandic⁸⁹,
 J. Maneira^{136a}, L. Manhaes de Andrade Filho^{78a}, J. Manjarres Ramos⁴⁶, K.H. Mankinen⁹⁴, A. Mann¹¹²,
 A. Manousos⁷⁴, B. Mansoulie¹⁴², J.D. Mansour^{15a}, M. Mantoani⁵¹, S. Manzoni^{66a,66b}, G. Marceca³⁰,
 L. March⁵², L. Marchese¹³¹, G. Marchiori¹³², M. Marcisovsky¹³⁷, C.A. Marin Tobon³⁵,
 M. Marjanovic³⁷, D.E. Marley¹⁰³, F. Marroquim^{78b}, Z. Marshall¹⁸, M.U.F Martensson¹⁶⁹,
 S. Marti-Garcia¹⁷¹, C.B. Martin¹²², T.A. Martin¹⁷⁵, V.J. Martin⁴⁸, B. Martin dit Latour¹⁷,
 M. Martinez^{14,x}, V.I. Martinez Outschoorn¹⁰⁰, S. Martin-Haugh¹⁴¹, V.S. Martoiu^{27b}, A.C. Martyniuk⁹²,
 A. Marzin³⁵, L. Masetti⁹⁷, T. Mashimo¹⁶⁰, R. Mashinistov¹⁰⁸, J. Masik⁹⁸, A.L. Maslennikov^{120b,120a},
 L.H. Mason¹⁰², L. Massa^{71a,71b}, P. Mastrandrea⁵, A. Mastroberardino^{40b,40a}, T. Masubuchi¹⁶⁰,
 P. Mättig¹⁷⁹, J. Maurer^{27b}, B. Maček⁸⁹, S.J. Maxfield⁸⁸, D.A. Maximov^{120b,120a}, R. Mazini¹⁵⁵,
 I. Maznas¹⁵⁹, S.M. Mazza¹⁴³, N.C. Mc Fadden¹¹⁶, G. Mc Goldrick¹⁶⁴, S.P. Mc Kee¹⁰³, A. McCarn¹⁰³,
 T.G. McCarthy¹¹³, L.I. McClymont⁹², E.F. McDonald¹⁰², J.A. McFayden³⁵, G. Mchedlidze⁵¹,
 M.A. McKay⁴¹, K.D. McLean¹⁷³, S.J. McMahon¹⁴¹, P.C. McNamara¹⁰², C.J. McNicol¹⁷⁵,
 R.A. McPherson^{173,ab}, J.E. Mdhuli^{32c}, Z.A. Meadows¹⁰⁰, S. Meehan¹⁴⁵, T. Megy⁵⁰, S. Mehlhase¹¹²,
 A. Mehta⁸⁸, T. Meideck⁵⁶, B. Meirose⁴², D. Melini^{171,g}, B.R. Mellado Garcia^{32c}, J.D. Mellenthin⁵¹,
 M. Melo^{28a}, F. Meloni⁴⁴, A. Melzer²⁴, S.B. Menary⁹⁸, E.D. Mendes Gouveia^{136a}, L. Meng⁸⁸,
 X.T. Meng¹⁰³, A. Mengarelli^{23b,23a}, S. Menke¹¹³, E. Meoni^{40b,40a}, S. Mergelmeyer¹⁹, C. Merlassino²⁰,
 P. Mermod⁵², L. Merola^{67a,67b}, C. Meroni^{66a}, F.S. Merritt³⁶, A. Messina^{70a,70b}, J. Metcalf⁶,
 A.S. Mete¹⁶⁸, C. Meyer¹³³, J. Meyer¹⁵⁷, J-P. Meyer¹⁴², H. Meyer Zu Theenhausen^{59a}, F. Miano¹⁵³,
 R.P. Middleton¹⁴¹, L. Mijovic⁴⁸, G. Mikenberg¹⁷⁷, M. Mikestikova¹³⁷, M. Mikuž⁸⁹, M. Milesi¹⁰²,

A. Milic¹⁶⁴, D.A. Millar⁹⁰, D.W. Miller³⁶, A. Milov¹⁷⁷, D.A. Milstead^{43a,43b}, A.A. Minaenko¹⁴⁰,
 M. Miñano Moya¹⁷¹, I.A. Minashvili^{156b}, A.I. Mincer¹²¹, B. Mindur^{81a}, M. Mineev⁷⁷, Y. Minegishi¹⁶⁰,
 Y. Ming¹⁷⁸, L.M. Mir¹⁴, A. Mirta^{65a,65b}, K.P. Mistry¹³³, T. Mitani¹⁷⁶, J. Mitrevski¹¹², V.A. Mitsou¹⁷¹,
 A. Miucci²⁰, P.S. Miyagawa¹⁴⁶, A. Mizukami⁷⁹, J.U. Mjörnmark⁹⁴, T. Mkrtchyan¹⁸¹, M. Mlynarikova¹³⁹,
 T. Moa^{43a,43b}, K. Mochizuki¹⁰⁷, P. Mogg⁵⁰, S. Mohapatra³⁸, S. Molander^{43a,43b}, R. Moles-Valls²⁴,
 M.C. Mondragon¹⁰⁴, K. Mönig⁴⁴, J. Monk³⁹, E. Monnier⁹⁹, A. Montalbano¹⁴⁹, J. Montejo Berlingen³⁵,
 F. Monticelli⁸⁶, S. Monzani^{66a}, R.W. Moore³, N. Morange¹²⁸, D. Moreno²², M. Moreno Llácer³⁵,
 P. Morettini^{53b}, M. Morgenstern¹¹⁸, S. Morgenstern⁴⁶, D. Mori¹⁴⁹, T. Mori¹⁶⁰, M. Morii⁵⁷,
 M. Morinaga¹⁷⁶, V. Morisbak¹³⁰, A.K. Morley³⁵, G. Mornacchi³⁵, A.P. Morris⁹², J.D. Morris⁹⁰,
 L. Morvaj¹⁵², P. Moschovakos¹⁰, M. Mosidze^{156b}, H.J. Moss¹⁴⁶, J. Moss^{150,m}, K. Motohashi¹⁶²,
 R. Mount¹⁵⁰, E. Mountricha³⁵, E.J.W. Moyse¹⁰⁰, S. Muanza⁹⁹, F. Mueller¹¹³, J. Mueller¹³⁵,
 R.S.P. Mueller¹¹², D. Muenstermann⁸⁷, P. Mullen⁵⁵, G.A. Mullier²⁰, F.J. Munoz Sanchez⁹⁸, P. Murin^{28b},
 W.J. Murray^{175,141}, A. Murrone^{66a,66b}, M. Muškinja⁸⁹, C. Mwewa^{32a}, A.G. Myagkov^{140,ai}, J. Myers¹²⁷,
 M. Myska¹³⁸, B.P. Nachman¹⁸, O. Nackenhorst⁴⁵, K. Nagai¹³¹, K. Nagano⁷⁹, Y. Nagasaka⁶⁰,
 K. Nagata¹⁶⁶, M. Nagel⁵⁰, E. Nagy⁹⁹, A.M. Nairz³⁵, Y. Nakahama¹¹⁵, K. Nakamura⁷⁹, T. Nakamura¹⁶⁰,
 I. Nakano¹²³, H. Nanjo¹²⁹, F. Napolitano^{59a}, R.F. Naranjo Garcia⁴⁴, R. Narayan¹¹, D.I. Narrias Villar^{59a},
 I. Naryshkin¹³⁴, T. Naumann⁴⁴, G. Navarro²², R. Nayyar⁷, H.A. Neal¹⁰³, P.Y. Nechaeva¹⁰⁸, T.J. Neep¹⁴²,
 A. Negri^{68a,68b}, M. Negrini^{23b}, S. Nektarijevic¹¹⁷, C. Nellist⁵¹, M.E. Nelson¹³¹, S. Nemecek¹³⁷,
 P. Nemethy¹²¹, M. Nessi^{35,e}, M.S. Neubauer¹⁷⁰, M. Neumann¹⁷⁹, P.R. Newman²¹, T.Y. Ng^{61c}, Y.S. Ng¹⁹,
 H.D.N. Nguyen⁹⁹, T. Nguyen Manh¹⁰⁷, E. Nibigira³⁷, R.B. Nickerson¹³¹, R. Nicolaïdou¹⁴²,
 J. Nielsen¹⁴³, N. Nikiforou¹¹, V. Nikolaenko^{140,ai}, I. Nikolic-Audit¹³², K. Nikolopoulos²¹, P. Nilsson²⁹,
 Y. Ninomiya⁷⁹, A. Nisati^{70a}, N. Nishu^{58c}, R. Nisius¹¹³, I. Nitsche⁴⁵, T. Nitta¹⁷⁶, T. Nobe¹⁶⁰,
 Y. Noguchi⁸³, M. Nomachi¹²⁹, I. Nomidis¹³², M.A. Nomura²⁹, T. Nooney⁹⁰, M. Nordberg³⁵,
 N. Norjoharuddeen¹³¹, T. Novak⁸⁹, O. Novgorodova⁴⁶, R. Novotny¹³⁸, L. Nozka¹²⁶, K. Ntekas¹⁶⁸,
 E. Nurse⁹², F. Nuti¹⁰², F.G. Oakham^{33,ad}, H. Oberlack¹¹³, T. Obermann²⁴, J. Ocariz¹³², A. Ochi⁸⁰,
 I. Ochoa³⁸, J.P. Ochoa-Ricoux^{144a}, K. O'Connor²⁶, S. Oda⁸⁵, S. Odaka⁷⁹, S. Oerdekk⁵¹, A. Oh⁹⁸,
 S.H. Oh⁴⁷, C.C. Ohm¹⁵¹, H. Oide^{53b,53a}, H. Okawa¹⁶⁶, Y. Okazaki⁸³, Y. Okumura¹⁶⁰, T. Okuyama⁷⁹,
 A. Olariu^{27b}, L.F. Oleiro Seabra^{136a}, S.A. Olivares Pino^{144a}, D. Oliveira Damazio²⁹, J.L. Oliver¹,
 M.J.R. Olsson³⁶, A. Olszewski⁸², J. Olszowska⁸², D.C. O'Neil¹⁴⁹, A. Onofre^{136a,136e}, K. Onogi¹¹⁵,
 P.U.E. Onyisi¹¹, H. Oppen¹³⁰, M.J. Oreglia³⁶, Y. Oren¹⁵⁸, D. Orestano^{72a,72b}, E.C. Orgill⁹⁸,
 N. Orlando^{61b}, A.A. O'Rourke⁴⁴, R.S. Orr¹⁶⁴, B. Osculati^{53b,53a,*}, V. O'Shea⁵⁵, R. Ospanov^{58a},
 G. Otero y Garzon³⁰, H. Otono⁸⁵, M. Ouchrif^{34d}, F. Ould-Saada¹³⁰, A. Ouraou¹⁴², Q. Ouyang^{15a},
 M. Owen⁵⁵, R.E. Owen²¹, V.E. Ozcan^{12c}, N. Ozturk⁸, J. Pacalt¹²⁶, H.A. Pacey³¹, K. Pachal¹⁴⁹,
 A. Pacheco Pages¹⁴, L. Pacheco Rodriguez¹⁴², C. Padilla Aranda¹⁴, S. Pagan Griso¹⁸, M. Paganini¹⁸⁰,
 G. Palacino⁶³, S. Palazzo^{40b,40a}, S. Palestini³⁵, M. Palka^{81b}, D. Pallin³⁷, I. Panagoulias¹⁰, C.E. Pandini³⁵,
 J.G. Panduro Vazquez⁹¹, P. Pani³⁵, G. Panizzo^{64a,64c}, L. Paolozzi⁵², T.D. Papadopoulou¹⁰,
 K. Papageorgiou^{9,i}, A. Paramonov⁶, D. Paredes Hernandez^{61b}, S.R. Paredes Saenz¹³¹, B. Parida^{58c},
 A.J. Parker⁸⁷, K.A. Parker⁴⁴, M.A. Parker³¹, F. Parodi^{53b,53a}, J.A. Parsons³⁸, U. Parzefall⁵⁰,
 V.R. Pascuzzi¹⁶⁴, J.M.P. Pasner¹⁴³, E. Pasqualucci^{70a}, S. Passaggio^{53b}, F. Pastore⁹¹, P. Pasuwan^{43a,43b},
 S. Pataria⁹⁷, J.R. Pater⁹⁸, A. Pathak^{178,j}, T. Pauly³⁵, B. Pearson¹¹³, M. Pedersen¹³⁰, L. Pedraza Diaz¹¹⁷,
 R. Pedro^{136a,136b}, S.V. Peleganchuk^{120b,120a}, O. Penc¹³⁷, C. Peng^{15d}, H. Peng^{58a}, B.S. Peralva^{78a},
 M.M. Perego¹⁴², A.P. Pereira Peixoto^{136a}, D.V. Perepelitsa²⁹, F. Peri¹⁹, L. Perini^{66a,66b}, H. Pernegger³⁵,
 S. Perrella^{67a,67b}, V.D. Peshekhanov^{77,*}, K. Peters⁴⁴, R.F.Y. Peters⁹⁸, B.A. Petersen³⁵, T.C. Petersen³⁹,
 E. Petit⁵⁶, A. Petridis¹, C. Petridou¹⁵⁹, P. Petroff¹²⁸, E. Petrolo^{70a}, M. Petrov¹³¹, F. Petrucci^{72a,72b},
 M. Pettee¹⁸⁰, N.E. Pettersson¹⁰⁰, A. Peyaud¹⁴², R. Pezoa^{144b}, T. Pham¹⁰², F.H. Phillips¹⁰⁴,
 P.W. Phillips¹⁴¹, G. Piacquadro¹⁵², E. Pianori¹⁸, A. Picazio¹⁰⁰, M.A. Pickering¹³¹, R. Piegaia³⁰,
 J.E. Pilcher³⁶, A.D. Pilkington⁹⁸, M. Pinamonti^{71a,71b}, J.L. Pinfold³, M. Pitt¹⁷⁷, M.-A. Pleier²⁹,

V. Pleskot¹³⁹, E. Plotnikova⁷⁷, D. Pluth⁷⁶, P. Podberezko^{120b,120a}, R. Poettgen⁹⁴, R. Poggi⁵²,
 L. Poggioli¹²⁸, I. Pogrebnyak¹⁰⁴, D. Pohl²⁴, I. Pokharej⁵¹, G. Polesello^{68a}, A. Poley⁴⁴,
 A. Policicchio^{40b,40a}, R. Polifka³⁵, A. Polini^{23b}, C.S. Pollard⁴⁴, V. Polychronakos²⁹, D. Ponomarenko¹¹⁰,
 L. Pontecorvo^{70a}, G.A. Popeneciu^{27d}, D.M. Portillo Quintero¹³², S. Pospisil¹³⁸, K. Potamianos⁴⁴,
 I.N. Potrap⁷⁷, C.J. Potter³¹, H. Potti¹¹, T. Poulsen⁹⁴, J. Poveda³⁵, T.D. Powell¹⁴⁶,
 M.E. Pozo Astigarraga³⁵, P. Pralavorio⁹⁹, S. Prell⁷⁶, D. Price⁹⁸, M. Primavera^{65a}, S. Prince¹⁰¹,
 N. Proklova¹¹⁰, K. Prokofiev^{61c}, F. Prokoshin^{144b}, S. Protopopescu²⁹, J. Proudfoot⁶, M. Przybycien^{81a},
 A. Puri¹⁷⁰, P. Puzo¹²⁸, J. Qian¹⁰³, Y. Qin⁹⁸, A. Quadt⁵¹, M. Queitsch-Maitland⁴⁴, A. Qureshi¹,
 P. Rados¹⁰², F. Ragusa^{66a,66b}, G. Rahal⁹⁵, J.A. Raine⁹⁸, S. Rajagopalan²⁹, A. Ramirez Morales⁹⁰,
 T. Rashid¹²⁸, S. Raspopov⁵, M.G. Ratti^{66a,66b}, D.M. Rauch⁴⁴, F. Rauscher¹¹², S. Rave⁹⁷, B. Ravina¹⁴⁶,
 I. Ravinovich¹⁷⁷, J.H. Rawling⁹⁸, M. Raymond³⁵, A.L. Read¹³⁰, N.P. Readioff⁵⁶, M. Reale^{65a,65b},
 D.M. Rebuzzi^{68a,68b}, A. Redelbach¹⁷⁴, G. Redlinger²⁹, R. Reece¹⁴³, R.G. Reed^{32c}, K. Reeves⁴²,
 L. Rehnisch¹⁹, J. Reichert¹³³, A. Reiss⁹⁷, C. Rembser³⁵, H. Ren^{15d}, M. Rescigno^{70a}, S. Resconi^{66a},
 E.D. Ressegue¹³³, S. Rettie¹⁷², E. Reynolds²¹, O.L. Rezanova^{120b,120a}, P. Reznicek¹³⁹, R. Richter¹¹³,
 S. Richter⁹², E. Richter-Was^{81b}, O. Ricken²⁴, M. Ridel¹³², P. Rieck¹¹³, C.J. Riegel¹⁷⁹, O. Rifki⁴⁴,
 M. Rijssenbeek¹⁵², A. Rimoldi^{68a,68b}, M. Rimoldi²⁰, L. Rinaldi^{23b}, G. Ripellino¹⁵¹, B. Ristić⁸⁷,
 E. Ritsch³⁵, I. Riu¹⁴, J.C. Rivera Vergara^{144a}, F. Rizatdinova¹²⁵, E. Rizvi⁹⁰, C. Rizzi¹⁴, R.T. Roberts⁹⁸,
 S.H. Robertson^{101,ab}, A. Robichaud-Veronneau¹⁰¹, D. Robinson³¹, J.E.M. Robinson⁴⁴, A. Robson⁵⁵,
 E. Rocco⁹⁷, C. Roda^{69a,69b}, Y. Rodina⁹⁹, S. Rodriguez Bosca¹⁷¹, A. Rodriguez Perez¹⁴,
 D. Rodriguez Rodriguez¹⁷¹, A.M. Rodríguez Vera^{165b}, S. Roe³⁵, C.S. Rogan⁵⁷, O. Røhne¹³⁰,
 R. Röhrlig¹¹³, C.P.A. Roland⁶³, J. Roloff⁵⁷, A. Romaniouk¹¹⁰, M. Romano^{23b,23a}, N. Rompotis⁸⁸,
 M. Ronzani¹²¹, L. Roos¹³², S. Rosati^{70a}, K. Rosbach⁵⁰, P. Rose¹⁴³, N-A. Rosien⁵¹, E. Rossi^{67a,67b},
 L.P. Rossi^{53b}, L. Rossini^{66a,66b}, J.H.N. Rosten³¹, R. Rosten¹⁴, M. Rotaru^{27b}, J. Rothberg¹⁴⁵,
 D. Rousseau¹²⁸, D. Roy^{32c}, A. Rozanov⁹⁹, Y. Rozen¹⁵⁷, X. Ruan^{32c}, F. Rubbo¹⁵⁰, F. Rühr⁵⁰,
 A. Ruiz-Martinez¹⁷¹, Z. Rurikova⁵⁰, N.A. Rusakovich⁷⁷, H.L. Russell¹⁰¹, J.P. Rutherford⁷,
 E.M. Rüttinger^{44,k}, Y.F. Ryabov¹³⁴, M. Rybar¹⁷⁰, G. Rybkin¹²⁸, S. Ryu⁶, A. Ryzhov¹⁴⁰, G.F. Rzechorz⁵¹,
 P. Sabatini⁵¹, G. Sabato¹¹⁸, S. Sacerdoti¹²⁸, H.F-W. Sadrozinski¹⁴³, R. Sadykov⁷⁷, F. Safai Tehrani^{70a},
 P. Saha¹¹⁹, M. Sahinsoy^{59a}, A. Sahu¹⁷⁹, M. Saimpert⁴⁴, M. Saito¹⁶⁰, T. Saito¹⁶⁰, H. Sakamoto¹⁶⁰,
 A. Sakharov^{121,ah}, D. Salamani⁵², G. Salamanna^{72a,72b}, J.E. Salazar Loyola^{144b}, D. Salek¹¹⁸,
 P.H. Sales De Bruin¹⁶⁹, D. Salihagic¹¹³, A. Salnikov¹⁵⁰, J. Salt¹⁷¹, D. Salvatore^{40b,40a}, F. Salvatore¹⁵³,
 A. Salvucci^{61a,61b,61c}, A. Salzburger³⁵, J. Samarati³⁵, D. Sammel⁵⁰, D. Sampsonidis¹⁵⁹,
 D. Sampsonidou¹⁵⁹, J. Sánchez¹⁷¹, A. Sanchez Pineda^{64a,64c}, H. Sandaker¹³⁰, C.O. Sander⁴⁴,
 M. Sandhoff¹⁷⁹, C. Sandoval²², D.P.C. Sankey¹⁴¹, M. Sannino^{53b,53a}, Y. Sano¹¹⁵, A. Sansoni⁴⁹,
 C. Santoni³⁷, H. Santos^{136a}, I. Santoyo Castillo¹⁵³, A. Sapronov⁷⁷, J.G. Saraiva^{136a,136d}, O. Sasaki⁷⁹,
 K. Sato¹⁶⁶, E. Sauvan⁵, P. Savard^{164,aq}, N. Savic¹¹³, R. Sawada¹⁶⁰, C. Sawyer¹⁴¹, L. Sawyer^{93,ag},
 C. Sbarra^{23b}, A. Sbrizzi^{23b,23a}, T. Scanlon⁹², J. Schaarschmidt¹⁴⁵, P. Schacht¹¹³, B.M. Schachtner¹¹²,
 D. Schaefer³⁶, L. Schaefer¹³³, J. Schaeffer⁹⁷, S. Schaepe³⁵, U. Schäfer⁹⁷, A.C. Schaffer¹²⁸, D. Schaile¹¹²,
 R.D. Schamberger¹⁵², N. Scharmberg⁹⁸, V.A. Schegelsky¹³⁴, D. Scheirich¹³⁹, F. Schenck¹⁹,
 M. Schernau¹⁶⁸, C. Schiavi^{53b,53a}, S. Schier¹⁴³, L.K. Schildgen²⁴, Z.M. Schillaci²⁶, E.J. Schioppa³⁵,
 M. Schioppa^{40b,40a}, K.E. Schleicher⁵⁰, S. Schlenker³⁵, K.R. Schmidt-Sommerfeld¹¹³, K. Schmieden³⁵,
 C. Schmitt⁹⁷, S. Schmitt⁴⁴, S. Schmitz⁹⁷, U. Schnoor⁵⁰, L. Schoeffel¹⁴², A. Schoening^{59b}, E. Schopf²⁴,
 M. Schott⁹⁷, J.F.P. Schouwenberg¹¹⁷, J. Schovancova³⁵, S. Schramm⁵², A. Schulte⁹⁷,
 H-C. Schultz-Coulon^{59a}, M. Schumacher⁵⁰, B.A. Schumm¹⁴³, Ph. Schune¹⁴², A. Schwartzman¹⁵⁰,
 T.A. Schwarz¹⁰³, H. Schweiger⁹⁸, Ph. Schwemling¹⁴², R. Schwienhorst¹⁰⁴, A. Sciandra²⁴, G. Sciolla²⁶,
 M. Scornajenghi^{40b,40a}, F. Scuri^{69a}, F. Scutti¹⁰², L.M. Scyboz¹¹³, J. Searcy¹⁰³, C.D. Sebastiani^{70a,70b},
 P. Seema²⁴, S.C. Seidel¹¹⁶, A. Seiden¹⁴³, T. Seiss³⁶, J.M. Seixas^{78b}, G. Sekhniaidze^{67a}, K. Sekhon¹⁰³,
 S.J. Sekula⁴¹, N. Semprini-Cesari^{23b,23a}, S. Sen⁴⁷, S. Senkin³⁷, C. Serfon¹³⁰, L. Serin¹²⁸, L. Serkin^{64a,64b},

M. Sessa^{72a,72b}, H. Severini¹²⁴, F. Sforza¹⁶⁷, A. Sfyrla⁵², E. Shabalina⁵¹, J.D. Shahinian¹⁴³,
 N.W. Shaikh^{43a,43b}, L.Y. Shan^{15a}, R. Shang¹⁷⁰, J.T. Shank²⁵, M. Shapiro¹⁸, A.S. Sharma¹, A. Sharma¹³¹,
 P.B. Shatalov¹⁰⁹, K. Shaw¹⁵³, S.M. Shaw⁹⁸, A. Shcherbakova¹³⁴, Y. Shen¹²⁴, N. Sherafati³³,
 A.D. Sherman²⁵, P. Sherwood⁹², L. Shi^{155,am}, S. Shimizu⁸⁰, C.O. Shimmin¹⁸⁰, M. Shimojima¹¹⁴,
 I.P.J. Shipsey¹³¹, S. Shirabe⁸⁵, M. Shiyakova⁷⁷, J. Shlomi¹⁷⁷, A. Shmeleva¹⁰⁸, D. Shoaleh Saadi¹⁰⁷,
 M.J. Shochet³⁶, S. Shojaii¹⁰², D.R. Shope¹²⁴, S. Shrestha¹²², E. Shulgá¹¹⁰, P. Sicho¹³⁷, A.M. Sickles¹⁷⁰,
 P.E. Sidebo¹⁵¹, E. Sideras Haddad^{32c}, O. Sidiropoulou¹⁷⁴, A. Sidoti^{23b,23a}, F. Siegert⁴⁶, Dj. Sijacki¹⁶,
 J. Silva^{136a}, M. Silva Jr.¹⁷⁸, M.V. Silva Oliveira^{78a}, S.B. Silverstein^{43a}, L. Simic⁷⁷, S. Simion¹²⁸,
 E. Simioni⁹⁷, M. Simon⁹⁷, R. Simoniello⁹⁷, P. Sinervo¹⁶⁴, N.B. Sinev¹²⁷, M. Sioli^{23b,23a}, G. Siragusa¹⁷⁴,
 I. Siral¹⁰³, S. Yu. Sivoklokov¹¹¹, J. Sjölin^{43a,43b}, M.B. Skinner⁸⁷, P. Skubic¹²⁴, M. Slater²¹, T. Slavicek¹³⁸,
 M. Slawinska⁸², K. Sliwa¹⁶⁷, R. Slovak¹³⁹, V. Smakhtin¹⁷⁷, B.H. Smart⁵, J. Smiesko^{28a}, N. Smirnov¹¹⁰,
 S. Yu. Smirnov¹¹⁰, Y. Smirnov¹¹⁰, L.N. Smirnova¹¹¹, O. Smirnova⁹⁴, J.W. Smith⁵¹, M.N.K. Smith³⁸,
 R.W. Smith³⁸, M. Smizanska⁸⁷, K. Smolek¹³⁸, A.A. Snesarev¹⁰⁸, I.M. Snyder¹²⁷, S. Snyder²⁹,
 R. Sobie^{173,ab}, A.M. Soffa¹⁶⁸, A. Soffer¹⁵⁸, A. Søgaard⁴⁸, D.A. Soh¹⁵⁵, G. Sokhrannyi⁸⁹,
 C.A. Solans Sanchez³⁵, M. Solar¹³⁸, E.Yu. Soldatov¹¹⁰, U. Soldevila¹⁷¹, A.A. Solodkov¹⁴⁰,
 A. Soloshenko⁷⁷, O.V. Solovyanov¹⁴⁰, V. Solovyev¹³⁴, P. Sommer¹⁴⁶, H. Son¹⁶⁷, W. Song¹⁴¹,
 A. Sopczak¹³⁸, F. Sopkova^{28b}, D. Sosa^{59b}, C.L. Sotiropoulou^{69a,69b}, S. Sottocornola^{68a,68b},
 R. Soualah^{64a,64c,h}, A.M. Soukharev^{120b,120a}, D. South⁴⁴, B.C. Sowden⁹¹, S. Spagnolo^{65a,65b},
 M. Spalla¹¹³, M. Spangenberg¹⁷⁵, F. Spanò⁹¹, D. Sperlich¹⁹, F. Spettel¹¹³, T.M. Spieker^{59a}, R. Spighi^{23b},
 G. Spigo³⁵, L.A. Spiller¹⁰², D.P. Spiteri⁵⁵, M. Spousta¹³⁹, A. Stabile^{66a,66b}, R. Stamen^{59a}, S. Stamm¹⁹,
 E. Stanecka⁸², R.W. Stanek⁶, C. Stanescu^{72a}, B. Stanislaus¹³¹, M.M. Stanitzki⁴⁴, B.S. Stapf¹¹⁸,
 S. Stapnes¹³⁰, E.A. Starchenko¹⁴⁰, G.H. Stark³⁶, J. Stark⁵⁶, S.H Stark³⁹, P. Staroba¹³⁷, P. Starovoitov^{59a},
 S. Stärz³⁵, R. Staszewski⁸², M. Stegler⁴⁴, P. Steinberg²⁹, B. Stelzer¹⁴⁹, H.J. Stelzer³⁵,
 O. Stelzer-Chilton^{165a}, H. Stenzel⁵⁴, T.J. Stevenson⁹⁰, G.A. Stewart⁵⁵, M.C. Stockton¹²⁷, G. Stoicea^{27b},
 P. Stolte⁵¹, S. Stonjek¹¹³, A. Straessner⁴⁶, J. Strandberg¹⁵¹, S. Strandberg^{43a,43b}, M. Strauss¹²⁴,
 P. Strizenec^{28b}, R. Ströhmer¹⁷⁴, D.M. Strom¹²⁷, R. Stroynowski⁴¹, A. Strubig⁴⁸, S.A. Stucci²⁹,
 B. Stugu¹⁷, J. Stupak¹²⁴, N.A. Styles⁴⁴, D. Su¹⁵⁰, J. Su¹³⁵, S. Suchek^{59a}, Y. Sugaya¹²⁹, M. Suk¹³⁸,
 V.V. Sulin¹⁰⁸, D.M.S. Sultan⁵², S. Sultansoy^{4c}, T. Sumida⁸³, S. Sun¹⁰³, X. Sun³, K. Suruliz¹⁵³,
 C.J.E. Suster¹⁵⁴, M.R. Sutton¹⁵³, S. Suzuki⁷⁹, M. Svatos¹³⁷, M. Swiatlowski³⁶, S.P. Swift²,
 A. Sydorenko⁹⁷, I. Sykora^{28a}, T. Sykora¹³⁹, D. Ta⁹⁷, K. Tackmann^{44,y}, J. Taenzer¹⁵⁸, A. Taffard¹⁶⁸,
 R. Tafirout^{165a}, E. Tahirovic⁹⁰, N. Taiblum¹⁵⁸, H. Takai²⁹, R. Takashima⁸⁴, E.H. Takasugi¹¹³,
 K. Takeda⁸⁰, T. Takeshita¹⁴⁷, Y. Takubo⁷⁹, M. Talby⁹⁹, A.A. Talyshев^{120b,120a}, J. Tanaka¹⁶⁰,
 M. Tanaka¹⁶², R. Tanaka¹²⁸, R. Tanioka⁸⁰, B.B. Tannenwald¹²², S. Tapia Araya^{144b}, S. Tapprogge⁹⁷,
 A. Tarek Abouelfadl Mohamed¹³², S. Tarem¹⁵⁷, G. Tarna^{27b,d}, G.F. Tartarelli^{66a}, P. Tas¹³⁹,
 M. Tasevsky¹³⁷, T. Tashiro⁸³, E. Tassi^{40b,40a}, A. Tavares Delgado^{136a,136b}, Y. Tayalati^{34e}, A.C. Taylor¹¹⁶,
 A.J. Taylor⁴⁸, G.N. Taylor¹⁰², P.T.E. Taylor¹⁰², W. Taylor^{165b}, A.S. Tee⁸⁷, P. Teixeira-Dias⁹¹,
 H. Ten Kate³⁵, P.K. Teng¹⁵⁵, J.J. Teoh¹¹⁸, F. Tepel¹⁷⁹, S. Terada⁷⁹, K. Terashi¹⁶⁰, J. Terron⁹⁶, S. Terzo¹⁴,
 M. Testa⁴⁹, R.J. Teuscher^{164,ab}, S.J. Thais¹⁸⁰, T. Theveneaux-Pelzer⁴⁴, F. Thiele³⁹, J.P. Thomas²¹,
 A.S. Thompson⁵⁵, P.D. Thompson²¹, L.A. Thomsen¹⁸⁰, E. Thomson¹³³, Y. Tian³⁸, R.E. Ticse Torres⁵¹,
 V.O. Tikhomirov^{108,aj}, Yu.A. Tikhonov^{120b,120a}, S. Timoshenko¹¹⁰, P. Tipton¹⁸⁰, S. Tisserant⁹⁹,
 K. Todome¹⁶², S. Todorova-Nova⁵, S. Todt⁴⁶, J. Tojo⁸⁵, S. Tokár^{28a}, K. Tokushuku⁷⁹, E. Tolley¹²²,
 K.G. Tomiwa^{32c}, M. Tomoto¹¹⁵, L. Tompkins¹⁵⁰, K. Toms¹¹⁶, B. Tong⁵⁷, P. Tornambe⁵⁰, E. Torrence¹²⁷,
 H. Torres⁴⁶, E. Torró Pastor¹⁴⁵, C. Toscri¹³¹, J. Toth^{99,aa}, F. Touchard⁹⁹, D.R. Tovey¹⁴⁶, C.J. Treado¹²¹,
 T. Trefzger¹⁷⁴, F. Tresoldi¹⁵³, A. Tricoli²⁹, I.M. Trigger^{165a}, S. Trincaz-Duvoid¹³², M.F. Tripiana¹⁴,
 W. Trischuk¹⁶⁴, B. Trocmé⁵⁶, A. Trofymov¹²⁸, C. Troncon^{66a}, M. Trovatelli¹⁷³, F. Trovato¹⁵³,
 L. Truong^{32b}, M. Trzebinski⁸², A. Trzupek⁸², F. Tsai⁴⁴, J.C.-L. Tseng¹³¹, P.V. Tsiareshka¹⁰⁵,
 N. Tsirintanis⁹, V. Tsiskaridze¹⁵², E.G. Tskhadadze^{156a}, I.I. Tsukerman¹⁰⁹, V. Tsulaia¹⁸, S. Tsuno⁷⁹,

D. Tsybychev¹⁵², Y. Tu^{61b}, A. Tudorache^{27b}, V. Tudorache^{27b}, T.T. Tulbure^{27a}, A.N. Tuna⁵⁷,
 S. Turchikhin⁷⁷, D. Turgeman¹⁷⁷, I. Turk Cakir^{4b,s}, R. Turra^{66a}, P.M. Tuts³⁸, E. Tzovara⁹⁷,
 G. Ucchielli^{23b,23a}, I. Ueda⁷⁹, M. Ughetto^{43a,43b}, F. Ukegawa¹⁶⁶, G. Unal³⁵, A. Undrus²⁹, G. Unel¹⁶⁸,
 F.C. Ungaro¹⁰², Y. Unno⁷⁹, K. Uno¹⁶⁰, J. Urban^{28b}, P. Urquijo¹⁰², P. Urrejola⁹⁷, G. Usai⁸, J. Usui⁷⁹,
 L. Vacavant⁹⁹, V. Vacek¹³⁸, B. Vachon¹⁰¹, K.O.H. Vadla¹³⁰, A. Vaidya⁹², C. Valderanis¹¹²,
 E. Valdes Santurio^{43a,43b}, M. Valente⁵², S. Valentineti^{23b,23a}, A. Valero¹⁷¹, L. Valéry⁴⁴, R.A. Vallance²¹,
 A. Vallier⁵, J.A. Valls Ferrer¹⁷¹, T.R. Van Daalen¹⁴, W. Van Den Wollenberg¹¹⁸, H. Van der Graaf¹¹⁸,
 P. Van Gemmeren⁶, J. Van Nieuwkoop¹⁴⁹, I. Van Vulpen¹¹⁸, M. Vanadia^{71a,71b}, W. Vandelli³⁵,
 A. Vaniachine¹⁶³, P. Vankov¹¹⁸, R. Vari^{70a}, E.W. Varnes⁷, C. Varni^{53b,53a}, T. Varol⁴¹, D. Varouchas¹²⁸,
 K.E. Varvell¹⁵⁴, G.A. Vasquez^{144b}, J.G. Vasquez¹⁸⁰, F. Vazeille³⁷, D. Vazquez Furelos¹⁴,
 T. Vazquez Schroeder¹⁰¹, J. Veatch⁵¹, V. Vecchio^{72a,72b}, L.M. Veloce¹⁶⁴, F. Veloso^{136a,136c},
 S. Veneziano^{70a}, A. Ventura^{65a,65b}, M. Venturi¹⁷³, N. Venturi³⁵, V. Vercesi^{68a}, M. Verducci^{72a,72b},
 C.M. Vergel Infante⁷⁶, W. Verkerke¹¹⁸, A.T. Vermeulen¹¹⁸, J.C. Vermeulen¹¹⁸, M.C. Vetterli^{149,aq},
 N. Viaux Maira^{144b}, M. Vicente Barreto Pinto⁵², I. Vichou^{170,*}, T. Vickey¹⁴⁶, O.E. Vickey Boeriu¹⁴⁶,
 G.H.A. Viehhäuser¹³¹, S. Viel¹⁸, L. Vigani¹³¹, M. Villa^{23b,23a}, M. Villaplana Perez^{66a,66b}, E. Vilucchi⁴⁹,
 M.G. Vincter³³, V.B. Vinogradov⁷⁷, A. Vishwakarma⁴⁴, C. Vittori^{23b,23a}, I. Vivarelli¹⁵³, S. Vlachos¹⁰,
 M. Vogel¹⁷⁹, P. Vokac¹³⁸, G. Volpi¹⁴, S.E. Von Buddenbrock^{32c}, E. Von Toerne²⁴, V. Vorobel¹³⁹,
 K. Vorobev¹¹⁰, M. Vos¹⁷¹, J.H. Vossebeld⁸⁸, N. Vranjes¹⁶, M. Vranjes Milosavljevic¹⁶, V. Vrba¹³⁸,
 M. Vreeswijk¹¹⁸, T. Šfiligoj⁸⁹, R. Vuillermet³⁵, I. Vukotic³⁶, T. Ženiš^{28a}, L. Živković¹⁶, P. Wagner²⁴,
 W. Wagner¹⁷⁹, J. Wagner-Kuhr¹¹², H. Wahlberg⁸⁶, S. Wahrmund⁴⁶, K. Wakamiya⁸⁰, V.M. Walbrecht¹¹³,
 J. Walder⁸⁷, R. Walker¹¹², S.D. Walker⁹¹, W. Walkowiak¹⁴⁸, V. Wallangen^{43a,43b}, A.M. Wang⁵⁷,
 C. Wang^{58b,d}, F. Wang¹⁷⁸, H. Wang¹⁸, H. Wang³, J. Wang¹⁵⁴, J. Wang^{59b}, P. Wang⁴¹, Q. Wang¹²⁴,
 R.-J. Wang¹³², R. Wang^{58a}, R. Wang⁶, S.M. Wang¹⁵⁵, W.T. Wang^{58a}, W. Wang^{15b,ac}, W.X. Wang^{58a,ac},
 Y. Wang^{58a}, Z. Wang^{58c}, C. Wanotayaroj⁴⁴, A. Warburton¹⁰¹, C.P. Ward³¹, D.R. Wardrope⁹²,
 A. Washbrook⁴⁸, P.M. Watkins²¹, A.T. Watson²¹, M.F. Watson²¹, G. Watts¹⁴⁵, S. Watts⁹⁸, B.M. Waugh⁹²,
 A.F. Webb¹¹, S. Webb⁹⁷, C. Weber¹⁸⁰, M.S. Weber²⁰, S.A. Weber³³, S.M. Weber^{59a}, J.S. Webster⁶,
 A.R. Weidberg¹³¹, B. Weinert⁶³, J. Weingarten⁵¹, M. Weirich⁹⁷, C. Weiser⁵⁰, P.S. Wells³⁵, T. Wenaus²⁹,
 T. Wengler³⁵, S. Wenig³⁵, N. Wermes²⁴, M.D. Werner⁷⁶, P. Werner³⁵, M. Wessels^{59a}, T.D. Weston²⁰,
 K. Whalen¹²⁷, N.L. Whallon¹⁴⁵, A.M. Wharton⁸⁷, A.S. White¹⁰³, A. White⁸, M.J. White¹, R. White^{144b},
 D. Whiteson¹⁶⁸, B.W. Whitmore⁸⁷, F.J. Wickens¹⁴¹, W. Wiedenmann¹⁷⁸, M. Wielers¹⁴¹,
 C. Wiglesworth³⁹, L.A.M. Wiik-Fuchs⁵⁰, A. Wildauer¹¹³, F. Wilk⁹⁸, H.G. Wilkens³⁵, L.J. Wilkins⁹¹,
 H.H. Williams¹³³, S. Williams³¹, C. Willis¹⁰⁴, S. Willocq¹⁰⁰, J.A. Wilson²¹, I. Wingerter-Seez⁵,
 E. Winkels¹⁵³, F. Winklmeier¹²⁷, O.J. Winston¹⁵³, B.T. Winter²⁴, M. Wittgen¹⁵⁰, M. Wobisch⁹³,
 A. Wolf⁹⁷, T.M.H. Wolf¹¹⁸, R. Wolff⁹⁹, M.W. Wolter⁸², H. Wolters^{136a,136c}, V.W.S. Wong¹⁷²,
 N.L. Woods¹⁴³, S.D. Worm²¹, B.K. Wosiek⁸², K.W. Woźniak⁸², K. Wraith⁵⁵, M. Wu³⁶, S.L. Wu¹⁷⁸,
 X. Wu⁵², Y. Wu^{58a}, T.R. Wyatt⁹⁸, B.M. Wynne⁴⁸, S. Xella³⁹, Z. Xi¹⁰³, L. Xia¹⁷⁵, D. Xu^{15a}, H. Xu^{58a},
 L. Xu²⁹, T. Xu¹⁴², W. Xu¹⁰³, B. Yabsley¹⁵⁴, S. Yacoob^{32a}, K. Yajima¹²⁹, D.P. Yallup⁹², D. Yamaguchi¹⁶²,
 Y. Yamaguchi¹⁶², A. Yamamoto⁷⁹, T. Yamanaka¹⁶⁰, F. Yamane⁸⁰, M. Yamatani¹⁶⁰, T. Yamazaki¹⁶⁰,
 Y. Yamazaki⁸⁰, Z. Yan²⁵, H.J. Yang^{58c,58d}, H.T. Yang¹⁸, S. Yang⁷⁵, Y. Yang¹⁶⁰, Z. Yang¹⁷, W-M. Yao¹⁸,
 Y.C. Yap⁴⁴, Y. Yasu⁷⁹, E. Yatsenko^{58c,58d}, J. Ye⁴¹, S. Ye²⁹, I. Yeletskikh⁷⁷, E. Yigitbasi²⁵, E. Yildirim⁹⁷,
 K. Yorita¹⁷⁶, K. Yoshihara¹³³, C.J.S. Young³⁵, C. Young¹⁵⁰, J. Yu⁸, J. Yu⁷⁶, X. Yue^{59a}, S.P.Y. Yuen²⁴,
 B. Zabinski⁸², G. Zacharis¹⁰, E. Zaffaroni⁵², R. Zaidan¹⁴, A.M. Zaitsev^{140,ai}, N. Zakharchuk⁴⁴,
 J. Zalieckas¹⁷, S. Zambito⁵⁷, D. Zanzi³⁵, D.R. Zaripovas⁵⁵, S.V. Zeißner⁴⁵, C. Zeitnitz¹⁷⁹,
 G. Zemaityte¹³¹, J.C. Zeng¹⁷⁰, Q. Zeng¹⁵⁰, O. Zenin¹⁴⁰, D. Zerwas¹²⁸, M. Zgubič¹³¹, D.F. Zhang^{58b},
 D. Zhang¹⁰³, F. Zhang¹⁷⁸, G. Zhang^{58a}, H. Zhang^{15b}, J. Zhang⁶, L. Zhang^{15b}, L. Zhang^{58a}, M. Zhang¹⁷⁰,
 P. Zhang^{15b}, R. Zhang^{58a}, R. Zhang²⁴, X. Zhang^{58b}, Y. Zhang^{15d}, Z. Zhang¹²⁸, X. Zhao⁴¹,
 Y. Zhao^{58b,128,af}, Z. Zhao^{58a}, A. Zhemchugov⁷⁷, B. Zhou¹⁰³, C. Zhou¹⁷⁸, L. Zhou⁴¹, M.S. Zhou^{15d},

M. Zhou¹⁵², N. Zhou^{58c}, Y. Zhou⁷, C.G. Zhu^{58b}, H.L. Zhu^{58a}, H. Zhu^{15a}, J. Zhu¹⁰³, Y. Zhu^{58a}, X. Zhuang^{15a}, K. Zhukov¹⁰⁸, V. Zhulanov^{120b,120a}, A. Zibell¹⁷⁴, D. Ziemska⁶³, N.I. Zimine⁷⁷, S. Zimmermann⁵⁰, Z. Zinonos¹¹³, M. Zinser⁹⁷, M. Ziolkowski¹⁴⁸, G. Zobernig¹⁷⁸, A. Zoccoli^{23b,23a}, K. Zoch⁵¹, T.G. Zorbas¹⁴⁶, R. Zou³⁶, M. Zur Nedden¹⁹, L. Zwalski³⁵.

¹Department of Physics, University of Adelaide, Adelaide; Australia.

²Physics Department, SUNY Albany, Albany NY; United States of America.

³Department of Physics, University of Alberta, Edmonton AB; Canada.

^{4(a)}Department of Physics, Ankara University, Ankara;^(b)Istanbul Aydin University, Istanbul;^(c)Division of Physics, TOBB University of Economics and Technology, Ankara; Turkey.

⁵LAPP, Université Grenoble Alpes, Université Savoie Mont Blanc, CNRS/IN2P3, Annecy; France.

⁶High Energy Physics Division, Argonne National Laboratory, Argonne IL; United States of America.

⁷Department of Physics, University of Arizona, Tucson AZ; United States of America.

⁸Department of Physics, University of Texas at Arlington, Arlington TX; United States of America.

⁹Physics Department, National and Kapodistrian University of Athens, Athens; Greece.

¹⁰Physics Department, National Technical University of Athens, Zografou; Greece.

¹¹Department of Physics, University of Texas at Austin, Austin TX; United States of America.

^{12(a)}Bahcesehir University, Faculty of Engineering and Natural Sciences, Istanbul;^(b)Istanbul Bilgi University, Faculty of Engineering and Natural Sciences, Istanbul;^(c)Department of Physics, Bogazici University, Istanbul;^(d)Department of Physics Engineering, Gaziantep University, Gaziantep; Turkey.

¹³Institute of Physics, Azerbaijan Academy of Sciences, Baku; Azerbaijan.

¹⁴Institut de Física d'Altes Energies (IFAE), Barcelona Institute of Science and Technology, Barcelona; Spain.

^{15(a)}Institute of High Energy Physics, Chinese Academy of Sciences, Beijing;^(b)Department of Physics, Nanjing University, Nanjing;^(c)Physics Department, Tsinghua University, Beijing;^(d)University of Chinese Academy of Science (UCAS), Beijing; China.

¹⁶Institute of Physics, University of Belgrade, Belgrade; Serbia.

¹⁷Department for Physics and Technology, University of Bergen, Bergen; Norway.

¹⁸Physics Division, Lawrence Berkeley National Laboratory and University of California, Berkeley CA; United States of America.

¹⁹Institut für Physik, Humboldt Universität zu Berlin, Berlin; Germany.

²⁰Albert Einstein Center for Fundamental Physics and Laboratory for High Energy Physics, University of Bern, Bern; Switzerland.

²¹School of Physics and Astronomy, University of Birmingham, Birmingham; United Kingdom.

²²Centro de Investigaciones, Universidad Antonio Nariño, Bogota; Colombia.

^{23(a)}Dipartimento di Fisica e Astronomia, Università di Bologna, Bologna;^(b)INFN Sezione di Bologna; Italy.

²⁴Physikalisches Institut, Universität Bonn, Bonn; Germany.

²⁵Department of Physics, Boston University, Boston MA; United States of America.

²⁶Department of Physics, Brandeis University, Waltham MA; United States of America.

^{27(a)}Transilvania University of Brasov, Brasov;^(b)Horia Hulubei National Institute of Physics and Nuclear Engineering, Bucharest;^(c)Department of Physics, Alexandru Ioan Cuza University of Iasi, Iasi;^(d)National Institute for Research and Development of Isotopic and Molecular Technologies, Physics Department, Cluj-Napoca;^(e)University Politehnica Bucharest, Bucharest;^(f)West University in Timisoara, Timisoara; Romania.

^{28(a)}Faculty of Mathematics, Physics and Informatics, Comenius University, Bratislava;^(b)Department of Subnuclear Physics, Institute of Experimental Physics of the Slovak Academy of Sciences, Kosice;

Slovak Republic.

²⁹Physics Department, Brookhaven National Laboratory, Upton NY; United States of America.

³⁰Departamento de Física, Universidad de Buenos Aires, Buenos Aires; Argentina.

³¹Cavendish Laboratory, University of Cambridge, Cambridge; United Kingdom.

^{32(a)}Department of Physics, University of Cape Town, Cape Town;^(b)Department of Mechanical Engineering Science, University of Johannesburg, Johannesburg;^(c)School of Physics, University of the Witwatersrand, Johannesburg; South Africa.

³³Department of Physics, Carleton University, Ottawa ON; Canada.

^{34(a)}Faculté des Sciences Ain Chock, Réseau Universitaire de Physique des Hautes Energies - Université Hassan II, Casablanca;^(b)Centre National de l'Energie des Sciences Techniques Nucleaires (CNESTEN), Rabat;^(c)Faculté des Sciences Semlalia, Université Cadi Ayyad, LPHEA-Marrakech;^(d)Faculté des Sciences, Université Mohamed Premier and LPTPM, Oujda;^(e)Faculté des sciences, Université Mohammed V, Rabat; Morocco.

³⁵CERN, Geneva; Switzerland.

³⁶Enrico Fermi Institute, University of Chicago, Chicago IL; United States of America.

³⁷LPC, Université Clermont Auvergne, CNRS/IN2P3, Clermont-Ferrand; France.

³⁸Nevis Laboratory, Columbia University, Irvington NY; United States of America.

³⁹Niels Bohr Institute, University of Copenhagen, Copenhagen; Denmark.

^{40(a)}Dipartimento di Fisica, Università della Calabria, Rende;^(b)INFN Gruppo Collegato di Cosenza, Laboratori Nazionali di Frascati; Italy.

⁴¹Physics Department, Southern Methodist University, Dallas TX; United States of America.

⁴²Physics Department, University of Texas at Dallas, Richardson TX; United States of America.

^{43(a)}Department of Physics, Stockholm University;^(b)Oskar Klein Centre, Stockholm; Sweden.

⁴⁴Deutsches Elektronen-Synchrotron DESY, Hamburg and Zeuthen; Germany.

⁴⁵Lehrstuhl für Experimentelle Physik IV, Technische Universität Dortmund, Dortmund; Germany.

⁴⁶Institut für Kern- und Teilchenphysik, Technische Universität Dresden, Dresden; Germany.

⁴⁷Department of Physics, Duke University, Durham NC; United States of America.

⁴⁸SUPA - School of Physics and Astronomy, University of Edinburgh, Edinburgh; United Kingdom.

⁴⁹INFN e Laboratori Nazionali di Frascati, Frascati; Italy.

⁵⁰Physikalischs Institut, Albert-Ludwigs-Universität Freiburg, Freiburg; Germany.

⁵¹II. Physikalischs Institut, Georg-August-Universität Göttingen, Göttingen; Germany.

⁵²Département de Physique Nucléaire et Corpusculaire, Université de Genève, Genève; Switzerland.

^{53(a)}Dipartimento di Fisica, Università di Genova, Genova;^(b)INFN Sezione di Genova; Italy.

⁵⁴II. Physikalischs Institut, Justus-Liebig-Universität Giessen, Giessen; Germany.

⁵⁵SUPA - School of Physics and Astronomy, University of Glasgow, Glasgow; United Kingdom.

⁵⁶LPSC, Université Grenoble Alpes, CNRS/IN2P3, Grenoble INP, Grenoble; France.

⁵⁷Laboratory for Particle Physics and Cosmology, Harvard University, Cambridge MA; United States of America.

^{58(a)}Department of Modern Physics and State Key Laboratory of Particle Detection and Electronics, University of Science and Technology of China, Hefei;^(b)Institute of Frontier and Interdisciplinary Science and Key Laboratory of Particle Physics and Particle Irradiation (MOE), Shandong University, Qingdao;^(c)School of Physics and Astronomy, Shanghai Jiao Tong University, KLPPAC-MoE, SKLPPC, Shanghai;^(d)Tsung-Dao Lee Institute, Shanghai; China.

^{59(a)}Kirchhoff-Institut für Physik, Ruprecht-Karls-Universität Heidelberg, Heidelberg;^(b)Physikalischs Institut, Ruprecht-Karls-Universität Heidelberg, Heidelberg; Germany.

⁶⁰Faculty of Applied Information Science, Hiroshima Institute of Technology, Hiroshima; Japan.

^{61(a)}Department of Physics, Chinese University of Hong Kong, Shatin, N.T., Hong Kong;^(b)Department

of Physics, University of Hong Kong, Hong Kong;^(c)Department of Physics and Institute for Advanced Study, Hong Kong University of Science and Technology, Clear Water Bay, Kowloon, Hong Kong; China.

⁶²Department of Physics, National Tsing Hua University, Hsinchu; Taiwan.

⁶³Department of Physics, Indiana University, Bloomington IN; United States of America.

^{64(a)}INFN Gruppo Collegato di Udine, Sezione di Trieste, Udine;^(b)ICTP, Trieste;^(c)Dipartimento di Chimica, Fisica e Ambiente, Università di Udine, Udine; Italy.

^{65(a)}INFN Sezione di Lecce;^(b)Dipartimento di Matematica e Fisica, Università del Salento, Lecce; Italy.

^{66(a)}INFN Sezione di Milano;^(b)Dipartimento di Fisica, Università di Milano, Milano; Italy.

^{67(a)}INFN Sezione di Napoli;^(b)Dipartimento di Fisica, Università di Napoli, Napoli; Italy.

^{68(a)}INFN Sezione di Pavia;^(b)Dipartimento di Fisica, Università di Pavia, Pavia; Italy.

^{69(a)}INFN Sezione di Pisa;^(b)Dipartimento di Fisica E. Fermi, Università di Pisa, Pisa; Italy.

^{70(a)}INFN Sezione di Roma;^(b)Dipartimento di Fisica, Sapienza Università di Roma, Roma; Italy.

^{71(a)}INFN Sezione di Roma Tor Vergata;^(b)Dipartimento di Fisica, Università di Roma Tor Vergata, Roma; Italy.

^{72(a)}INFN Sezione di Roma Tre;^(b)Dipartimento di Matematica e Fisica, Università Roma Tre, Roma; Italy.

^{73(a)}INFN-TIFPA;^(b)Università degli Studi di Trento, Trento; Italy.

⁷⁴Institut für Astro- und Teilchenphysik, Leopold-Franzens-Universität, Innsbruck; Austria.

⁷⁵University of Iowa, Iowa City IA; United States of America.

⁷⁶Department of Physics and Astronomy, Iowa State University, Ames IA; United States of America.

⁷⁷Joint Institute for Nuclear Research, Dubna; Russia.

^{78(a)}Departamento de Engenharia Elétrica, Universidade Federal de Juiz de Fora (UFJF), Juiz de Fora;^(b)Universidade Federal do Rio De Janeiro COPPE/EE/IF, Rio de Janeiro;^(c)Universidade Federal de São João del Rei (UFSJ), São João del Rei;^(d)Instituto de Física, Universidade de São Paulo, São Paulo; Brazil.

⁷⁹KEK, High Energy Accelerator Research Organization, Tsukuba; Japan.

⁸⁰Graduate School of Science, Kobe University, Kobe; Japan.

^{81(a)}AGH University of Science and Technology, Faculty of Physics and Applied Computer Science, Krakow;^(b)Marian Smoluchowski Institute of Physics, Jagiellonian University, Krakow; Poland.

⁸²Institute of Nuclear Physics Polish Academy of Sciences, Krakow; Poland.

⁸³Faculty of Science, Kyoto University, Kyoto; Japan.

⁸⁴Kyoto University of Education, Kyoto; Japan.

⁸⁵Research Center for Advanced Particle Physics and Department of Physics, Kyushu University, Fukuoka ; Japan.

⁸⁶Instituto de Física La Plata, Universidad Nacional de La Plata and CONICET, La Plata; Argentina.

⁸⁷Physics Department, Lancaster University, Lancaster; United Kingdom.

⁸⁸Oliver Lodge Laboratory, University of Liverpool, Liverpool; United Kingdom.

⁸⁹Department of Experimental Particle Physics, Jožef Stefan Institute and Department of Physics, University of Ljubljana, Ljubljana; Slovenia.

⁹⁰School of Physics and Astronomy, Queen Mary University of London, London; United Kingdom.

⁹¹Department of Physics, Royal Holloway University of London, Egham; United Kingdom.

⁹²Department of Physics and Astronomy, University College London, London; United Kingdom.

⁹³Louisiana Tech University, Ruston LA; United States of America.

⁹⁴Fysiska institutionen, Lunds universitet, Lund; Sweden.

⁹⁵Centre de Calcul de l’Institut National de Physique Nucléaire et de Physique des Particules (IN2P3), Villeurbanne; France.

- ⁹⁶Departamento de Física Teórica C-15 and CIAFF, Universidad Autónoma de Madrid, Madrid; Spain.
- ⁹⁷Institut für Physik, Universität Mainz, Mainz; Germany.
- ⁹⁸School of Physics and Astronomy, University of Manchester, Manchester; United Kingdom.
- ⁹⁹CPPM, Aix-Marseille Université, CNRS/IN2P3, Marseille; France.
- ¹⁰⁰Department of Physics, University of Massachusetts, Amherst MA; United States of America.
- ¹⁰¹Department of Physics, McGill University, Montreal QC; Canada.
- ¹⁰²School of Physics, University of Melbourne, Victoria; Australia.
- ¹⁰³Department of Physics, University of Michigan, Ann Arbor MI; United States of America.
- ¹⁰⁴Department of Physics and Astronomy, Michigan State University, East Lansing MI; United States of America.
- ¹⁰⁵B.I. Stepanov Institute of Physics, National Academy of Sciences of Belarus, Minsk; Belarus.
- ¹⁰⁶Research Institute for Nuclear Problems of Byelorussian State University, Minsk; Belarus.
- ¹⁰⁷Group of Particle Physics, University of Montreal, Montreal QC; Canada.
- ¹⁰⁸P.N. Lebedev Physical Institute of the Russian Academy of Sciences, Moscow; Russia.
- ¹⁰⁹Institute for Theoretical and Experimental Physics (ITEP), Moscow; Russia.
- ¹¹⁰National Research Nuclear University MEPhI, Moscow; Russia.
- ¹¹¹D.V. Skobeltsyn Institute of Nuclear Physics, M.V. Lomonosov Moscow State University, Moscow; Russia.
- ¹¹²Fakultät für Physik, Ludwig-Maximilians-Universität München, München; Germany.
- ¹¹³Max-Planck-Institut für Physik (Werner-Heisenberg-Institut), München; Germany.
- ¹¹⁴Nagasaki Institute of Applied Science, Nagasaki; Japan.
- ¹¹⁵Graduate School of Science and Kobayashi-Maskawa Institute, Nagoya University, Nagoya; Japan.
- ¹¹⁶Department of Physics and Astronomy, University of New Mexico, Albuquerque NM; United States of America.
- ¹¹⁷Institute for Mathematics, Astrophysics and Particle Physics, Radboud University Nijmegen/Nikhef, Nijmegen; Netherlands.
- ¹¹⁸Nikhef National Institute for Subatomic Physics and University of Amsterdam, Amsterdam; Netherlands.
- ¹¹⁹Department of Physics, Northern Illinois University, DeKalb IL; United States of America.
- ^{120(a)}Budker Institute of Nuclear Physics, SB RAS, Novosibirsk;^(b)Novosibirsk State University Novosibirsk; Russia.
- ¹²¹Department of Physics, New York University, New York NY; United States of America.
- ¹²²Ohio State University, Columbus OH; United States of America.
- ¹²³Faculty of Science, Okayama University, Okayama; Japan.
- ¹²⁴Homer L. Dodge Department of Physics and Astronomy, University of Oklahoma, Norman OK; United States of America.
- ¹²⁵Department of Physics, Oklahoma State University, Stillwater OK; United States of America.
- ¹²⁶Palacký University, RCPTM, Joint Laboratory of Optics, Olomouc; Czech Republic.
- ¹²⁷Center for High Energy Physics, University of Oregon, Eugene OR; United States of America.
- ¹²⁸LAL, Université Paris-Sud, CNRS/IN2P3, Université Paris-Saclay, Orsay; France.
- ¹²⁹Graduate School of Science, Osaka University, Osaka; Japan.
- ¹³⁰Department of Physics, University of Oslo, Oslo; Norway.
- ¹³¹Department of Physics, Oxford University, Oxford; United Kingdom.
- ¹³²LPNHE, Sorbonne Université, Paris Diderot Sorbonne Paris Cité, CNRS/IN2P3, Paris; France.
- ¹³³Department of Physics, University of Pennsylvania, Philadelphia PA; United States of America.
- ¹³⁴Konstantinov Nuclear Physics Institute of National Research Centre "Kurchatov Institute", PNPI, St. Petersburg; Russia.

¹³⁵Department of Physics and Astronomy, University of Pittsburgh, Pittsburgh PA; United States of America.

^{136(a)}Laboratório de Instrumentação e Física Experimental de Partículas - LIP;^(b)Departamento de Física, Faculdade de Ciências, Universidade de Lisboa, Lisboa;^(c)Departamento de Física, Universidade de Coimbra, Coimbra;^(d)Centro de Física Nuclear da Universidade de Lisboa, Lisboa;^(e)Departamento de Física, Universidade do Minho, Braga;^(f)Departamento de Física Teorica y del Cosmos, Universidad de Granada, Granada (Spain);^(g)Dep Física and CEFITEC of Faculdade de Ciências e Tecnologia, Universidade Nova de Lisboa, Caparica; Portugal.

¹³⁷Institute of Physics, Academy of Sciences of the Czech Republic, Prague; Czech Republic.

¹³⁸Czech Technical University in Prague, Prague; Czech Republic.

¹³⁹Charles University, Faculty of Mathematics and Physics, Prague; Czech Republic.

¹⁴⁰State Research Center Institute for High Energy Physics, NRC KI, Protvino; Russia.

¹⁴¹Particle Physics Department, Rutherford Appleton Laboratory, Didcot; United Kingdom.

¹⁴²IRFU, CEA, Université Paris-Saclay, Gif-sur-Yvette; France.

¹⁴³Santa Cruz Institute for Particle Physics, University of California Santa Cruz, Santa Cruz CA; United States of America.

^{144(a)}Departamento de Física, Pontificia Universidad Católica de Chile, Santiago;^(b)Departamento de Física, Universidad Técnica Federico Santa María, Valparaíso; Chile.

¹⁴⁵Department of Physics, University of Washington, Seattle WA; United States of America.

¹⁴⁶Department of Physics and Astronomy, University of Sheffield, Sheffield; United Kingdom.

¹⁴⁷Department of Physics, Shinshu University, Nagano; Japan.

¹⁴⁸Department Physik, Universität Siegen, Siegen; Germany.

¹⁴⁹Department of Physics, Simon Fraser University, Burnaby BC; Canada.

¹⁵⁰SLAC National Accelerator Laboratory, Stanford CA; United States of America.

¹⁵¹Physics Department, Royal Institute of Technology, Stockholm; Sweden.

¹⁵²Departments of Physics and Astronomy, Stony Brook University, Stony Brook NY; United States of America.

¹⁵³Department of Physics and Astronomy, University of Sussex, Brighton; United Kingdom.

¹⁵⁴School of Physics, University of Sydney, Sydney; Australia.

¹⁵⁵Institute of Physics, Academia Sinica, Taipei; Taiwan.

^{156(a)}E. Andronikashvili Institute of Physics, Iv. Javakhishvili Tbilisi State University, Tbilisi;^(b)High Energy Physics Institute, Tbilisi State University, Tbilisi; Georgia.

¹⁵⁷Department of Physics, Technion, Israel Institute of Technology, Haifa; Israel.

¹⁵⁸Raymond and Beverly Sackler School of Physics and Astronomy, Tel Aviv University, Tel Aviv; Israel.

¹⁵⁹Department of Physics, Aristotle University of Thessaloniki, Thessaloniki; Greece.

¹⁶⁰International Center for Elementary Particle Physics and Department of Physics, University of Tokyo, Tokyo; Japan.

¹⁶¹Graduate School of Science and Technology, Tokyo Metropolitan University, Tokyo; Japan.

¹⁶²Department of Physics, Tokyo Institute of Technology, Tokyo; Japan.

¹⁶³Tomsk State University, Tomsk; Russia.

¹⁶⁴Department of Physics, University of Toronto, Toronto ON; Canada.

^{165(a)}TRIUMF, Vancouver BC;^(b)Department of Physics and Astronomy, York University, Toronto ON; Canada.

¹⁶⁶Division of Physics and Tomonaga Center for the History of the Universe, Faculty of Pure and Applied Sciences, University of Tsukuba, Tsukuba; Japan.

¹⁶⁷Department of Physics and Astronomy, Tufts University, Medford MA; United States of America.

¹⁶⁸Department of Physics and Astronomy, University of California Irvine, Irvine CA; United States of

America.

¹⁶⁹Department of Physics and Astronomy, University of Uppsala, Uppsala; Sweden.

¹⁷⁰Department of Physics, University of Illinois, Urbana IL; United States of America.

¹⁷¹Instituto de Física Corpuscular (IFIC), Centro Mixto Universidad de Valencia - CSIC, Valencia; Spain.

¹⁷²Department of Physics, University of British Columbia, Vancouver BC; Canada.

¹⁷³Department of Physics and Astronomy, University of Victoria, Victoria BC; Canada.

¹⁷⁴Fakultät für Physik und Astronomie, Julius-Maximilians-Universität Würzburg, Würzburg; Germany.

¹⁷⁵Department of Physics, University of Warwick, Coventry; United Kingdom.

¹⁷⁶Waseda University, Tokyo; Japan.

¹⁷⁷Department of Particle Physics, Weizmann Institute of Science, Rehovot; Israel.

¹⁷⁸Department of Physics, University of Wisconsin, Madison WI; United States of America.

¹⁷⁹Fakultät für Mathematik und Naturwissenschaften, Fachgruppe Physik, Bergische Universität Wuppertal, Wuppertal; Germany.

¹⁸⁰Department of Physics, Yale University, New Haven CT; United States of America.

¹⁸¹Yerevan Physics Institute, Yerevan; Armenia.

^a Also at Borough of Manhattan Community College, City University of New York, NY; United States of America.

^b Also at Centre for High Performance Computing, CSIR Campus, Rosebank, Cape Town; South Africa.

^c Also at CERN, Geneva; Switzerland.

^d Also at CPPM, Aix-Marseille Université, CNRS/IN2P3, Marseille; France.

^e Also at Département de Physique Nucléaire et Corpusculaire, Université de Genève, Genève; Switzerland.

^f Also at Departament de Fisica de la Universitat Autonoma de Barcelona, Barcelona; Spain.

^g Also at Departamento de Física Teorica y del Cosmos, Universidad de Granada, Granada (Spain); Spain.

^h Also at Department of Applied Physics and Astronomy, University of Sharjah, Sharjah; United Arab Emirates.

ⁱ Also at Department of Financial and Management Engineering, University of the Aegean, Chios; Greece.

^j Also at Department of Physics and Astronomy, University of Louisville, Louisville, KY; United States of America.

^k Also at Department of Physics and Astronomy, University of Sheffield, Sheffield; United Kingdom.

^l Also at Department of Physics, California State University, Fresno CA; United States of America.

^m Also at Department of Physics, California State University, Sacramento CA; United States of America.

ⁿ Also at Department of Physics, King's College London, London; United Kingdom.

^o Also at Department of Physics, St. Petersburg State Polytechnical University, St. Petersburg; Russia.

^p Also at Department of Physics, University of Fribourg, Fribourg; Switzerland.

^q Also at Department of Physics, University of Michigan, Ann Arbor MI; United States of America.

^r Also at Dipartimento di Fisica E. Fermi, Università di Pisa, Pisa; Italy.

^s Also at Giresun University, Faculty of Engineering, Giresun; Turkey.

^t Also at Graduate School of Science, Osaka University, Osaka; Japan.

^u Also at Hellenic Open University, Patras; Greece.

^v Also at Horia Hulubei National Institute of Physics and Nuclear Engineering, Bucharest; Romania.

^w Also at II. Physikalisches Institut, Georg-August-Universität Göttingen, Göttingen; Germany.

^x Also at Institucio Catalana de Recerca i Estudis Avancats, ICREA, Barcelona; Spain.

^y Also at Institut für Experimentalphysik, Universität Hamburg, Hamburg; Germany.

^z Also at Institute for Mathematics, Astrophysics and Particle Physics, Radboud University

Nijmegen/Nikhef, Nijmegen; Netherlands.

aa Also at Institute for Particle and Nuclear Physics, Wigner Research Centre for Physics, Budapest; Hungary.

ab Also at Institute of Particle Physics (IPP); Canada.

ac Also at Institute of Physics, Academia Sinica, Taipei; Taiwan.

ad Also at Institute of Physics, Azerbaijan Academy of Sciences, Baku; Azerbaijan.

ae Also at Institute of Theoretical Physics, Ilia State University, Tbilisi; Georgia.

af Also at LAL, Université Paris-Sud, CNRS/IN2P3, Université Paris-Saclay, Orsay; France.

ag Also at Louisiana Tech University, Ruston LA; United States of America.

ah Also at Manhattan College, New York NY; United States of America.

ai Also at Moscow Institute of Physics and Technology State University, Dolgoprudny; Russia.

aj Also at National Research Nuclear University MEPhI, Moscow; Russia.

ak Also at Near East University, Nicosia, North Cyprus, Mersin; Turkey.

al Also at Physikalisches Institut, Albert-Ludwigs-Universität Freiburg, Freiburg; Germany.

am Also at School of Physics, Sun Yat-sen University, Guangzhou; China.

an Also at The City College of New York, New York NY; United States of America.

ao Also at The Collaborative Innovation Center of Quantum Matter (CICQM), Beijing; China.

ap Also at Tomsk State University, Tomsk, and Moscow Institute of Physics and Technology State University, Dolgoprudny; Russia.

aq Also at TRIUMF, Vancouver BC; Canada.

ar Also at Universita di Napoli Parthenope, Napoli; Italy.

* Deceased